NASA CR 137574

HIGH-PURITY SILICA REFLECTING HEAT SHIELD DEVELOPMENT

By William M. Congdon

August 1974

Prepared under Contract No. NAS2-7912 by
MARTIN MARIETTA CORPORATION
Denver, Colo.

for

AMES RESEARCH CENTER

NATIONAL AERONAUTICS AND SPACE ADMINISTRATION

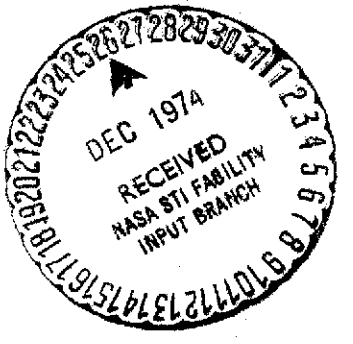

FOREWORD

This report is prepared by the Denver Division of Martin Marietta Corporation under National Aeronautics and Space Administration Contract NAS2-7912, *Study of Factors that Determine the Heat Shield Performance of Silica-Bonded Silica Materials and Fabrication of Selected Material Billets*. The program was conducted by the Structures and Materials Department of the Engineering Research and Development organization from December 1973 to October 1974. Mr. William M. Congdon was the Principal Investigator. The Ames Research Center, Moffett Field, California, directed the administration of this contract. Dr. Phillip R. Nachtsheim, Assistant Branch Chief of the Thermal Protection Branch, served as the NASA Technical Monitor.

Invaluable assistance and guidance were received from the following Martin Marietta personnel:

E. L. Strauss	Program Manager
J. W. Maccalous	Supervisor, Plastics Laboratory
G. J. Schmidt	Supervisor, Plasma Arc Facility
J. M. Mann	Ceramics Laboratory
A. E. Blair	Plasma Arc Laboratory
E. R. Freeman	Failure Analysis Laboratory
P. J. Pizzolato	Thermal Engineering Laboratory
P. N. Peece	Materials Analysis Laboratory
M. B. Congdon	Quality Control Laboratory
W. E. Precht	Materials Department (MML)
S. E. Stokowski	Physics Department (MML)
W. M. Mularie	Physics Department (MML)

TABLE OF CONTENTS

LIST OF ILLUSTRATIONS

LIST OF TABLES

HIGH-PURITY REFLECTING HEAT SHIELD DEVELOPMENT

By William M. Congdon
Martin Marietta Corporation

SUMMARY

The purpose of this program was to develop a high-purity, fused-silica reflecting heat shield for the thermal protection of outer-planet probes. Such a heat shield reflects shock-layer radiation by diffuse scattering due to the dissimilar refractive index of the silica and void phases. The program also included a study of factors that strongly influence the performance of a silica heat shield, such as the microstructure and degree of purity. Three different silica-bonded silica configurations, each prepared by a different technique, were investigated. These were slip-cast, foamed-slip, and pressure-sintered fused silica. Each configuration was rated according to its relative merits. Slip-casting was selected as the preferred fabrication method because it produced good reflectivity and good strength, and is relatively easy to scale up for a full-size outer-planet probe.

The slips were cast using a variety of different particle sizes. Besides the continuous-particle-size slips generally used in slip casting, we also studied monodisperse particle-size slips and blends of monodisperse particle-size slips. Of the monodisperse slips studied, the slip that was composed of particles between 5 and 11 μm in diameter produced the highest reflectance for a given material. Of the blend slips studied, the one whose major component consisted of the 5- to 11-μm particles gave the highest reflectance. In general, over the particle sizes studied, smaller particles gave the highest reflectance. In addition, both the monodisperse slips as well as the blend slips gave a higher reflectance than the continuous-particle-size slips for a given material and a given model thickness.

An upgraded and fused natural quartz was used to study the effects of microstructure on reflectance and as the baseline to ascertain the increase in reflectance obtained from using a higher-purity synthetic material. A noticeable improvement in reflectance in the near-UV was obtained by using a synthetic fused silica prepared by the vapor-phase hydrolysis of silicon tetrachloride.

I. INTRODUCTION

A. Program Objective and Scope

The objective of this program was to develop a high-purity-silica reflecting heat shield material. This included fabricating and evaluating three types of silica-bonded silica configurations--slip-cast, foamed-slip, and pressure-sintered fused silica--to determine their relative merits as reflecting heat shield candidates. The evaluation testing consisted of spectrophotometer tests, high-intensity-radiation tests, and mechanical tests to determine the modulus of rupture, and modulus of elasticity.

After selecting the best silica-bonded silica configuration, we studied producibility aspects for a full-size heat shield. This involved scaling up of the methods and techniques used to produce the test models, as well as investigating various attachment aspects.

The program concluded with the fabrication of five study billets to be evaluated by NASA-Ames Research Center. Specimens machined from these billets are to be tested in the Advanced Entry Heating Simulator (AEHS) facility.

B. Reflecting Heat Shield Concept

The reflecting heat shield is a promising means of thermal protection for entry environments containing large shock-layer radiation components. Such heat shields are being considered for upcoming outer-planet probe missions, particularly for the nominal-cool extremes in the uncertainty of the outer-planet atmospheres, where radiation is most severe.

Figure 1 from reference 1 shows analytically predicted entry heating associated with a probe entry into Saturn. The figure covers the full range of uncertainty in scale height and composition of the planet's atmosphere.

Note the large differences in entry heating rates and durations for the cool-, nominal-, and warm-atmosphere ranges. Entry into the cool atmosphere is dominated by shock-layer radiation pulses up to 23 kW/cm^2; radiative and convective pulses are intense, but of short duration. Entry into the warm atmosphere produces relatively mild pulses with very little radiation, but the pulses have a longer duration. The nominal atmosphere produces convective and radiative pulses of moderate duration that reach approximately 8 kW/cm^2 and 3 kW/cm^2, respectively.

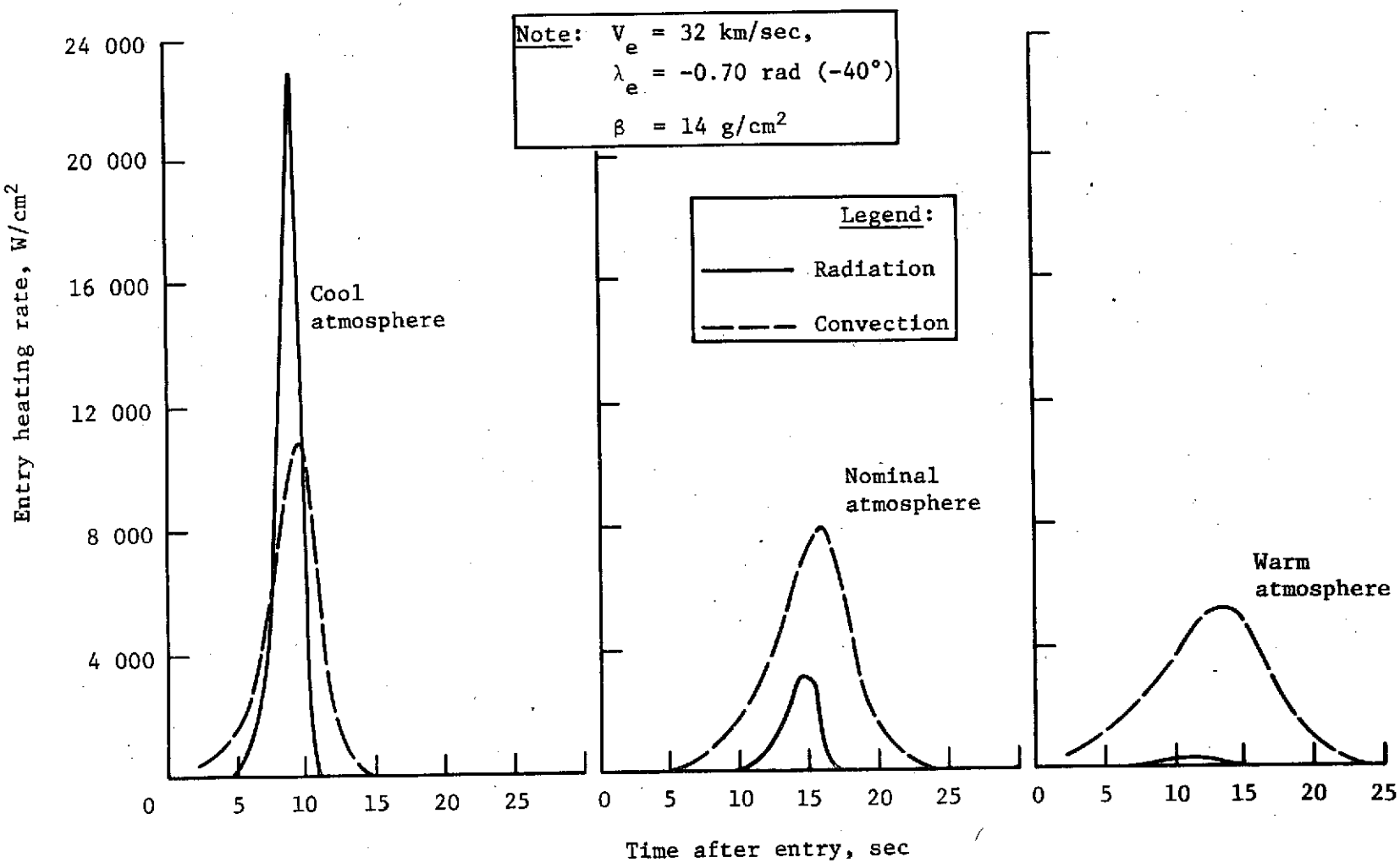

Figure 1.- Comparison of the cool-, nominal-, and warm-atmosphere heating rates for Saturn entry (ref. 1)

The Saturn heating rates are also representative of the heating environment encountered during Uranus entry. Table 1 compares cone edge heating experienced during entry into the cool planetary atmospheres at an entry angle of -0.70 rad (-40°). Compared with Saturn entry heating, the peak convective heating rate for Uranus is about 20% lower and the peak radiative heating rate is about 15% higher. Total convective heating during Uranus entry is 37% lower than for Saturn entry.

TABLE 1.- COMPARISON OF SATURN AND URANUS ENTRY HEATING*

Entry parameter	Saturn	Uranus
Entry velocity, km/sec (ft/sec)	29.3 (96 000)	26.8 (88 000)
Peak convective heating rate, kW/cm^2 (Btu/ft^2-sec)	24.8 (21 800)	19.6 (17 300)
Peak radiative heating rate, kW/cm^2 (Btu/ft^2-sec)	26.8 (23 600)	31.0 (27 300)
Total convective heating, $kW\text{-}sec/cm^2$ (Btu/ft^2)	86.2 (76 000)	54.5 (48 000)
Total radiative heating, $kW\text{-}sec/cm^2$ (Btu/ft^2)	53.4 (47 000)	51.1 (45 000)

*Cone edge heating; -0.70 rad (-40°) entry angle; cool atmosphere.

An important consideration in designing a reflecting heat shield is the spectral distribution of shock-layer radiation during entry. The spectrum will vary with the composition of the planet atmosphere and will be perturbed by the injection of ablation products. Figure 2 shows Nicolet's analytically predicted stagnation-point spectrum for a steep entry into the Saturn nominal atmosphere. As shown, the bulk of the radiation is in the visible and UV regions of the spectrum.

Fused silica has a good potential as an efficient reflecting heat shield material because of its high reflectivity over the wavelength range of interest, its high heat of sublimation, which is about 12.5 MJ/kg, and its excellent resistance to thermal shock (ref. 2).

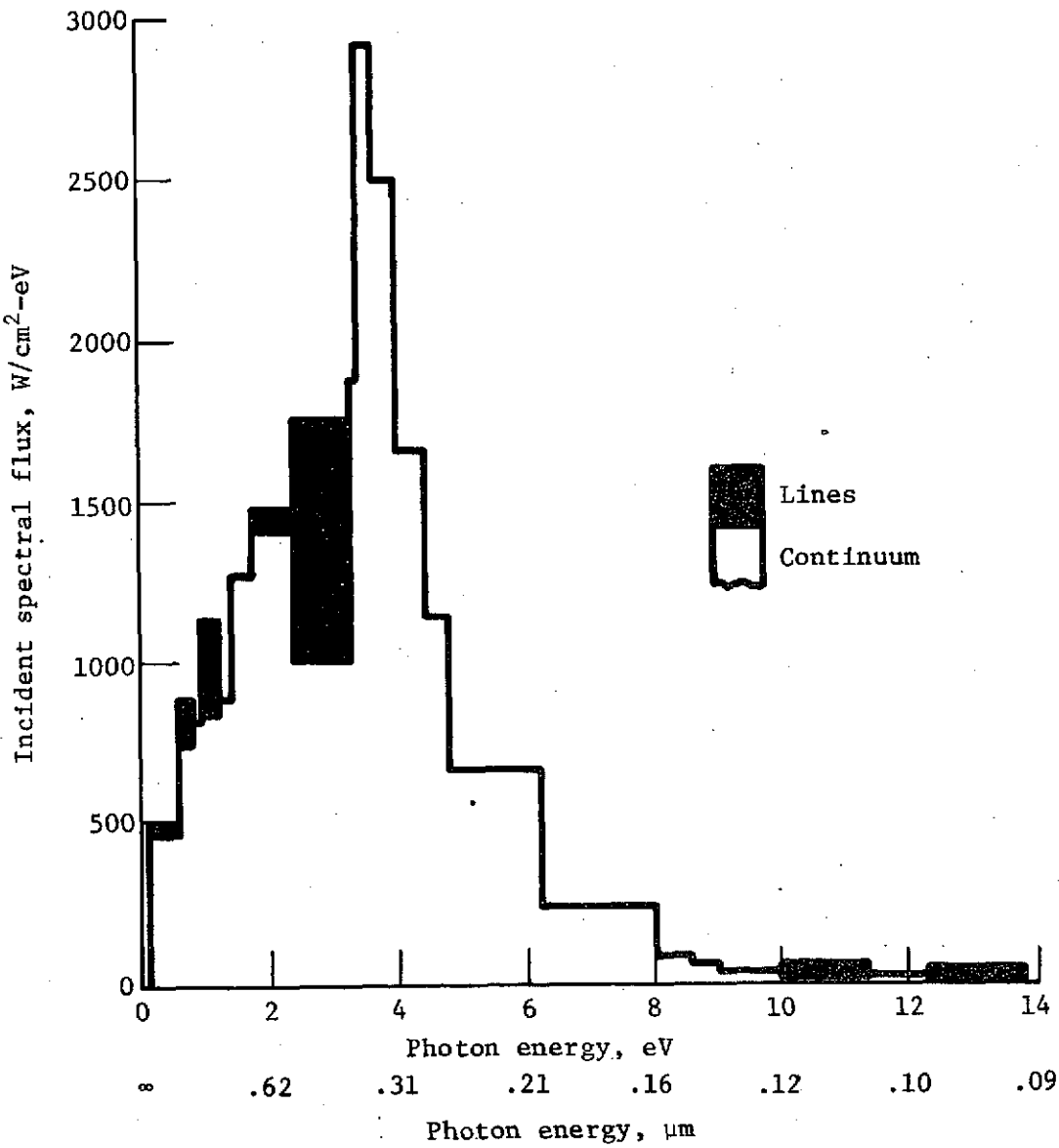

Figure 2.- Predicted spectral distribution of Saturn entry shock layer radiation to nonablating wall (ref. 1)

II. THEORETICAL INVESTIGATIONS

A. General Properties of Silica

1. Polymorphic forms.- The relationship of fused silica to its crystalline counterparts is often a source of confusion and is worth reviewing. Fused silica is a noncrystalline form of silicon dioxide. Essentially, it is a high-viscosity melt phase, or glass, that is thermodynamically unstable, but kinetically stable at ordinary temperatures. At atmospheric pressure, the crystalline forms of silica are quartz, tridymite, and cristobalite (ref. 3). The densities of these polymorphic forms are 2.65, 2.26, and 2.33 g/cm^3, respectively, whereas the density of fused silica is 2.20 g/cm^3.

Quartz is the stable crystalline form from room temperature up to 1140°K. Tridymite is stable from 1140°K to 1743°K, and cristobalite is stable from 1743°K up to its melting point, 1996°K. Each of these, in turn, has additional polymorphic forms within different temperature ranges.

Quartz, tridymite, and cristobalite are stable within their own temperature ranges and, as a result, exhibit properties that are constant over time at these temperatures. However, one silica crystalline phase can be thermally stranded for indefinite periods within the temperature range of another. Thus, for example, tridymite and cristobalite exist within the stability domains of quartz, and fused silica exists in the temperature ranges of all three crystalline forms. Metastable states such as these can change to stable states under particular conditions, or into some other phase that is also thermodynamically unstable but lower in free energy than the original state. Quartz, for instance, when heated to temperatures between 1140°K and 1743°K, usually changes to a disordered cristobalite rather than to tridymite (ref. 3).

The highest-temperature, stable crystalline form of silica at a pressure of 1 atmosphere is high cristobalite. This structure melts slowly to form fused silica at 1996°K, and has a heat of transformation of 0.128 J/kg. However, at 1957°K it is possible to observe the melting point of the metastable tridymite because of the slowness of the tridymite-cristobalite transformation. Thus, fusion can occur at this lower temperature. When the melted phase is cooled, fused silica is generally maintained. This noncrystalline form has no recognized melting point. It undergoes a gradual change in viscosity with temperature, as do other glass-like materials, but still remains very stiff up to its boiling point, which is about 3100°K.

The vaporization of fused silica involves the following reaction:

$$SiO_2(\ell) \longrightarrow SiO(g) + \tfrac{1}{2}O_2(g).$$

The thermodynamically calculated heat of vaporization, based on this reaction, is about 12.5 MJ/kg at 2000°K. Near 3000°K, the heat of reaction is about 12.0 MJ/kg (ref. 4).

Only fused silica has such a low coefficient of thermal expansion. This unique property is a result of its random structure. In contrast, the crystalline forms are susceptible to thermal shocking.

2. Optical characteristics.- For the purposes of this discussion, fused silica can be categorized into two general types, which differ in terms of their optical transmittance (fig. 3). Type A fused silica is a synthetically produced, ultrahigh-purity fused silica that is usually prepared by the vapor-phase hydrolysis of silicon tetrachloride. It has no UV absorption band at 0.243 μm, but does have IR absorption bands at 1.38, 2.22, and 2.73 μm.* Type B fused silica is produced by upgrading and fusing natural quartz. It can be produced in very high purity, but is generally less pure than Type A. Type B has an UV absorption band at 0.243 μm, but does not exhibit the IR bands at 1.38, 2.22, and 2.73 μm that are common to high-hydroxyl material. Generally, Type A silica is prepared in small quantities and is approximately 100 times more costly than Type B.

The UV absorption edge for fused silica corresponds to the transition of a valence electron of an oxygen ion in the glass network to an excited state (refs. 6 and 7). If the network is modified so that nonbridging oxygen ions are produced, then the excitation of the valence electrons of these singly-bonded oxygen ions shifts the UV edge to longer wavelengths.

The presence of alkali-metal impurities in fused silica apparently generates nonbridging oxygen ions, and small amounts produce a significant shift in the UV absorption edge. Figure 4 shows a two-dimensional representation of the creation of nonbridging oxygens by the introduction of sodium into the silica network. Sigel (ref. 6) studied the magnitude of the absorption edge shift as a function of the concentration of alkali metal. Figure 5 shows the shift to longer wavelength caused by percentages of sodium ranging from 0.015 to 0.12 mole (0.6 to 5.0 ppm).

---

*For the causes of these absorption bands, the reader is referred to ref. 5.

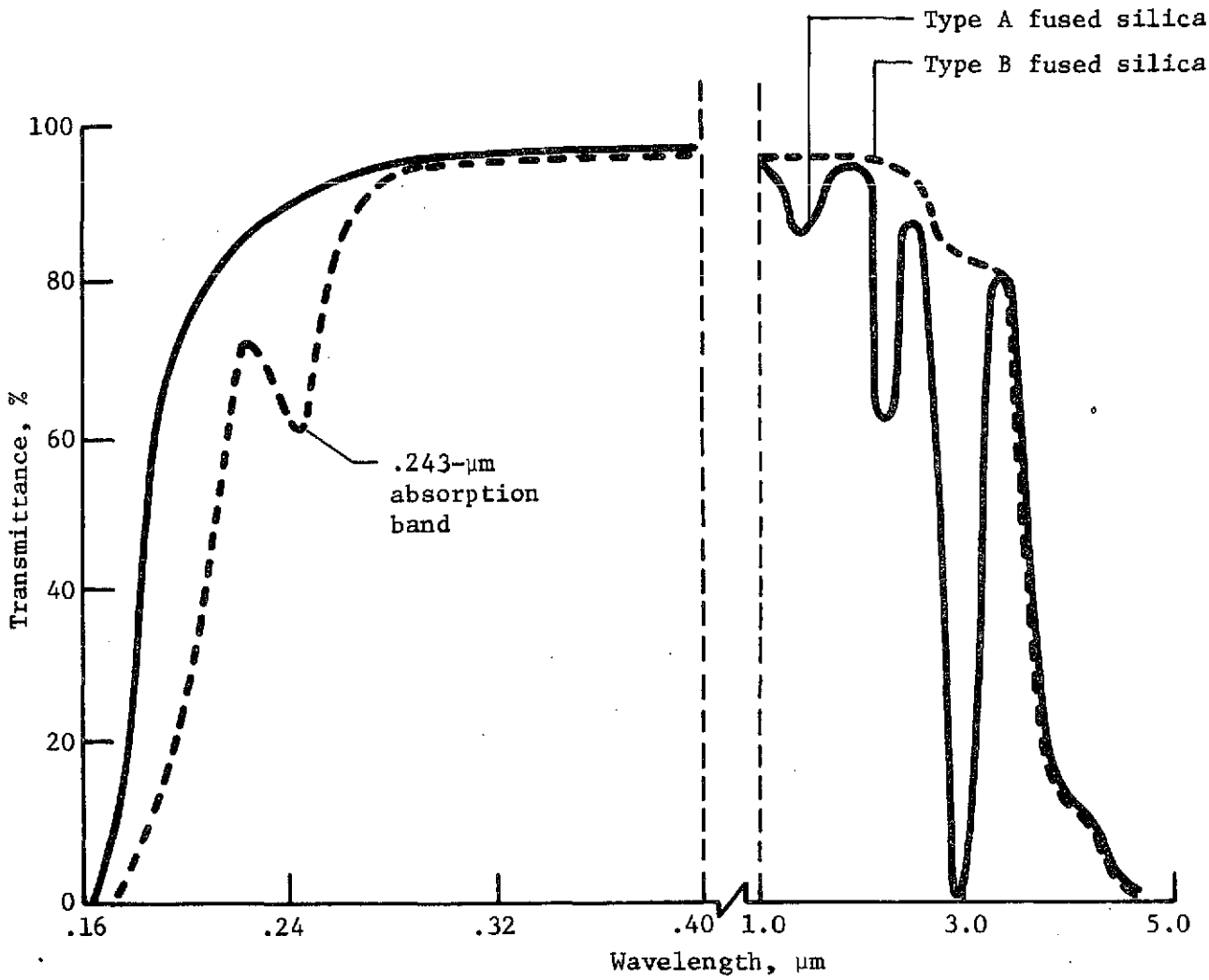

Figure 3.- Spectral transmittance for 1.0-cm-thick slabs of two types of clear fused silica (Ref. 5)

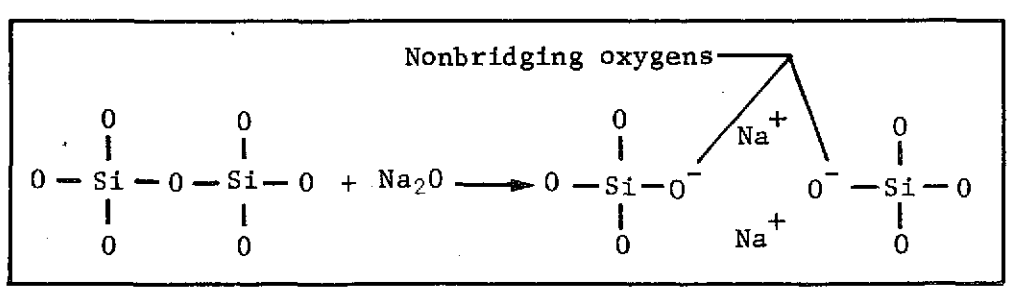

Figure 4.- Two-dimensional representation of the creation of nonbridging oxygens by the introduction of sodium into the fused silica network (Ref. 6)

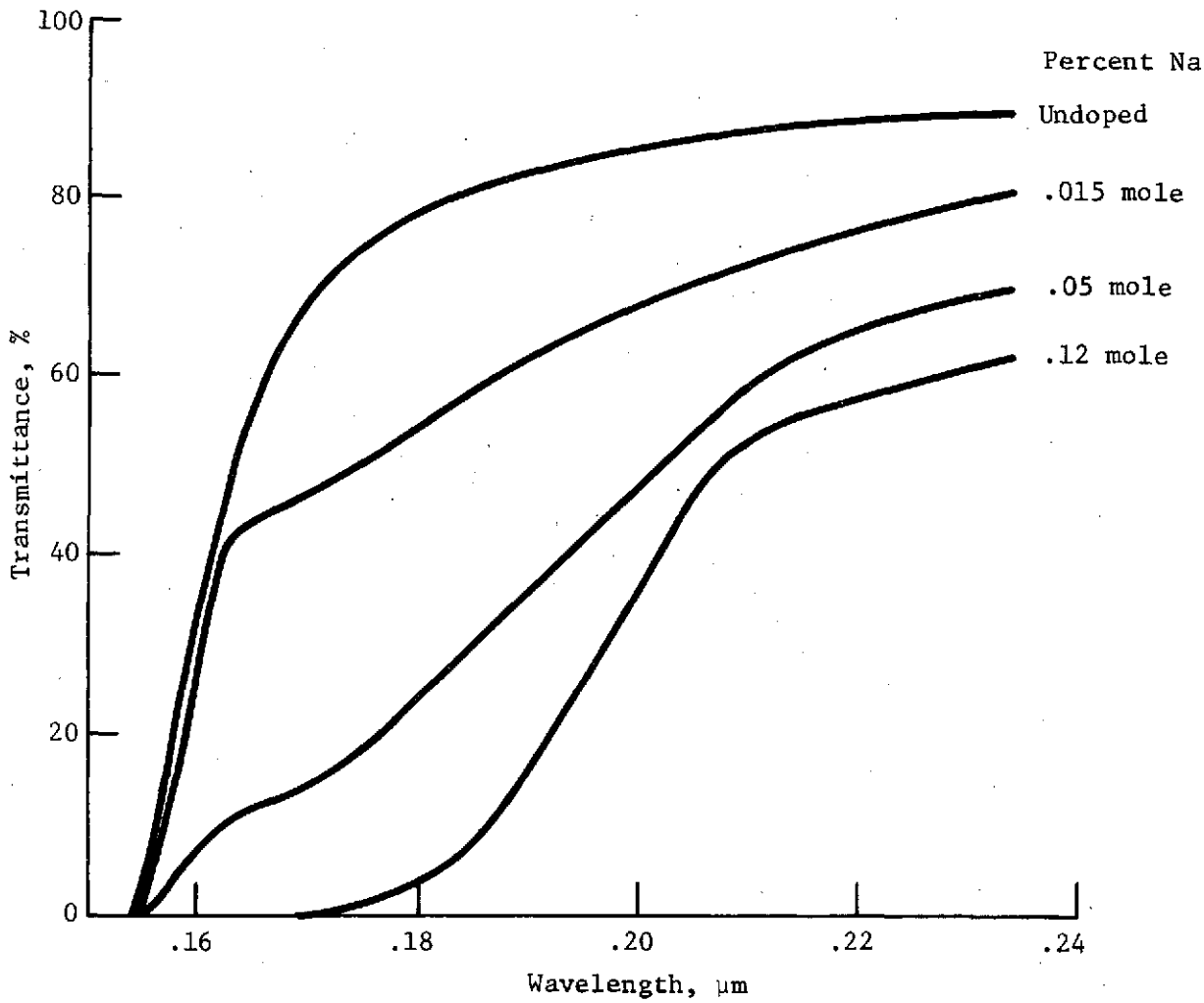

Figure 5.- Effects of the addition of sodium on the UV absorption of fused silica (Ref. 6)

Sigel also showed that for a given level of impurity, the intensity of absorption decreased in the following order--K, Na, and Li. When samples were doped with equal amounts of aluminum and alkali metal, the absorption was significantly less than that with alkali metal alone.

At elevated temperatures, the transparency of fused silica decreases. The absorption edge in the far-UV shifts to longer wavelengths, and that in the IR, to shorter wavelengths. Figure 6, taken from a paper by Beder, Bass, and Shackleford (ref. 8), shows the UV bathochromic shift of Type A fused silica from room temperature to 1773°K. At temperatures near the melting point of silica, the UV absorption edge moves to approximately 0.23 μm. The presence of impurities (such as sodium) in the fused-silica network shifts the edge to still longer wavelengths.

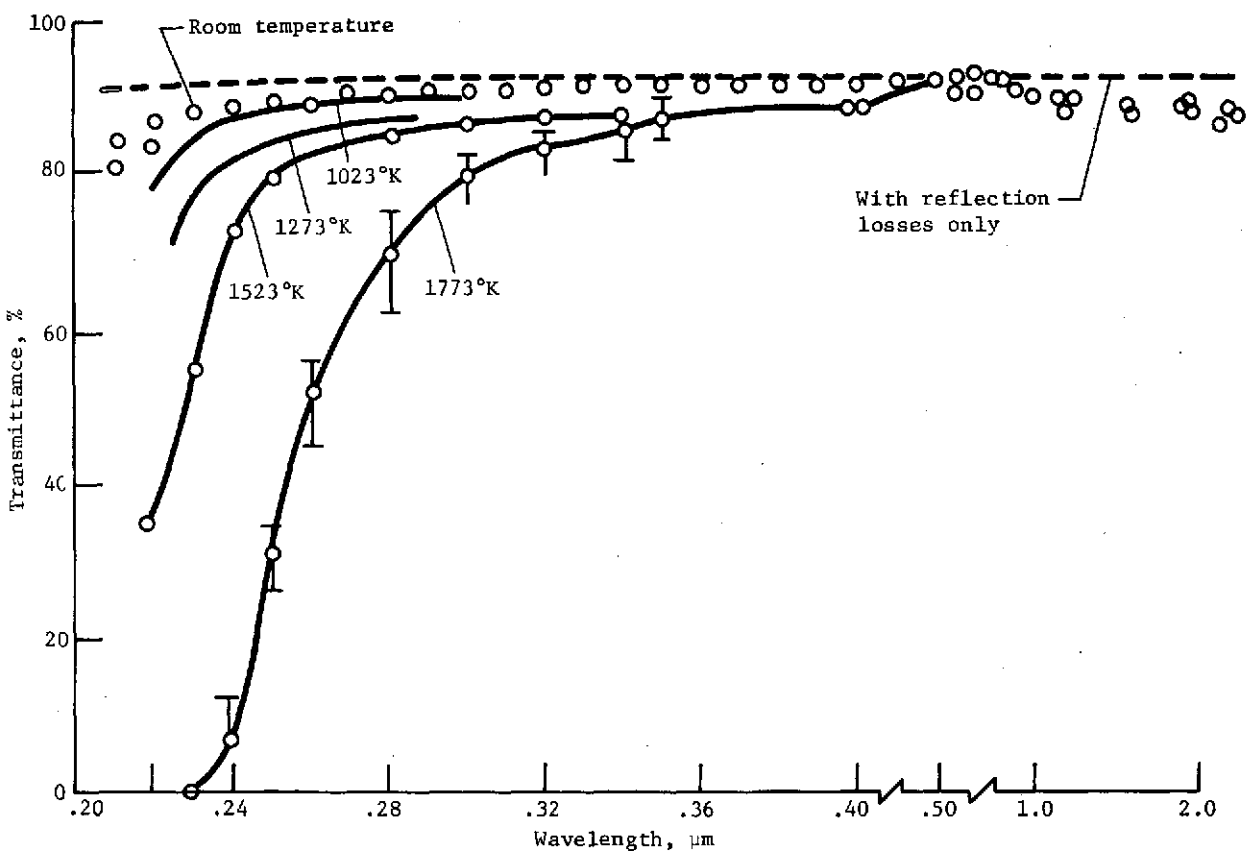

Figure 6.- Isothermal curves of spectral transmittance for a 0.95-cm-thick slab of Type A clear fused silica (Ref. 8)

B. Investigation of Scattering Properties

Martin Marietta's Multiple Scattering Analysis Program (MSAP) was used to theoretically investigate the scattering performance of a white fused-silica heat shield containing scattering voids. This program couples the exact Mie solutions of Maxwell's equations for single-particle scattering with the phenomenological theory of Kubelka-Munk, and relates the experimentally determined scattering parameters to the total hemispherical reflectance of an array of scatterers. The scattering, and hence, the reflectance of configurations of various materials, can be theoretically predicted by inputing basic material properties such as the absorption coefficient and complex refractive index, and sizing parameters such as the scattering center diameter and percent volume concentration of scatterers. This program can also optimize the reflectance of a configuration by systematically varying important parameters relative to a particular spectral distribution of incident radiation.

In our MSAP analyses of fused silica, complex refractive indices and temperature-dependent absorption coefficients were used to calculate the hemispherical reflectance of fused silica as a function of void size and volume density. The real part of the refractive index and the absorption coefficients were also input as functions of wavelength.

Table 2 lists the values for the real part of the refractive index (from ref. 9) and the absorption coefficients (from refs. 8 and 9) that were used in the analyses. These values are for GE 151 ultrahigh-purity synthetic fused silica, a Type A material. The 293°K values of the real refractive index were used for the 1773°K analysis, as well as for the 293°K analyses. (Normally, the refractive index would be higher at 1773°K, thereby giving a higher reflectance than that calculated with the 293°K data.)

Figure 7 shows a plot of hemispherical reflectance vs. wavelength, void size, and volume density for a Type A fused-silica heat shield at room temperature, as predicted by MSAP. The void size is a function of particle size, and the voids are basically the interparticle interstices. Note that larger void radii produce a higher reflectance. For a given void radius, a higher reflectance can be obtained by increasing the volume of void phase, which is, essentially, decreasing the density of the material by increasing the number of voids. Figure 7 also shows that the increase in reflectance obtained by increasing the number of voids is less for the larger voids than for the smaller voids.

TABLE 2.- REFRACTIVE INDICES AND ABSORPTION COEFFICIENTS (for GE 151 fused silica) USED IN THE MSAP ANALYSES (Refs. 8 and 9)

Wavelength, μm	Real refractive index (at 293°K)	Absorption coefficient, cm^{-1}	
		At 293°K	At 1773°K
0.25	1.5065	0.0408	1.3
0.30	1.4878	0.0202	.17
0.35	1.4770	0.010	.07
0.40	1.4703	0.004	.05
0.45	1.4653	--	.03
0.50	1.4622	--	.01
0.55	1.4598	--	.004
0.60	1.4580	--	--
0.65	1.4565	--	--
0.70	1.4553	--	--

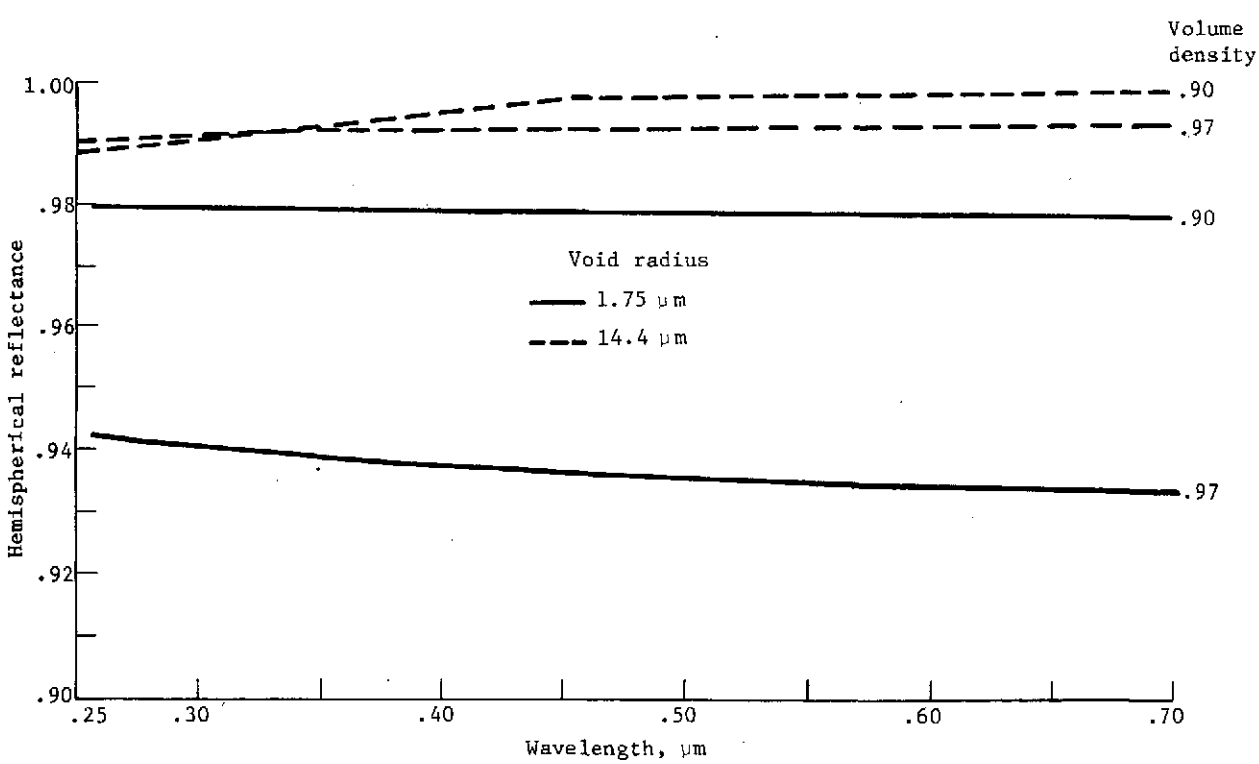

Figure 7.- MSAP predictions of the effects of void size and volume density on the hemispherical spectral reflectance of a 0.13-cm-thick slab of Type A fused silica at 293°K

Figure 8 shows MSAP predictions at 1773°K. Note that larger void radii produce a decreased reflectance in the UV region at higher temperatures--a larger decrease than with smaller void radii--due to the increased absorption and the changed scattering cross sections that result from this increased absorption. This phenomenon is significant because the surface of a silica reflecting heat shield will reach a temperature of 1773°K very rapidly, and the larger reflectance of the smaller voids could prevent or delay the occurrence of bulk vitrification* by decreasing the absorption.

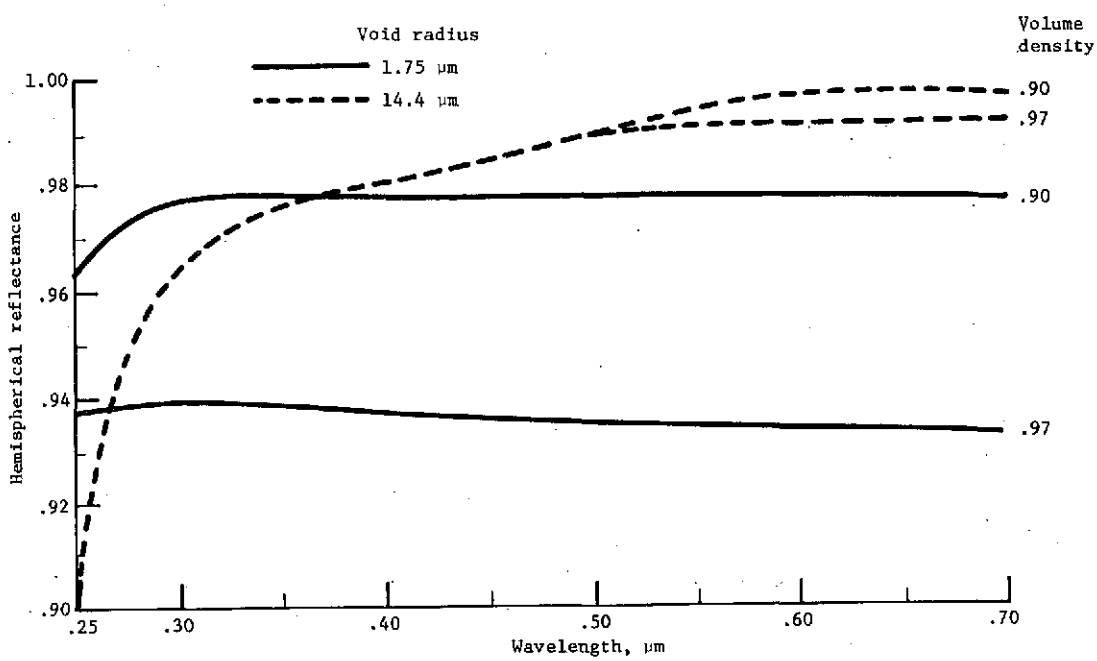

Figure 8.- MSAP predictions of the effects of void size and volume density on the hemispherical spectral reflectance of a 0.13-cm-thick slab of Type A fused silica at 1773°K

Figure 9 shows the results obtained by using MSAP to calculate the total hemispherical reflectance of a fused-silica heat shield, relative to the predicted Saturn entry shock layer radiation given in figure 2. Note that for a 70% dense material, the optimum reflectance is achieved by a void radius in the 2- to 3-μm region. For higher-density configurations, an optimum reflectance requires larger voids.

It should be mentioned that the important results of all the MSAP analyses are the trends they reveal, rather than the absolute reflectances they predict.

---

*The term "bulk vitrification" is used to describe the process where the silica particles coalesce at high temperature, eliminating scattering voids and leaving a transparent matrix.

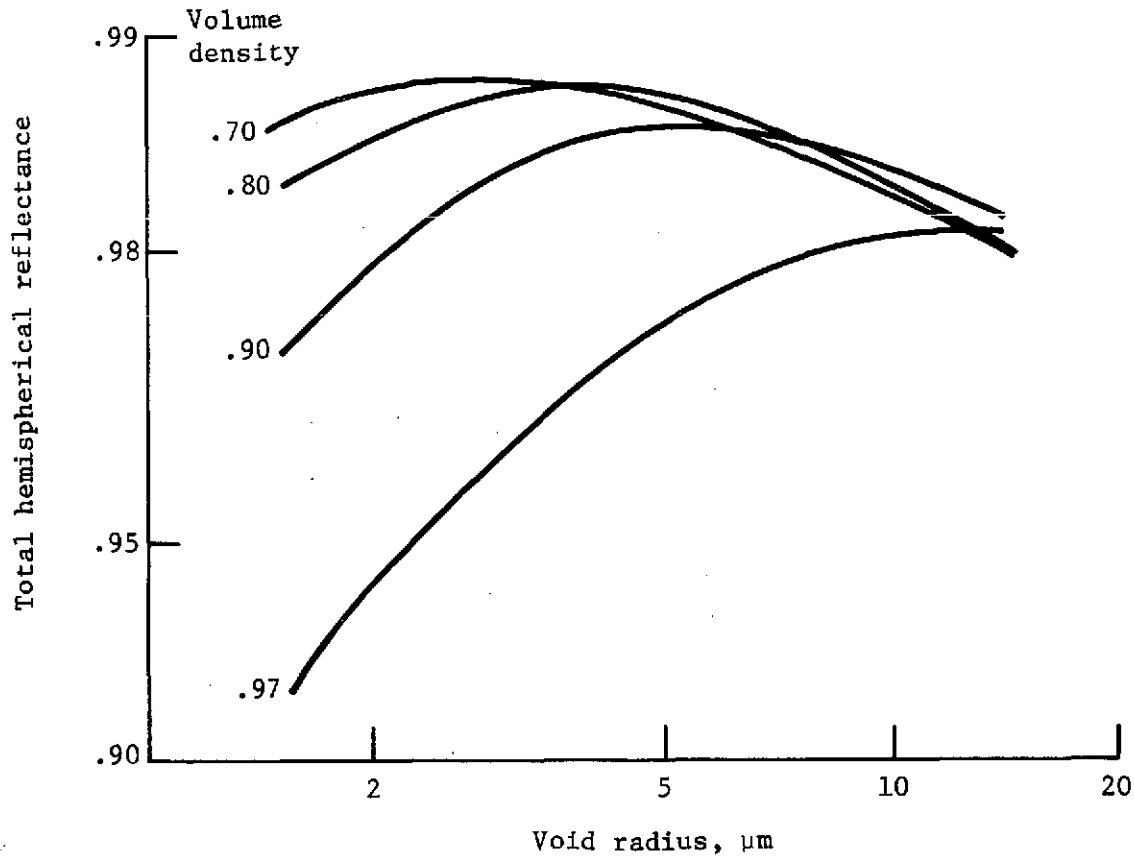

Figure 9.- MSAP predictions of the total hemispherical reflectance as a function of void size and volume density for Type A fused silica at 1773°K, relative to the Saturn entry spectrum of fig. 2

C. Investigation of Thermal Properties

After radiation reflection, thermal conductivity is perhaps the second most important parameter in making up a silica reflecting heat shield. Although the heat capacity of a silica configuration is a linear function of its density, and, therefore, can be easily predicted, estimating its thermal conductivity can be complex. Microstructure, as well as density, plays a significant part in establishing the conductivity of a silica heat shield.

Table 3 contains thermal conductivity data from several sources for silica configurations of varying densities. As is typical in comparing thermal conductivity measurements, some of the data is conflicting. Plotted in figure 10 are selected values of thermal conductivity vs. temperature taken from table 3 for 33%, 91%, and 100% dense fused silica.

TABLE 3.- THERMAL CONDUCTIVITY DATA FOR FUSED SILICA CONFIGURATIONS OF VARIOUS DENSITIES

Temperature, °K	Thermal conductivity, J/m-s-°K
100% dense, 2.20 g/cm^3 (ref. 10)	
273	1.33
300	1.38
350	1.46
400	1.52
450	1.58
500	1.63
600	1.76
700	1.95
800	2.20
900	2.47
1000	2.87
1100	3.36
1200	4.01
1300	4.93
1400	6.16
88% dense, 1.93 g/cm^3 (ref. 13)	
478	0.645
589	0.654
700	0.657
811	0.666
922	0.671
1033	0.690
1144	0.749
1256	0.865
1367	1.04
34% dense, 0.75 g/cm^3 (ref. 13)	
478	0.156
589	0.164
700	0.182
811	0.190
922	0.208
1144	0.259

Temperature, °K	Thermal conductivity, J/m-s-°K
100% dense, 2.20 g/cm^3 (ref. 11)	
367	1.52
589	2.13
811	3.94
367	----
91% dense, 2.00 g/cm^3 (ref. 11)	
367	0.571
589	0.605
811	0.657
1367	0.899
23% dense, 0.50 g/cm^3 (ref. 11)	
367	0.173
589	0.173
811	0.190
1367	0.363
33% dense, 0.72 g/cm^3 (ref. 12)	
422	0.116
533	0.144
700	0.187
811	0.202
978	0.216
1144	0.259
1256	0.303
1367	0.403
37% dense, 0.82 g/cm^3 (ref. 14)	
422	0.116
1367	0.398
20% dense, 0.45 g/cm^3 (ref. 14)	
422	0.144
1367	0.144

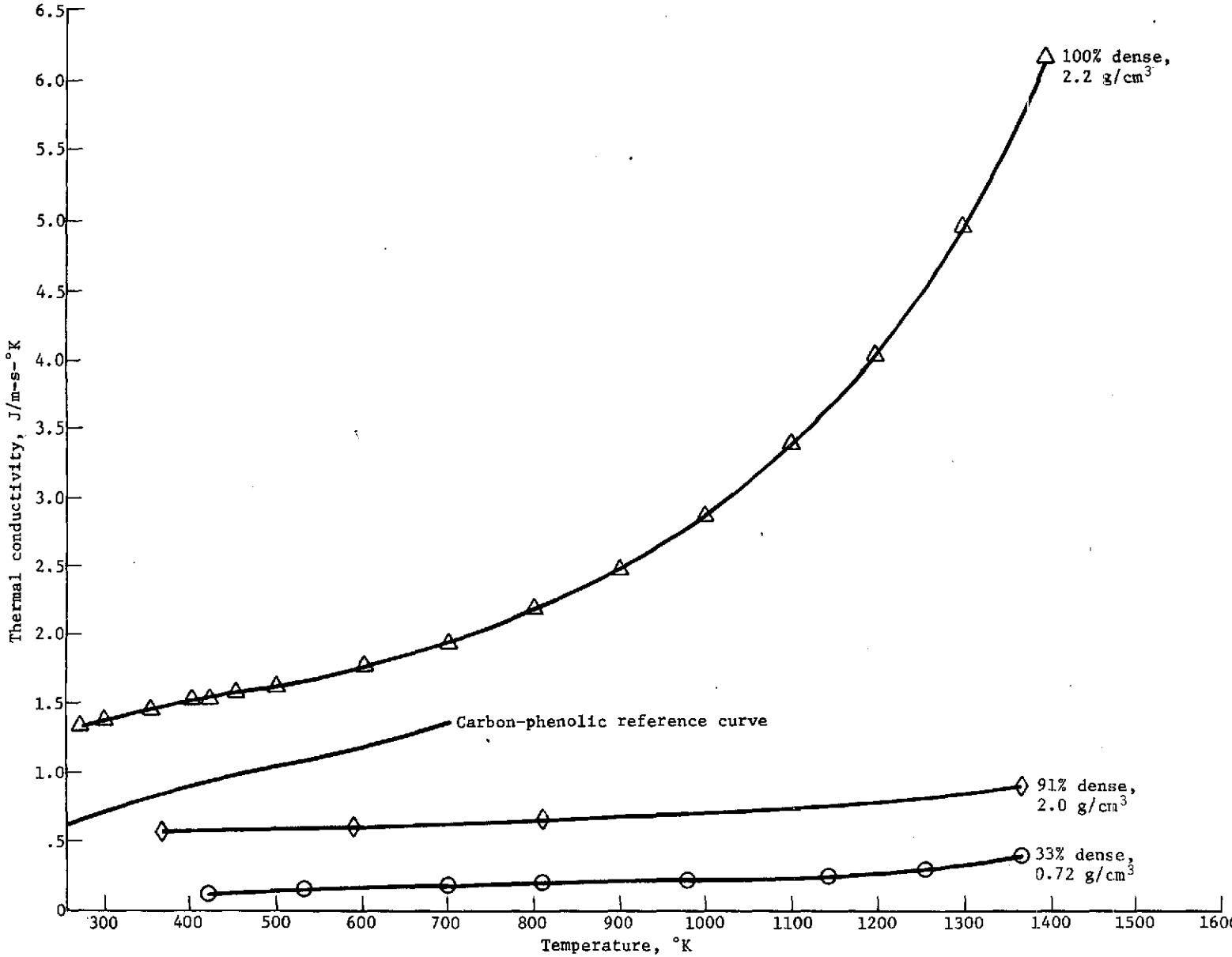

Figure 10.- Selected values of thermal conductivity for fused silica configurations of various densities

It is believed that an appropriate rule of thumb in developing a silica reflecting heat shield is that its thermal conductivity should be at least as low as that of carbon phenolic. Therefore, figure 10 also shows a reference curve of thermal conductivity vs. temperature for carbon phenolic, which was taken from reference 15.

During this contract we investigated various analytical expressions for thermal conductivity as a function of density and microstructure to study in more detail the parameters that influence it.

$$k_r = k_c \left[\frac{1 + 2V_v \left(1 - k_c/k_v\right)/\left(2\, k_c/k_v + 1\right)}{1 - V_v \left(1 - k_c/k_v\right)/\left(k_c/k_v + 1\right)} \right] \tag{1}$$

$$k_r = k_c \left[\frac{V_v^{2/3} + \left(k_c/k_v\right)\left(1 - V_v^{2/3}\right)}{V_v^{2/3} - V_v + \left(k_c/k_v\right)\left(1 - V_v^{2/3} + V_v\right)} \right] \tag{2}$$

$$k_r = k_c \left[\left(1 - P_C\right) + \frac{P_C}{\left(P_L\, k_c/4\sigma e \gamma d \bar{T}^3\right) + \left(1 - P_L\right)} \right] \tag{3}$$

where

d = dimension of void in the direction of heat flow (for spherical voids, this is the diameter)

e = emissivity of the void walls

k_c = thermal conductivity of the continuous phase

k_r = thermal conductivity of the resultant configuration

k_v = thermal conductivity of the void phase

P_C = fraction of a cross-sectional area occupied by voids (cut perpendicular to the direction of heat flow in a plane containing voids)

P_L = fraction of length of a line of heat flow occupied by voids (line passes through voids)

$\bar{T}^3$ = mean of the cube of the absolute temperature of a sample

V_v = volume fraction of voids

γ = a geometrical factor depending on the shape and orientation of voids (0.667 for spherical voids)

σ = Stefan-Boltzmann radiation constant

All three of these equations are presented for a thermal conductance model in which the voids are spherical and homogeneously dispersed throughout a continuous silica phase. Equation (1) was derived by Maxwell and Euken and was obtained from reference 16. Equation (2) was derived by Russell and obtained from reference 17, and equation (3) by Loeb was obtained from reference 18.

Paraphrasing a passage by Kingery in reference 16 gives insight into the role of microstructure and voids on thermal conductivity at high temperatures. If one thinks of the continuous material surrounding the voids in a porous ceramic as radiation shields that diminish the transfer of emitted thermal radiation, then the smaller the void size and the larger the void volume fraction, the more voids or shields there will be across the radiant flux. Thus the radiant transfer will be decreased. At the same time, the higher the emissivity of the continuous phase, then the greater the transfer between void walls and the larger the effective conductivity. The effect of translucency is to lower the efficency of these radiation shields and thereby increase the effective conductivity. This effect also depends on the thickness of the walls, because thinner walls have higher transmission.

Although decreasing the void size (and holding other factors constant) increases the number of radiation shields, it also diminishes the efficiency of each shield, and therefore, does not decrease the conductivity as much as it would if the material were opaque. Therefore, a tradeoff exists, and the net result is that the void size in a highly transparent material has little effect on the thermal transfer of radiant energy and, thus, little effect on the overall thermal conductance.

The significance of equation (3) is that it allows one to look quantitatively at the effects of thermal radiation across voids on the effective conductance. The analytical model of this equation also considers the geometrical aspects of the voids relative to the direction of heat transfer. For purposes of this discussion, consider that the spherical, homogeneously-dispersed voids are observed from a face so that the foremost voids eclipse the ones behind them. Thus, there are tunnels of silica-void-silica alternates and these tunnels are dispersed in a continuous silica matrix. The radiation term in equation (3), $4\sigma e\gamma\, d\bar{T}^3$, probably should be factored by the square of the refractive index in view of some work more recent than Loeb's, for instance, Gardon's (ref. 19), but for this discussion, the assumed model would radiate from the silica wall into the void, and thus the factor, being the square of the refractive index for air, would essentially have a value of one.

To study the thermal conductance effects of void size in a silica reflecting heat shield, we generated curves of conductance vs. temperature using equation (3). These curves are shown in figure 11 for 60%, 80%, and 100% dense fused silica with 5-μm and 500-μm void diameters. The emissivity of silica was obtained from the 1-mm curve of hemispherical emissivity vs. temperature in figure 12, which was taken from reference 19.

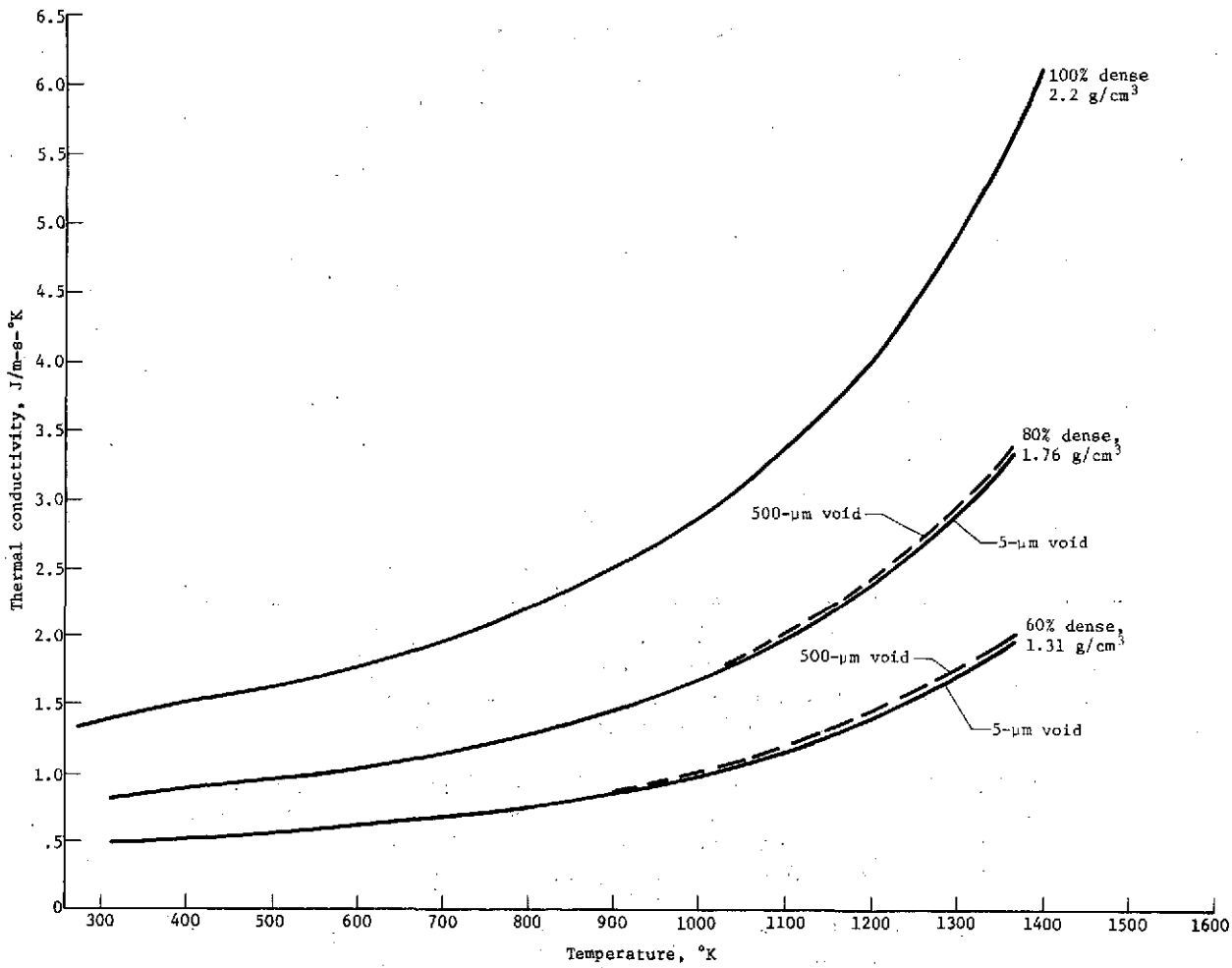

Figure 11.- Analytical prediction of density and void-size effects on the thermal conductivity of fused silica as a function of temperature (based on eq. 3)

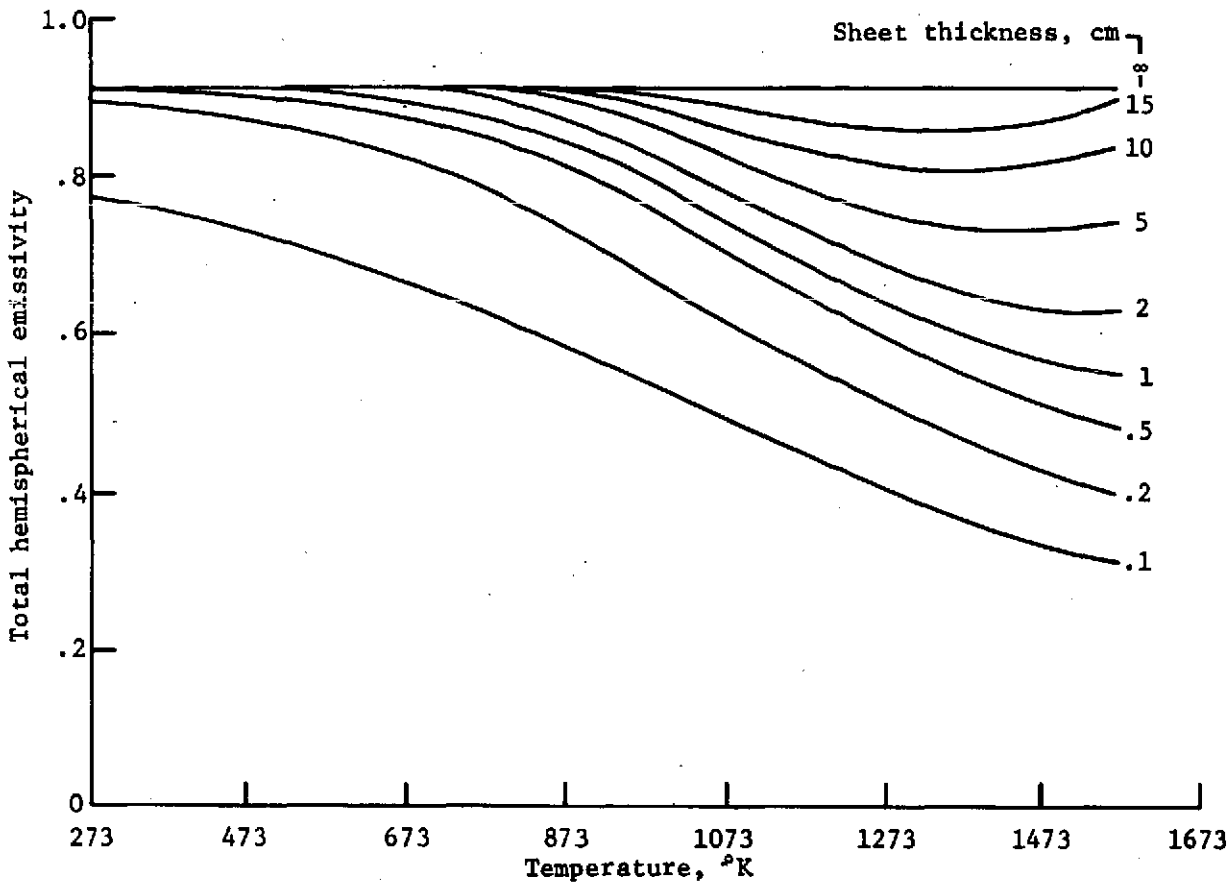

Figure 12.- Total hemispherical emissivity vs. temperature for glass slabs of various thicknesses (ref. 19)

Table 4 gives the values selected from figure 12. These values are conservative in that they assume a 1-mm wall thickness and because the absorption/emission of this alkali-metal-ladened glass would be higher than for high-purity silica.

TABLE 4.- TOTAL HEMISPHERICAL EMISSIVITY vs. TEMPERATURE FOR A 1-mm-THICK GLASS SLAB (determined from fig. 12)

Temperature, °K	Emissivity
311	0.77
367	0.76
478	0.73
589	0.69
700	0.65
811	0.61
922	0.57
1033	0.51
1144	0.46
1256	0.41
1367	0.37

The curves in figure 11 indicate that there is quite a bit of latitude in terms of affecting thermal conductivity by varying void size. There is only a minimal increase in conductivity by going from a 5-μm void to a 500-μm void. Thus, in fabricating slip-cast, foamed-slip, and pressure-sintered silica for a reflecting heat shield, the conductance effect of void sizes up to 500 μm in diameter should not be a large concern.

Although the analytical model for silica used in these calculations is not completely accurate, the above conclusion should remain valid. The true matrix is not entirely continuous because it is constructed of silica particles sintered together essentially at points. The result of this discontinuity is a resistance to heat transfer by true conduction modes. Thus, the curves of measured conductance for silica in figure 10 are lower than those of figure 11.

In addition to enabling a study of void size effects, equation (3) shows that the thermal conductivity of fused silica can be substantially reduced by the introduction of voids.

D. Investigation of Mechanical Properties

The mechanical strength of a silica reflecting heat shield material is related to its microstructure. The microstructure, in turn, is a function of the sintering temperature, pressure, and time, and the initial particle size and distribution. For instance, for a fixed and continuous-particle-size distribution, the modulus of rupture for slip-cast fused silica has been found to vary significantly with the firing conditions. Figure 13 from Fleming (ref. 13) shows that the ultimate strength can vary from 28 to 45 MN/m^2, depending on the firing schedule, for 88%-dense fused silica.

In the sintering process the driving force depends on the magnitude of the surface free energy of the particles, which varies inversely as the particle radii (ref. 16). The surface energy of very small particles is higher than that of large ones. Thus, fine particles disappear and coarser ones grow. Some investigators consider that very small particles have a lower melting point than larger ones (ref. 20). Therefore, the strength of a silica configuration is a complicated function of particle size and distribution, as well as firing conditions.

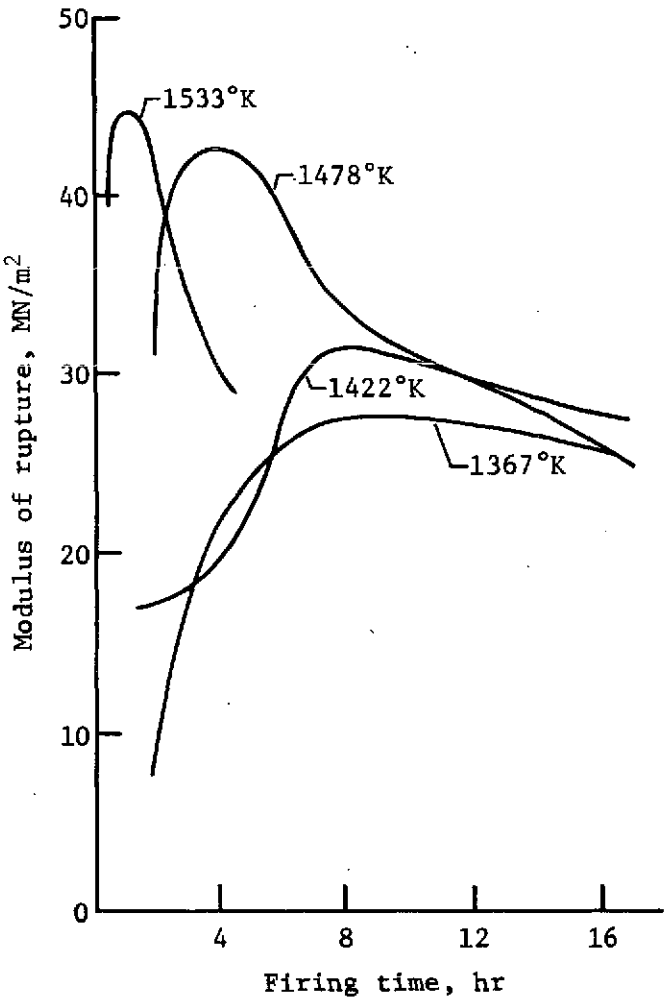

Figure 13.- Room-temperature modulus of rupture for fused silica as a function of firing time at different firing temperatures (ref. 13)

Data are available on the mechanical strength of various fused silica configurations covering a wide range of densities through technical information brochures from such commercial suppliers as Glasrock Products Company, Inc. (Glasrock), and the Fused Silica Products, Refractories and Electronics Division of the Carborundum Company (Silfrax). The modulus of rupture is the most frequently reported parameter, and is determined by methods such as ASTM 674. Table 5 contains data from several sources on the modulus of rupture of fused silica as a function of density. However, little or no information is available from these sources on the void size and general microstructure of the material, or its fabrication procedures.

TABLE 5.- MODULUS OF RUPTURE vs. DENSITY FOR FUSED-SILICA CONFIGURATIONS

% dense	Density, g/cm^3	Modulus of rupture, MN/m^2	Reference
18	0.40	0.52-1.4	12
18-22	0.40-0.48	0.55-1.6	14
23	0.51	1.4	11
33	0.73	0.52-2.1	12
35-39	0.77-0.86	0.55-2.2	14
88	1.9	28-45	13
91	2.0	41	11
100	2.2	69	11

Considerable data on the mechanical properties of fused silica are also available in references 21, 22, and 23. Figures 14 and 15, taken from reference 21, show the modulus of rupture vs. density and the modulus of elasticity vs. density, respectively, for high-purity, slip-cast fused silica.

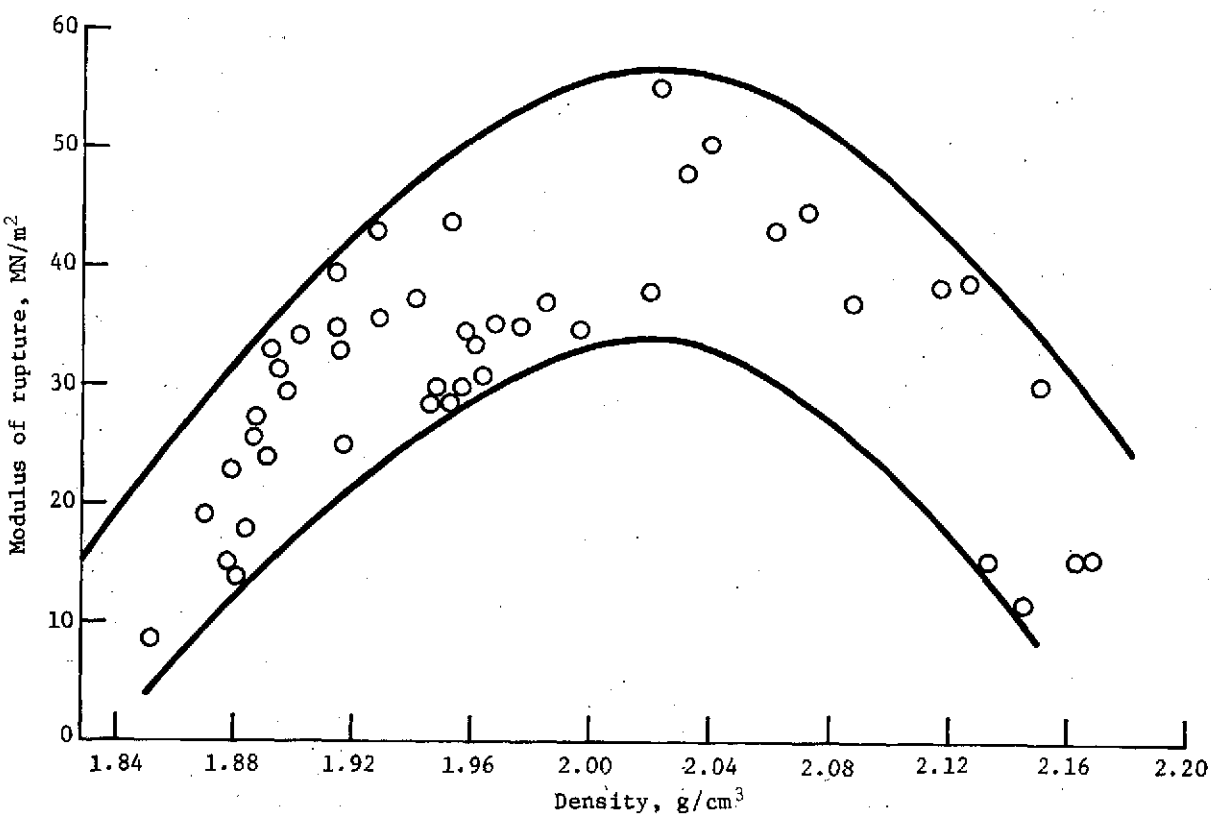

Figure 14.- Modulus of rupture vs. density for high-purity, slip-cast fused silica (ref. 21)

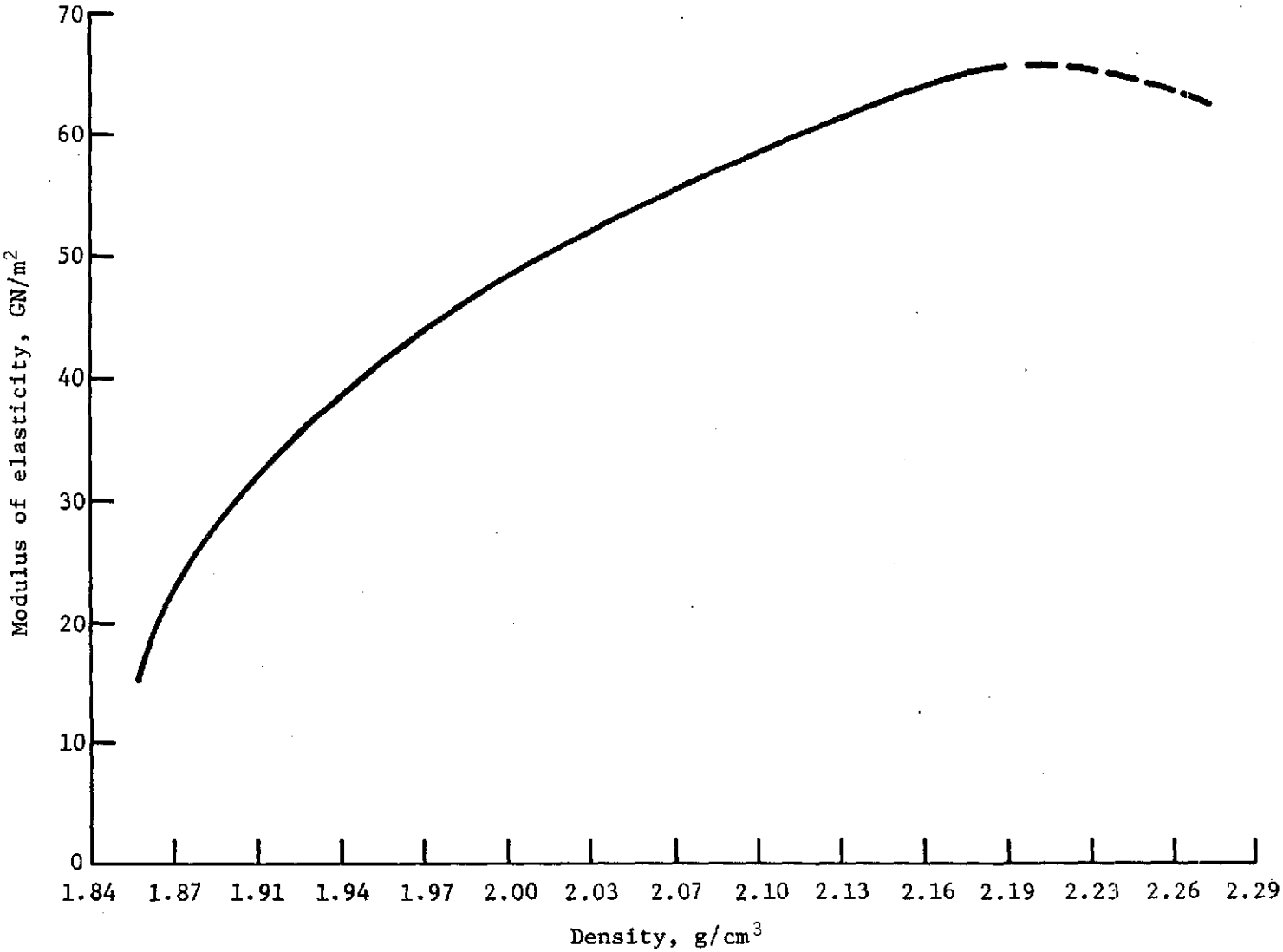

Figure 15.- Modulus of elasticity vs. density for high-purity, slip-cast fused silica (ref. 21)

III. LABORATORY DEVELOPMENT AND FABRICATION

Three types of fused-silica configurations were studied for potential application as reflecting heat shields. These configurations were slip-cast, foamed-slip, and pressure-sintered fused silica. Briefly, in slip casting, a slurry of suspended silica particles in water (i.e., a slip) is poured into a plaster mold, the water is drained away, and a cast part is left for drying and firing. In the foamed-slip method, air bubbles are introduced into the silica slurry and the slip is cast and processed in a similar manner as that for the slip-cast article. The resulting material has a lower density than conventional, slip-cast fused silica. The pressure-sintering process used in this program involved filling a chamber with silica powder, compressing the powder to between 2.1 and 2.8 GN/m^2 (30 000 to 40 000 $lb/in.^2$), and then postfiring the article. Most of the effort of this program pertained to slip-casting, since it became readily apparent that this configuration was the most suitable for use as a fused silica reflecting heat shield.

A. Preparation of Fused Silica Powders

1. Materials.- Two types of fused silica were used on this program. One, designated GE 204, was a high-purity, upgraded natural quartz obtained from General Electric. Table 6 shows typical impurity levels for this material.

TABLE 6.- GE 204 IMPURITIES

Element	Concentration, ppm (GE-supplied data)
Aluminum	26
Calcium	5.0
Iron	3.5
Lithium	<0.5
Magnesium	1.2
Potassium	3.3
Sodium	3.0

The GE 204 material was used for most of the fabrication and testing efforts, and for studying the effects of particle size on reflectance.

The second material was Suprasil, an ultrahigh-purity, synthetic fused silica obtained from Amersil Incorporated. This material is prepared by the vapor-phase hydrolysis of silicon tetrachloride. Table 7 shows typical impurity levels reported for Suprasil.

TABLE 7.- SUPRASIL IMPURITIES

Element	Concentration, ppm (Amersil-supplied data)
Aluminum	0.1
Calcium	0.1
Iron	0.2
Lithium	0.05
Magnesium	0.1
Potassium	0.001
Sodium	0.04

The Suprasil was used to determine the increase in reflectance that could be obtained from an ultrahigh-purity, synthetic fused silica.

2. Comminution of materials.- Two methods were used to reduce the size of the crushed, fused silica materials: ball milling, using an alumina ball mill, and fluid-energy milling. The GE 204 fused silica was comminuted entirely by ball milling with 85% alumina. The crushed material was added to the mill in the ratio of 82 parts of crushed silica to 18 parts of distilled water. Each batch was milled for about 48 hours, until the mean particle diameter (as determined by ASTM Method 152H) was about 8 μm.

The ultrahigh-purity Suprasil material was ball-milled and fluid energy-milled. In fluid-energy milling, the silica particles are allowed to grind themselves, rather than being ground by other materials. This produces a less contaminated powder. As shown in figure 16, the silica particles are carried by opposing, high-velocity air streams and collide and break up, forming smaller particles.

The fluid-energy milling of Suprasil caused some organic contamination by abrading the polyurethane liners of the mill and other polyurethane parts. This problem could be alleviated by using high-purity, slip-cast, fused silica liners and internal parts in the mill. Since such liners were not available, we decided to comminute the Suprasil using a 99% alumina ball mill.

3. Classification of powders.- The silica powder was classified into discrete particle-size ranges via sedimentation in aqueous media, applying Stoke's law. The fused silica slip that remained after ball-milling, which contained about 82% solids, was diluted and allowed to settle for successively longer times to obtain different ranges of particle size.

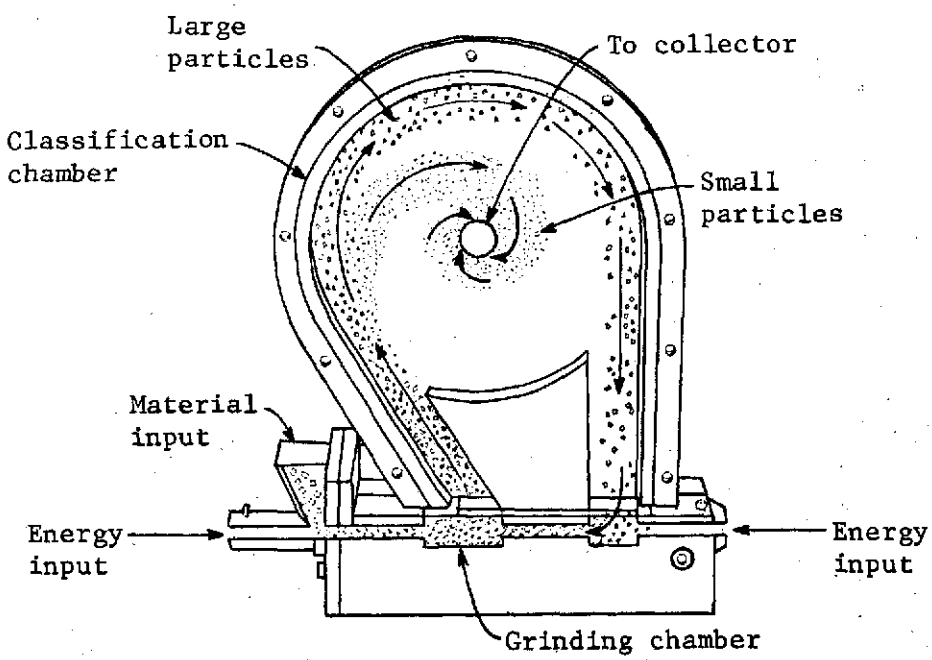

Figure 16.- Fluid-energy mill used to comminute the fused silica particles

Each batch consisted of 800 g of slip (656 g of fused silica solids) diluted with distilled water to a total volume of about 12 300 cm^3. This dilute suspension contained about 5% solids. The settling vessels were polyurethane-lined steel drums with an inner diameter of 28 cm and an inner height of about 34 cm. The diluted 800 g of 82% slip filled the buckets to a height of 20 cm.

The suspension in the first bucket was allowed to settle for 2 minutes, and all the supernatant liquid was decanted to the second bucket. The contents of the second bucket were then allowed to settle for 4 minutes, after which the supernatant liquid was transferred to the next bucket, where it was allowed to settle for 7 minutes, and so on. This process is shown in figure 17. The supernatant liquid was successively settled for 2, 4, 7, 10, 15, 60, 180, and 1440 minutes. The supernatant liquid was discarded after the 1440-minute settling.

After this, the residue in the first bucket (2-minute settling time) was resuspended by filling the bucket with distilled water to a height of 20 cm. The material was then resettled for 2 minutes and the supernatant liquid was successively poured into the remaining buckets, resettling all the residues a second time. After being decanted from the 1440-minute drum, the second batch of supernatant liquid was also discarded.

Figure 17.- Classification of milled, fused silica particles by sedimentation in aqueous media

The residues in each bucket were then transferred to drying dishes by rinsing them from the buckets with distilled water. These drying dishes were placed in a filtered, circulating-air oven and dried at about 340°K. The powders were then kiln-roasted at about 1070°K for 12 hours and transferred to individual storage containers, ready for use in producing the slips.

The results of our particle-size analyses for these classified powders are shown in figure 18. The distribution for the <2 minutes (Particle Size 1) material was not determined because this size was not used for preparing test samples. The distributions for the <180 minute (Particle Size 7) and the <1440 minute (Particle Size 8) material are not shown because the validity of this method is questionable for such small particles, and also because the particles tend to flocculate, giving misleading results. (See the appendix for scanning electron microscope photographs of some of the different particle sizes.)

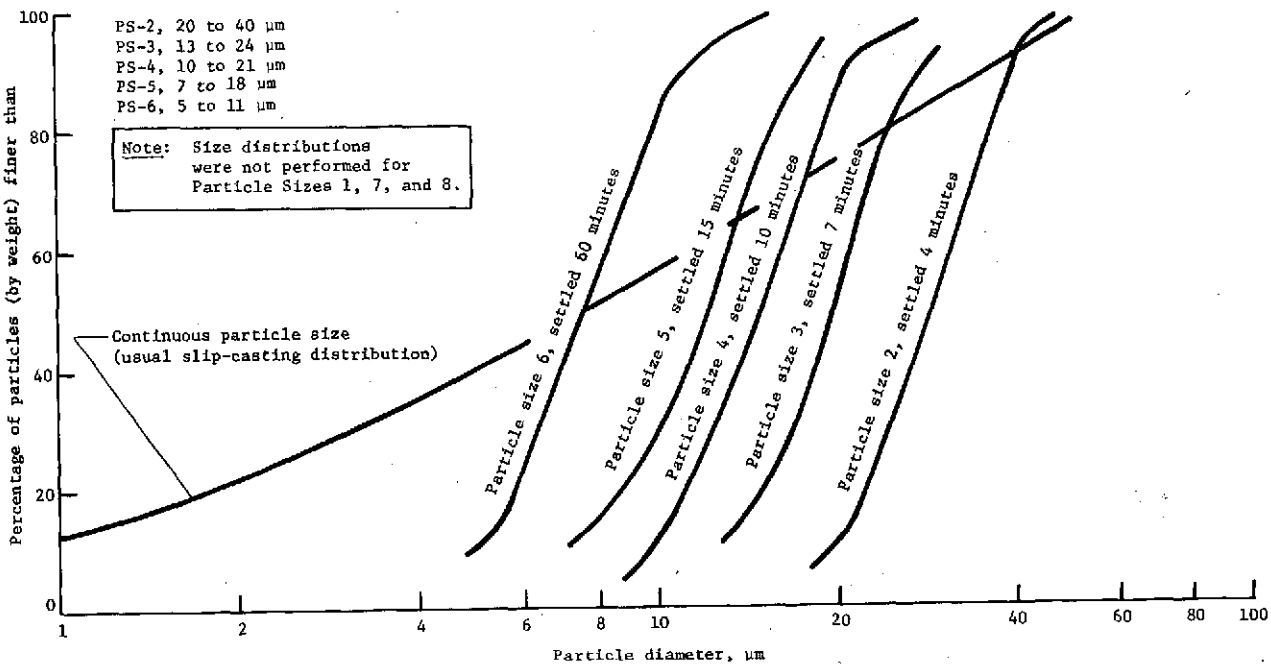

Figure 18.- Size determination for different fused silica particles

B. Preparation of Slip-Cast Configurations

Slip-cast, fused silica configurations were fabricated from GE 204 continuous-particle-size slip and from GE 204 monodisperse particle-size slips that had been prepared from the sedimentation-classified powders. Essentially 10 configurations, made from different-sized powders, were prepared and tested. The configurations are summarized in table 8. The first five configurations listed above were made entirely from one particle size; these are described as "100% monodisperse." The last five configurations were made from blends of two particle sizes; these configurations are described as "75/25% blend."

In addition, a continuous-particle-size slip was cast from the ball-milled Suprasil fused silica and tested.

TABLE 8.- SLIP-CAST FUSED SILICA CONFIGURATIONS MADE FROM DISCRETE PARTICLE SIZES

Configuration number	Primary Component, w/o	Secondary component, w/o	Description
1	Particle size 2, 100%	None	100% monodisperse
2	Particle size 3, 100%	None	100% monodisperse
3	Particle size 4, 100%	None	100% monodisperse
4	Particle size 5, 100%	None	100% monodisperse
5	Particle size 6, 100%	None	100% monodisperse
1B	Particle size 2, 75%	Particle size 6, 25%	75/25% blend
2B	Particle size 3, 75%	Particle size 7, 25%	75/25% blend
3B	Particle size 4, 75%	Particle size 7, 25%	75/25% blend
4B	Particle size 5, 75%	Particle size 8, 25%	75/25% blend
5B	Particle size 6, 75%	Particle size 8, 25%	75/25% blend

1. Plaster mold preparation.- The slip-cast configurations were cast in plaster molds. The plaster was No. 1 Molding Plaster obtained from the U.S. Gypsum Company and was mixed using 60 parts of plaster to 40 parts of water.

Three types of molds were used in preparing the test specimens. The spectrophotometer models were 3.18-cm-diameter discs that were cast using the 3-piece mold shown in figure 19 and machined to different thicknesses. The xenon-arc lamp models for high-intensity-radiation tests were 5.08-cm-diameter discs machined to different thicknesses that were cast using the type of mold shown in figure 20. The flexure models were cut from the 14.0 by 8.26 by 1.27-cm billets cast using the mold shown in figure 21.

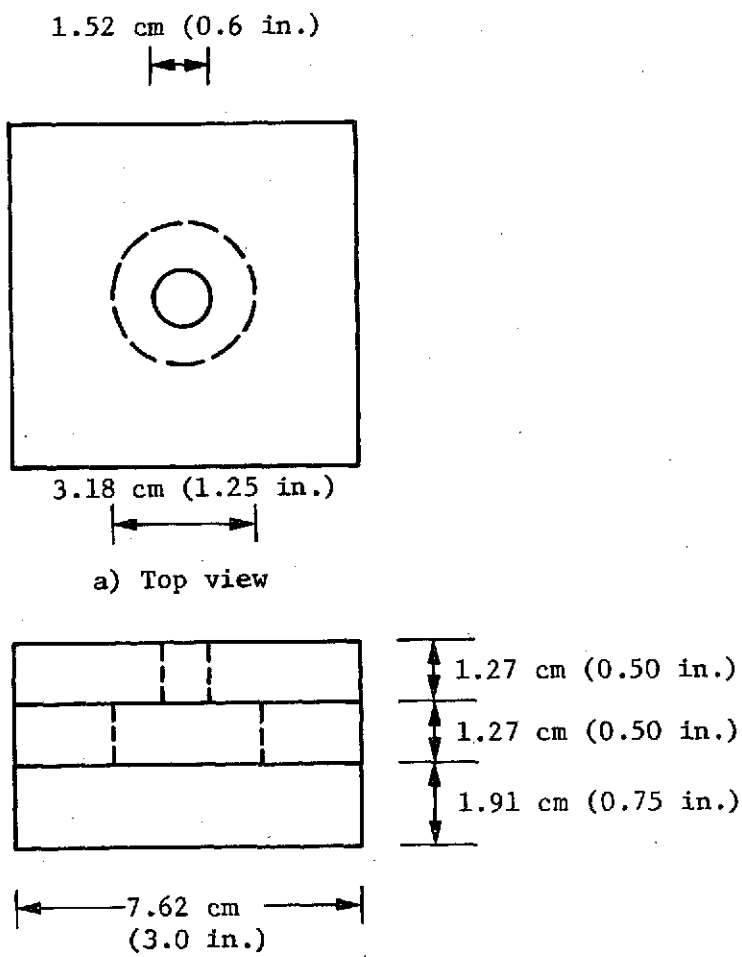

Figure 19.- Plaster mold used to prepare the slip-cast, fused silica models for the spectrophotometer tests

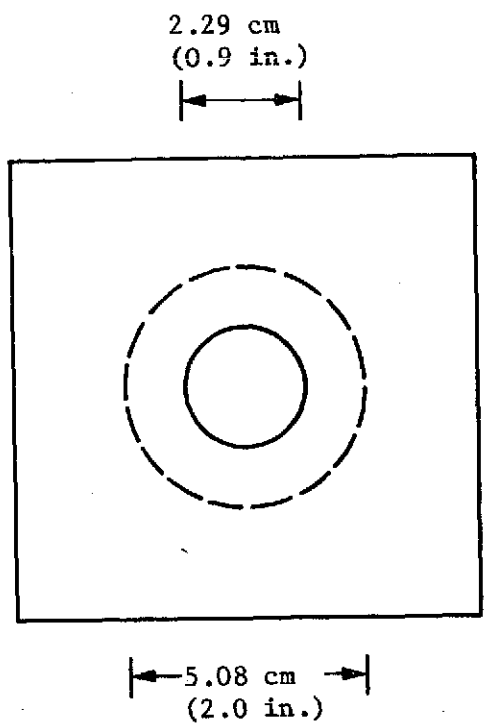

a) Top view

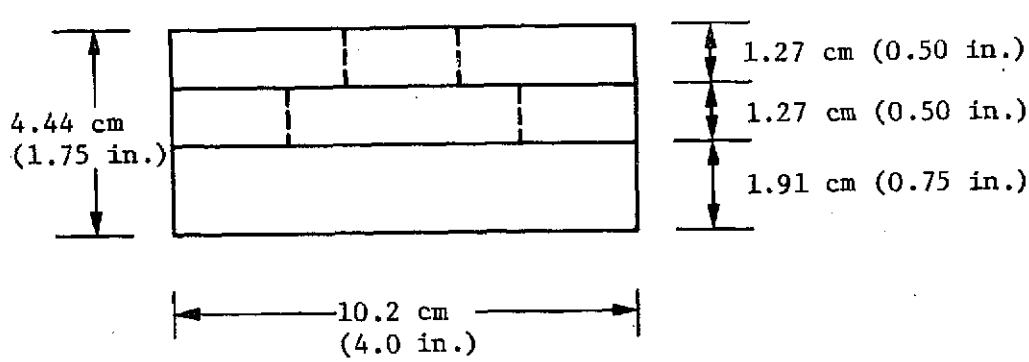

b) Front view

Figure 20.- Plaster mold used to prepare the slip-cast, fused silica models for the xenon arc-lamp tests

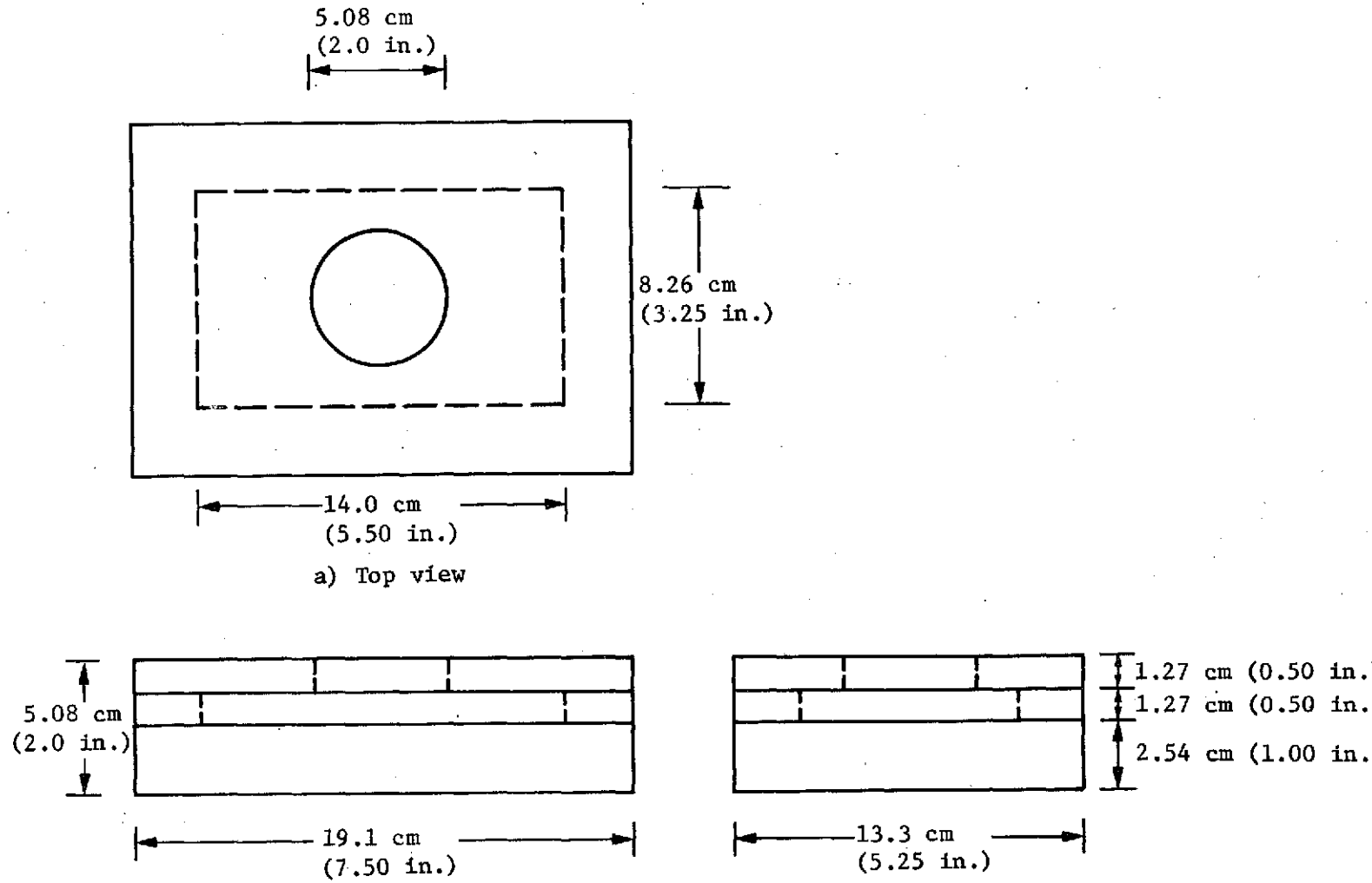

Figure 21.- Plaster mold used to prepare the slip-cast, fused silica billet for the flexure tests

2. Colloidal silica.- Colloidal silica was used in preparing the configurations from the 100% monodisperse and 75/25% blend slips, but was not used to prepare configurations from the continuous-particle-size slip (the latter slip contains essentially colloidal-size particle as a result of ball milling). In the discrete-particle-size slips, the colloidal silica acts as a dispersant, to aid in deflocculating the silica particles, and also as a binder, to strengthen the cast article before firing. Without colloidal silica, the cast articles made from the 100% monodisperse and 75/25% blend slips have almost no green strength. The solids content of the aqueous colloidal silica is typically about 30%.

Most commercially available colloidal silicas are sodium ion-stabilized. Because sodium increases the absorption of fused silica, such sols are undesirable. As a result, we considered the use of an ammonium ion-stabilized colloidal silica called Ludox AS, which is made by DuPont. However, atomic absorption and flame emission analyses on several lots of Ludox AS revealed sodium contamination of about 860 ppm of aqueous colloid. Even though small amounts of colloidal silica are used in preparing the reflecting silica configurations, this amount of sodium contamination was considered too high. We then turned to a low-sodium experimental Ludox AS, whose sodium content is only about 30 ppm of aqueous colloid. Samples of this low-sodium material were obtained from DuPont and used throughout this program.

Table 9 compares our chemical assay results for the regular Ludox AS and the experimental, low-sodium Ludox AS used on this program. Figure 22 shows the amount of sodium introduced in the final slip-cast configuration in terms of the proportion of colloidal silica used to prepare articles from the 100% monodisperse and 75/25% blend slips.

TABLE 9.- LUDOX AS IMPURITIES

Element	Concentration in solids, ppm	
	Regular Ludox AS	Experimental Ludox AS* (low sodium)
Aluminum	--	--
Calcium	<<5.0	<<5.0
Iron	140	37.5
Lithium	<<0.18	<< .18
Magnesium	33	5.0
Potassium	<13	.95
Sodium	2870	88
*Lot 1239-182, solids content = 29.1%		

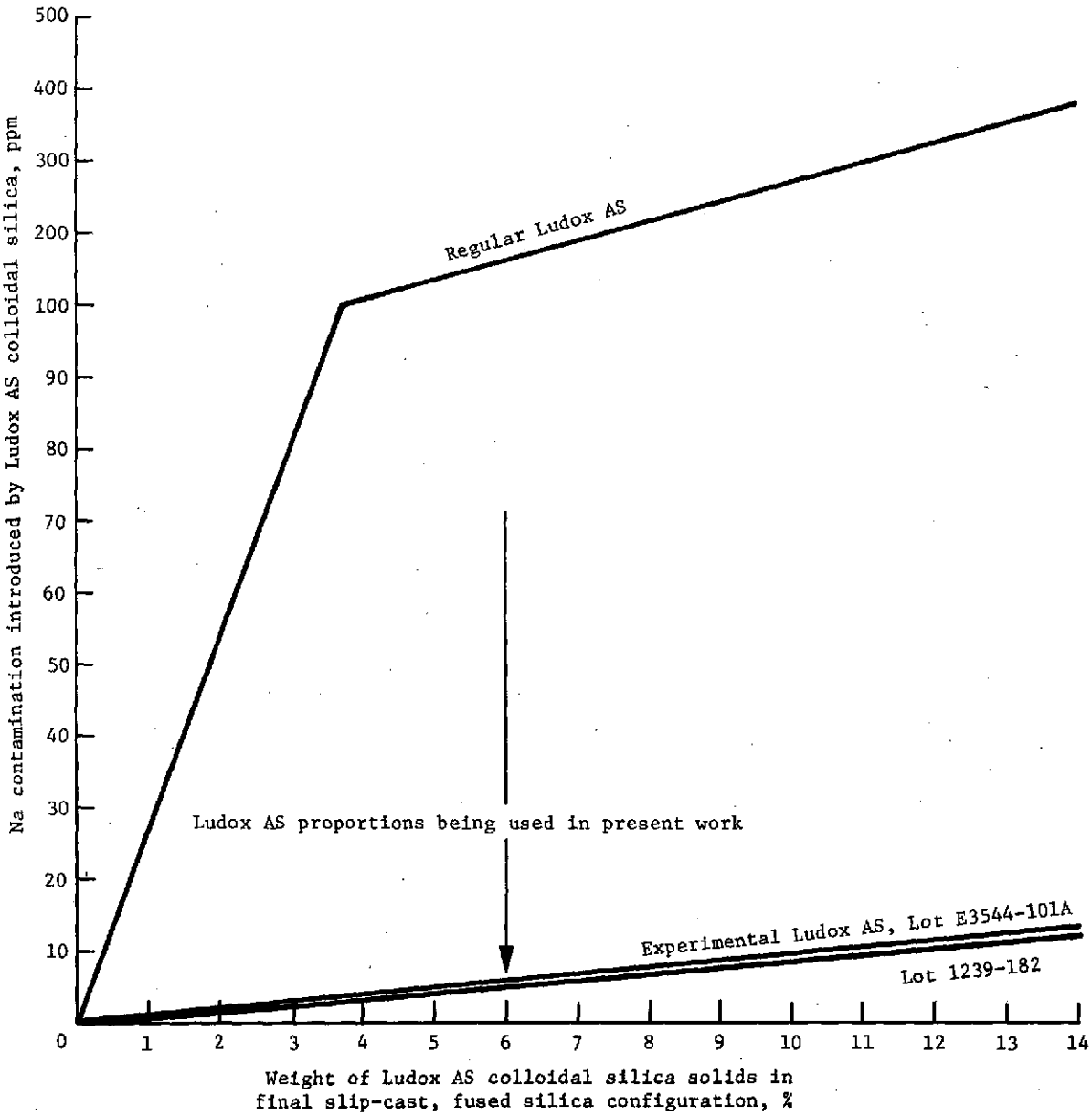

Figure 22.- Sodium contamination introduced by Ludox AS colloidal silicas in slip-cast fused silica

3. Slip preparation.- The continuous-particle-size slips made from GE 204 and Suprasil required essentially no preparation after ball milling. The solids content and pH were checked before the slips were cast, and necessary corrections were made as required. No colloidal silica was added to the continuous-particle-size slips.

In preparing the 100% monodisperse and 75/25% blend slips, the experimental, low-sodium colloidal silica constituted 6% of the total solids. These fused-silica slips could not be stored because particle settling occurs and the degree of mixing required to resuspend the particles changes the particle-size distribution. In addition, with time the colloidal silica begins to gel. Consequently, we prepared only enough slip for immediate casting.

In preparing the 100% monodisperse slips using 6% of colloidal silica solids and 94% of fused silica particles, we achieved a solids content of 72%. (Higher-solids-content slips can be made, but their high viscosity makes them difficult to use.) Distilled water was added to the aqueous colloidal silica and the pH was adjusted to 5.0 using 6N hydrochloric acid. Then the fused silica powder was added gradually until the solids content reached 72%. Adding the powder too rapidly can leave a dry paste.

When all the powder was added, we rolled the slip on a jar mill for 30 minutes to assure thorough mixing. Prolonged rolling produces smaller particles, so rolling should not exceed 30 minutes.

Adjusting the pH to 5.0 reduced the electronic double layer on the colloidal silica and fused silica particles and gradually allows them to cohere.

After being rolled, the slip was placed under a vacuum to remove entrapped air bubbles.

The preparation of the 75/25% blend slips was similar to that for the 100% monodisperse slips. The aqueous colloidal silica, which comprised 6% of the total solids, was mixed with distilled water and the pH was adjusted to 5.0. The fused silica powders were then added gradually to achieve a total solids content of 76%. As in the previous case, a solids content higher than this causes the slip to become too viscous. The slip was then rolled on a jar mill for 30 minutes and subsequently placed under a vacuum.

4. Casting.- The molds for the continuous-particle-size slips, the 100% monodisperse particle-size slips, and the 75/25% blend slips were all prepared for casting in the same way. First, they were dried overnight in a circulating air oven at about 350°K. Then they were disassembled and the inside surfaces were

generously sprayed with a 20% aqueous starch solution. The starch acts as a mold-release agent, allowing the casting to be easily separated from the mold, and allowing the draining away of water from the slip via capillary action.

The continuous-particle-size slips were thoroughly rolled on a jar mill for at least 2 hours before being cast. Afterward, the slip was placed under a vacuum to remove entrapped air, and then poured into the mold, making sure the reservoir was filled. As the water drained away from the slip and the particles compacted, more slip had to be added periodically to keep the mold reservoir full. The number of times that the reservoir needs to be refilled depends on the size of the article being cast. A wet cloth should be placed over the mold between fillings to keep the exposed surface of the slip from drying out.

The length of time required for the slip to drain depends on the size of the cast article, but generally takes longer than 1 hour.

To cast the 100% monodisperse and 75/25% blend slips, we used a slightly different procedure. After placing the slips under a vacuum for about 5 minutes to remove entrapped air, they were stirred slowly in a manner that does not introduce air bubbles, so that any settled particles would be resuspended. After this, the slips were poured into the plaster molds. Pouring has to be done rapidly because the slips drain very quickly, and the mold has to be completely filled before drainage occurs. Depending on the particle size of the 100% monodisperse and 75/25% blend slips, drainage generally takes between 10 and 60 seconds. The larger-particle slips drain more rapidly than the smaller ones.

For the 100% monodisperse and 75/25% blend slips, the mold reservoir generally had to be refilled only once. The degree of compacting for these slips was considerably less than that for the continuous-particle-size slips.

5. Drying and firing.- The amount of drying required depended on the size of the slip-cast article. For casting the 14.0 by 8.26 by 1.27-cm flexure model billets, we let them dry in their molds for about 48 hours at ambient temperature, then removed them from the molds and dried them in a circulating air oven at about 340°K for 24 hours. Finally, they were dried an additional 24 hours in the circulating air oven by gradually raising the temperature to 450°K and maintaining it at that level.

Different firing schedules were used for the continuous slips and for the 100% monodisperse and 75/25% blend slips. For the continuous slips, the firing schedule was 4 hours at 1478°K. For the 100% monodisperse and 75/25% blend slips, the firing schedule varied from 2 hours at 1534°K to 5 hours at 1534°K, depending on the size of particles used in the slips. Larger particles

required longer firing times. (See the appendix for scanning electron microscope photographs of different-sized particles under different firing conditions.)

C. Preparation of Foamed Slip Configuration

In this phase of the program we investigated foamed versions of the slip-cast, fused silica configurations, primarily because they have a significantly lower thermal conductivity than regular slip-cast silicas. The foam was produced using the small, laboratory-size foam generator shown in figure 23.

A surfactant called Arquad 16-50 (Armak Company, Chicago, Ill.), which is a quarternary ammonium salt, was used in conjunction with the low-sodium, experimental, Ludox AS colloidal silica to produce the silica foam. Thirty-three grams of colloidal silica and 0.80 g of Arquad 16-50 were added to the foam generator, mixed, and foamed until the foam reached a height of about 5.0 cm (about half the height of the foam generator cylinder), depending on the density of the foamed slip desired. Then 90 g of fused silica solids, in slip form, were blended in and thoroughly mixed. The foamed slip was then cast, dried, and fired in a similar fashion to the slip-cast configuration described in the previous section.

D. Preparation of Pressure Sintered Configuration

Various compacting methods were investigated during this program, including standard die compacting, hot pressing, and isostatic pressing at room temperature, followed by vacuum firing. The extensive lamination of the test pieces formed by die compacting made this approach appear impractical. Hot-pressing techniques showed considerable merit, but the best results thus far were obtained using isostatic pressing.

The procedures followed in this method include these principal steps:

1. The powder was loaded into a metal tube lined with a thin rubber (Gooch) tubing, and tamped to ensure uniform loading;

2. The Gooch tubing was closed at both ends with rubber stoppers;

3. A hypodermic needle was inserted through one of the rubber stoppers and connected to a vacuum pump to remove entrained gases;

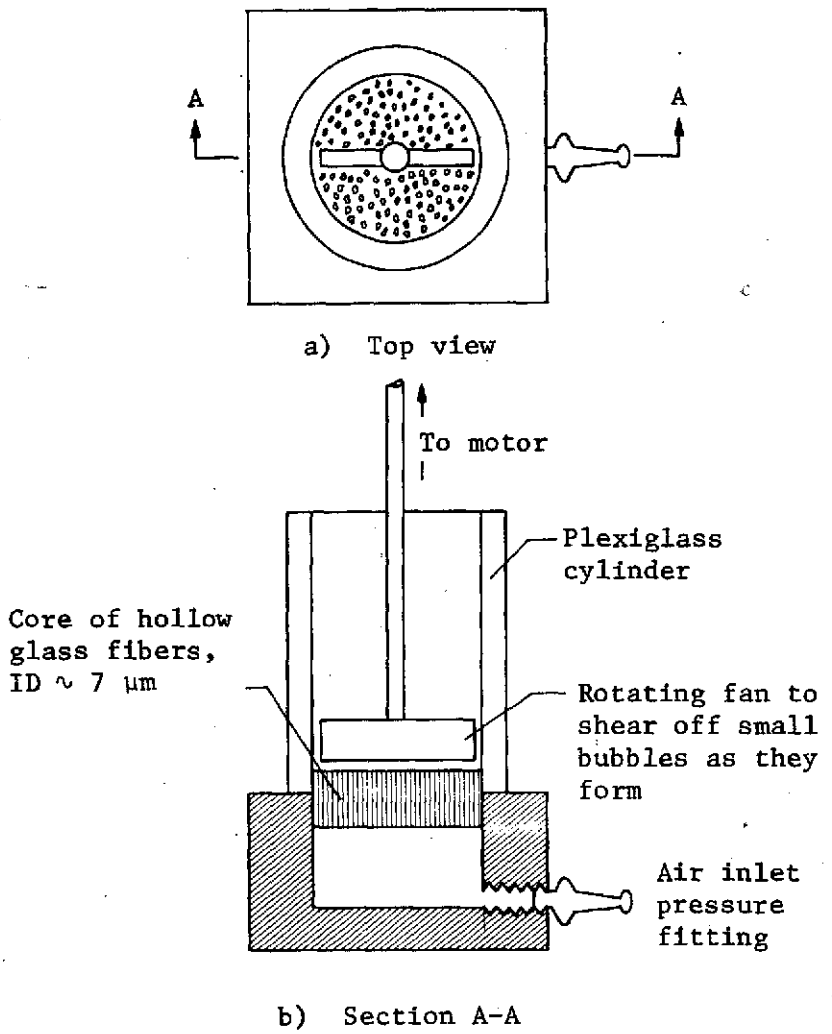

Figure 23.- Foam generator used to prepare the foamed-slip, fused silica configuration

4. The hypodermic needle was removed from the stopper, and the packed Gooch tubing was removed from the metal tube, taking care to avoid flexing the tubing;

5. The Gooch tubing was tied into a wire screen holder and suspended in an oil pressure-transmitting medium;

6. A pressure of 3.2 GN/m^2 (46 000 $lb/in.^2$) was applied to the specimen through the oil bath and the Gooch tubing for 5 minutes;

7. The compacted powders were carefully removed from the Gooch tubing and fired in a vacuum furnace at 10^{-3} N/m^2 and 1448°K to 1473°K for approximately 20 hours.

Figures 24, 25, and 26 show the equipment used to prepare the porous silica specimens from these powders. Figure 24 shows the pressing chamber; figure 25, the control console; and figure 26, the vacuum sintering furnace. The samples prepared in this manner are briefly described in table 10.

TABLE 10.- DESCRIPTION OF POROUS SILICA SPECIMENS

Starting powder	Compacting pressure, GN/m^2 ($lb/in.^2$)	Sintering conditions			Remarks
		Time, hr	Temperature, °K	Vacuum, N/m^2	
2	2.8 (46 000)	20	1333	5.3×10^{-3}	Powdery surface.
4	2.8 (46 000)	18	1438	8.0	
5	2.8 (46 000)	18	1393	6.7	
6	2.8 (46 000)	8	1445		
		16	1333	8.0	
6	2.1 (30 000)	16	1523	8.0	High shrinkage.

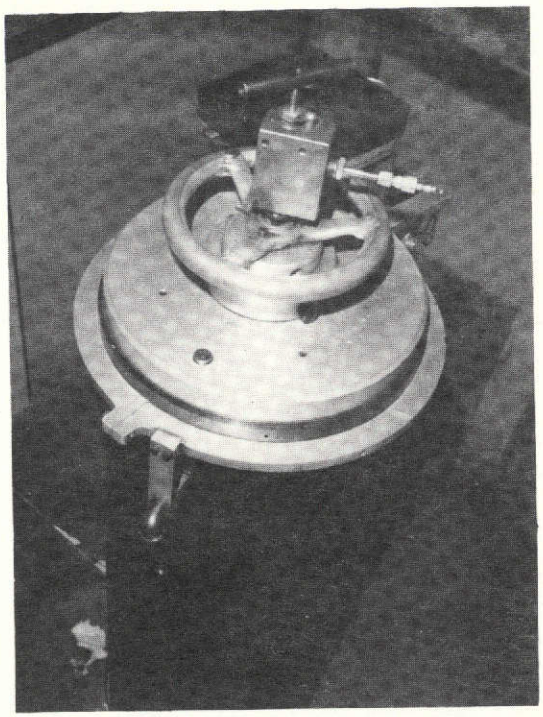

Figure 24.- Chamber of isostatic compacting unit

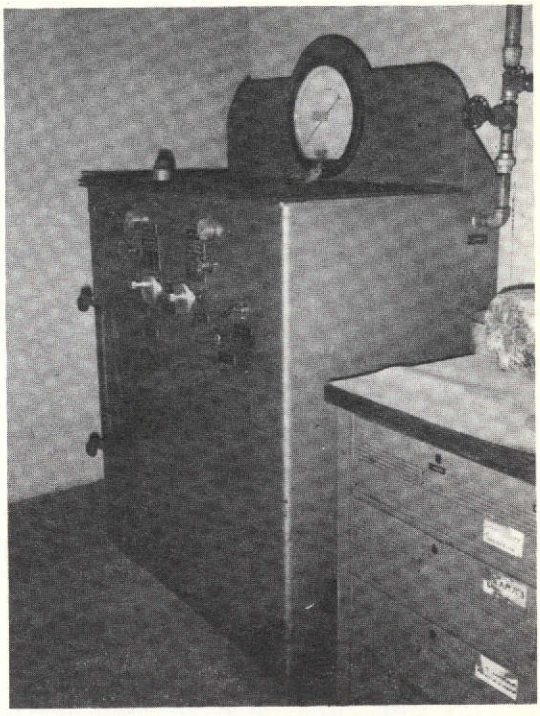

Figure 25.- Control console for isostatic unit

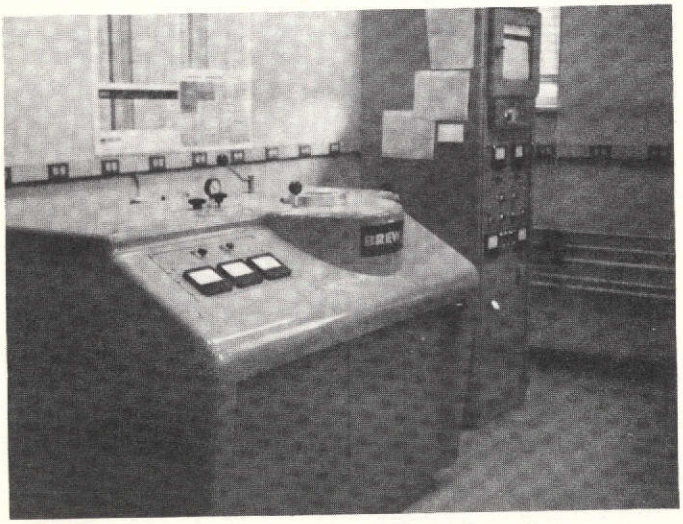

Figure 26.- Vacuum-sintering furnace

IV. LABORATORY EVALUATION TESTING

Test data and results were obtained for the slip-cast, foamed-slip, and pressure-sintered fused silica configurations. The different configurations and samples were primarily evaluated using three types of tests:

1) Spectrophotometer tests using a Beckman DK-2A spectrophotometer with an integrating sphere;

2) Xenon arc-lamp, high-intensity-radiation tests;

3) Flexure tests using four-point loading.

The spectrophotometer tests consisted of measuring the reflectance and transmittance at various wavelengths for sample discs of different thicknesses. The absorptance was calculated via a conservation-of-energy method, in which the sum of the reflectance, transmittance, and absorptance is equal to one. The wavelength ranged from 0.25 to 2.5 μm.

The discs were 3.18 cm (1.25 in.) in diameter and 0.25 cm (0.10 in.), 0.51 cm (0.20 in.), or 0.76 cm (0.30 in.) thick, and the inside of the integrating sphere had a white reference coating of MgO.

For the reflectance measurements the incident beam was 0.26 rad (15 deg) off normal; for the transmittance measurements, the incident beam was normal to the surface.

A Tamarac JP-50 xenon arc lamp was used in the high-intensity-radiation tests to determine the transmittance vs. time and the occurrence of surface melting. Because silica has a high boiling temperature, a high heat of sublimation, and a high reflectivity, the mass loss was insignificant in these tests. This lamp produced the approximate spectral distribution shown in figure 27. The incident radiation on the models ranged from 1100 to 1300 W/cm^2 (970 to 1140 Btu/ft^2-sec) for durations up to about 25 seconds.

The test models were 5.1-cm (2.00-in.) diameter discs with thicknesses of 0.25 cm (0.10 in.), 0.51 cm (0.20 in.), or 0.76 cm (0.30 in.). The models were mounted adjacent to a calormeter and the xenon lamp was operated at full power. A douser, or radiation shield, was raised and lowered to control the radiation exposure for precise time intervals. The radiant flux transmitted through the model to the substrate was measured by a copper-constantan, circular-foil, heat flux gage (Gardon-type calorimeter), and the millivolt-vs-time output was monitored using Bristol recorders.

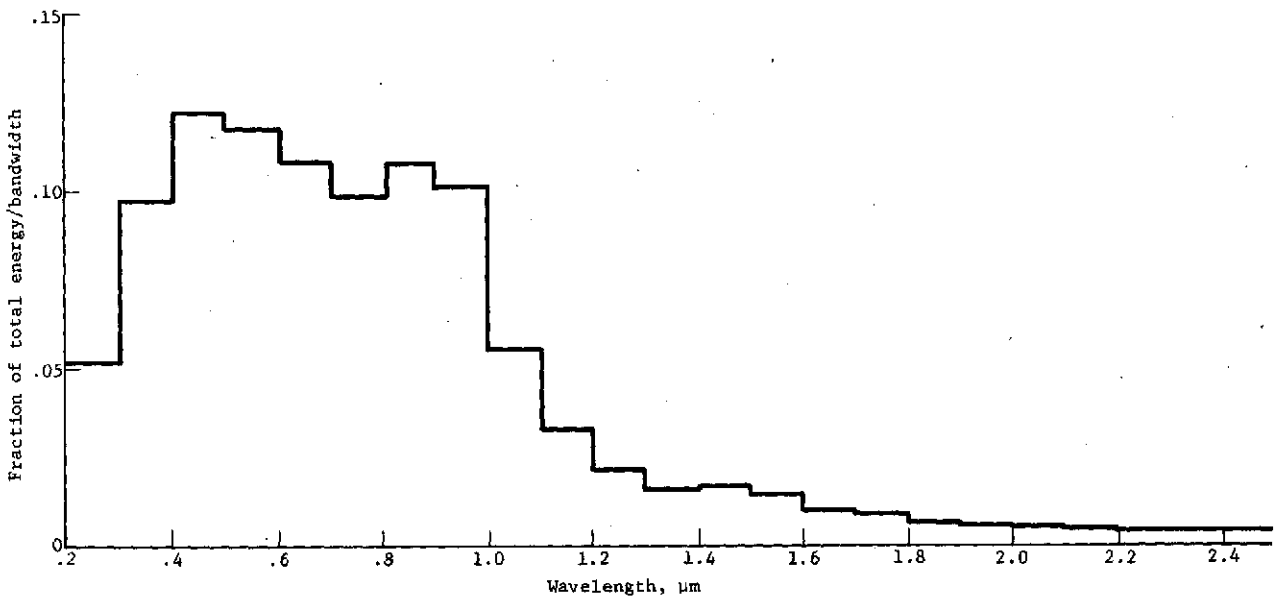

Figure 27.- Approximate spectral distribution for the Tamarac JP-50 high-intensity xenon arc lamp

The models were separated from the face of the calorimeter by a 0.10-cm (0.04-in.) thick, annular stainless steel shim, which had an i. d. of 3.81 cm (1.5 in.) and an o. d. of 5.89 cm (2.32 in.). This allowed the back of the model to be free-standing, which minimized the energy transfer to the calorimeter from thermal conduction.

Transmittance was calculated from

$$T = \frac{1}{I_0}\left[\frac{C \cdot E}{\alpha}\right] \tag{4}$$

where

I_0 = intensity of the radiant energy incident to the calorimeter without the model in place in W/cm^2

E = calorimeter output, in mV

α = absorptivity of the high-emittance black coating applied to the surface of the calorimeter

C = calibration constant for the calorimeter, in W/cm^2-mV;

The flexure tests were used to determine the modulus of rupture and modulus of elasticity. The flexural models were bars approximately 8.3 cm (3.25 in.) long, 1.9 cm (0.75 in.) wide, and 0.76 cm (0.30 in.) thick. These bars were tested as simply-supported beams spanning a distance of 7.15 cm (2.81 in.) with the load points located at the third span.

In addition to the above tests we determined the thermal conductivity for a selected fused silica configuration. The thermal conductivity was measured by the guarded hot plate method. Also, selected samples were examined using a scanning electron microscope to ascertain the degree of packing, degree of sintering, and other microstructural details.

A. Slip-Cast Configuration Testing

As mentioned in Section III, we prepared and tested essentially four types of slip-cast, fused-silica samples: continuous-particle-size GE 204; 100% monodisperse GE 204; 75/25% blend GE 204; and ultrahigh-purity, continuous-particle-size Suprasil.

1. Spectrophotometer tests.

a. Continuous-particle-size GE 204: Several test samples were made from continuous-particle-size GE 204 slips, primarily as a standard for comparing the performance of other slip-cast silica materials. Table 11 gives the reflectance, transmittance, and absorptance vs. wavelength for 0.25-cm (0.10-in.) and 0.51-cm (0.20-in.) thick discs prepared from continuous-particle-size GE 204 slip. As shown in the table, the sample-to-sample variation is very slight. At 0.25 μm, the average reflectance was 62.2%.

Atomic absorption and flame emission analyses made after the spectrophotometer tests showed that these samples contained about 9.2 ppm of sodium, 6.3 ppm of potassium, and less than 0.5 ppm of lithium.

As discussed in Section III, colloidal silica was used to prepare the 100% monodisperse and 75/25% blend configurations, but was not used for the continuous-particle-size configurations. The colloidal silica contains some sodium and thus introduces some contamination into the slip-cast silica material. The proportion used in preparing the 100% monodisperse and 75/25% blend slips introduced about 6 ppm of additional sodium contamination into the slip-cast article.

TABLE 11.- SPECTROPHOTOMETER TEST RESULTS FOR SLIP-CAST MODELS MADE FROM CONTINUOUS-PARTICLE-SIZE GE 204 SLIP*

Wavelength, μm	SNC-62, t = 0.25 cm (0.10 in.)			SNC-63, t = 0.25 cm (0.10 in.)			SNC-58, t = 0.51 cm (0.20 in.)			SNC-59, t = 0.51 cm (0.20 in.)			SNC-60, t = 0.51 cm (0.20 in.)			SNC-61, t = 0.51 cm (0.20 in.)		
	R, %	T, %	A, %	R, %	T, %	A, %	R, %	T, %	A, %	R, %	T, %	A, %	R, %	T, %	A, %	R, %	T, %	A, %
0.25	62.6	0.0	37.4	62.7	0.0	37.3	62.4	0.0	37.6	61.6	0.0	38.4	61.9	0.0	38.1	62.1	0.0	37.9
0.30	70.0	0.0	30.0	70.2	0.0	29.8	70.9	0.0	29.1	71.2	0.0	28.8	70.8	0.0	29.2	70.9	0.0	29.1
0.35	84.4	0.0	15.6	84.4	0.0	15.6	85.0	0.0	15.0	85.5	0.0	14.5	85.4	0.0	14.6	85.4	0.0	14.6
0.40	89.7	0.3	10.0	89.5	0.3	10.2	90.8	0.0	9.2	91.2	0.2	8.6	90.7	0.3	9.0	91.0	0.2	8.8
0.45	91.8	0.8	7.4	91.7	0.7	7.6	92.6	0.1	7.3	93.4	0.2	6.4	92.3	0.3	7.4	92.8	0.3	6.9
0.50	92.9	0.9	6.2	92.8	0.9	6.3	94.0	0.1	5.9	95.2	0.3	4.5	93.9	0.4	5.7	94.3	0.3	5.4
0.60	94.1	1.3	4.6	94.0	1.3	4.7	95.3	0.2	4.5	95.8	0.4	3.8	94.7	0.5	4.8	95.2	0.4	4.4
0.70	96.0	1.7	2.3	95.9	1.8	2.3	96.2	0.8	3.0	96.1	0.6	3.3	96.4	0.7	2.9	96.2	0.6	3.2
0.80	96.0	2.3	1.7	95.9	2.3	1.8	96.3	0.9	2.8	96.2	0.8	3.0	96.5	0.8	2.7	96.3	0.7	3.0
0.90	96.0	2.8	1.2	95.9	2.7	1.4	96.5	1.1	2.4	96.2	1.0	2.8	96.6	1.0	2.4	96.3	1.0	2.7
1.00	95.8	3.1	1.1	95.7	3.0	1.3	96.6	1.4	2.0	96.4	1.2	2.4	96.8	1.2	2.0	96.5	1.3	2.2
1.20	95.3	3.5	1.2	95.0	3.6	1.4	96.2	1.6	2.2	95.9	1.5	2.6	96.3	1.5	2.2	96.1	1.4	2.5
1.40	94.0	3.7	2.3	93.8	3.7	2.5	94.6	1.3	4.1	94.4	1.2	4.4	94.8	1.2	4.0	94.5	1.2	4.3
1.60	94.4	4.7	.9	94.5	4.9	.6	96.1	2.1	1.8	95.9	2.0	2.1	96.3	2.0	1.7	96.1	2.0	1.9
1.80	94.0	5.6	.4	94.0	5.7	.3	95.7	2.6	1.7	95.2	2.4	2.4	96.1	2.1	1.8	95.8	2.4	1.8
1.90	94.0	5.7	.3	93.9	5.7	.4	95.2	2.0	2.8	94.8	2.3	2.9	95.7	2.0	2.3	95.3	2.2	2.5
2.00	93.9	6.3	.2	94.0	6.4	.4	95.5	2.7	1.8	95.2	2.5	2.3	96.0	2.5	1.5	95.6	2.6	1.8
2.10	92.3	6.9	.8	92.2	7.0	.8	93.5	2.1	4.4	92.9	2.3	4.8	93.7	2.0	4.3	93.5	2.2	4.3
2.20	88.0	5.0	7.0	87.9	5.0	7.1	89.8	0.8	9.4	98.1	1.1	.8	94.6	2.0	3.4	94.3	1.4	4.3
2.40	90.2	6.3	3.5	90.3	6.4	3.3	91.3	1.3	7.4	91.0	1.5	7.5	92.1	1.3	6.6	91.5	1.3	7.2
2.50	87.8	5.1	7.1	87.9	5.1	7.0	87.9	0.2	11.9	87.3	0.5	12.2	88.2	0.2	11.6	87.8	0.3	11.9

*R = reflectance, T = transmittance, A = absorptance.

To provide a better comparison with the 100% monodisperse and 75/25% blend configurations, some continuous-particle-size samples were prepared with 6% colloidal silica solids. The effect of this added sodium contamination was very noticeable at near-UV wavelengths, but had little effect at longer wavelengths.

Table 12 shows the spectrophotometer results for the colloidal silica-doped, continuous-particle-size, GE 204 slip-cast models. At 0.25 μm, the reflectance has fallen to about 53.0%, as compared to 63% for samples without colloidal silica.

After the reflectance tests, atomic absorption and flame emission analyses of the colloidal silica-containing models showed that adding the colloidal silica raised the sodium contamination to about 14.5 ppm, as compared to 9.2 ppm for the undoped continuous-particle-size samples.

b. 100% monodisperse GE 204: Five different configurations were studied that used 100% monodisperse slips made from GE 204, with 6% colloidal silica solids. Each of these configurations was made from a different particle-size powder:

Particle size	Diameter, μm
2	20 to 40
3	13 to 24
4	10 to 21
5	7 to 18
6	5 to 11

TABLE 12.- SPECTROPHOTOMETER TEST RESULTS FOR SLIP-CAST MODELS MADE FROM CONTINUOUS-PARTICLE-SIZE GE 204 SLIP WITH 6% COLLOIDAL SILICA SOLIDS*

Wavelength, μm	SNC-68, t = 0.25 cm (0.10 in.)			SNC-69, t = 0.25 cm (0.10 in.)			SNC-64, t = 0.51 cm (0.20 in.)			SNC-65, t = 0.51 cm (0.20 in.)			SNC-66, t = 0.51 cm (0.20 in.)			SNC-67, t = 0.51 cm (0.20 in.)		
	R, %	T, %	A, %	R, %	T, %	A, %	R, %	T, %	A, %	R, %	T, %	A, %	R, %	T, %	A, %	R, %	T, %	A, %
0.25	52.7	0.0	47.3	53.4	0.0	46.6	53.5	0.0	47.8	52.1	0.0	47.9	53.1	0.0	46.9	53.3	0.0	46.7
0.30	64.9	0.0	35.1	65.6	0.0	34.4	64.9	0.0	35.1	64.3	0.0	35.7	66.3	0.0	33.7	65.3	0.0	34.7
0.35	82.0	0.0	18.0	82.3	0.0	17.7	82.2	0.0	17.8	80.1	0.0	19.9	84.0	0.0	16.0	82.1	0.0	17.9
0.40	89.2	0.3	10.8	89.6	0.3	10.1	89.7	0.2	10.1	88.6	0.3	11.1	90.1	0.2	9.7	89.6	0.1	10.3
0.45	91.5	0.7	7.8	92.0	0.8	7.2	92.1	0.5	7.4	91.4	0.3	8.3	92.5	0.3	7.2	92.0	0.1	7.9
0.50	93.7	0.9	5.4	93.8	0.9	5.3	94.3	0.5	5.2	93.9	0.3	5.8	93.5	0.3	6.2	94.3	0.1	5.6
0.60	94.4	1.2	4.4	95.0	1.2	3.8	95.4	0.6	4.0	95.0	0.4	4.6	95.1	0.4	4.5	95.3	0.2	4.5
0.70	96.3	1.8	1.9	95.9	1.7	2.4	96.1	0.5	3.4	95.8	0.5	3.7	96.4	0.7	2.9	96.1	0.7	3.2
0.80	96.3	2.2	1.5	96.1	2.3	1.6	96.2	0.5	3.3	96.0	0.7	3.3	96.3	0.8	2.9	96.3	0.8	2.9
0.90	96.2	2.7	1.1	96.2	2.7	1.1	96.4	1.1	2.5	96.4	1.0	2.6	96.2	1.1	2.7	96.2	1.2	2.6
1.00	95.8	3.1	1.1	95.8	3.0	1.2	96.5	1.3	2.2	96.7	1.2	2.1	96.7	1.4	1.9	96.5	1.3	2.2
1.20	95.4	3.6	1.0	95.5	3.3	1.2	96.4	1.3	2.3	96.3	1.5	2.2	95.9	1.6	2.5	96.2	1.6	2.2
1.40	94.2	3.8	2.0	94.3	3.6	2.1	94.8	1.4	3.8	94.6	1.2	4.2	94.7	1.3	4.0	94.7	1.3	4.0
1.60	94.4	4.9	.7	94.9	4.4	.7	96.6	1.8	1.6	96.2	2.1	1.7	96.0	2.1	1.9	96.4	2.0	1.6
1.80	94.2	5.6	.2	94.2	5.3	.5	95.5	2.0	2.5	95.4	2.6	2.0	95.7	2.5	1.8	95.8	2.5	1.7
1.90	94.0	5.7	.3	94.8	5.7	.5	95.1	1.8	3.1	95.0	2.0	3.0	95.0	2.2	2.8	94.9	2.0	3.1
2.00	94.0	6.3	.3	93.5	6.2	.3	95.3	2.0	2.7	95.3	2.7	2.0	95.8	2.7	1.5	95.2	2.6	2.2
2.10	92.6	7.0	.4	92.7	6.7	.6	93.7	2.3	4.0	93.4	2.3	4.3	93.9	2.2	3.9	93.4	2.0	4.6
2.20	88.2	4.9	6.9	89.2	4.4	6.4	94.4	1.3	4.3	94.3	1.3	4.4	94.4	1.4	4.2	94.1	1.2	4.7
2.40	90.4	6.4	3.2	90.7	6.3	3.0	91.3	1.4	7.3	91.5	1.5	7.0	91.5	1.4	7.1	91.3	1.3	7.4
2.50	88.0	5.0	7.0	88.2	4.9	6.9	87.8	0.5	11.7	88.0	0.5	11.5	87.4	0.3	12.3	88.0	0.3	11.7

*R = reflectance, T = transmittance, A = absorptance.

Spectrophotometer tests were performed on representative samples to measure the reflectance and transmittance of these configurations. The results for Particle Sizes 2 through 6 are given in tables 13 through 17, respectively. These results show that smaller particle sizes produce higher reflectance and lower transmittance than larger particle sizes. The increased reflectance for smaller particles is especially noticeable at shorter wavelengths.

TABLE 13.- SPECTROPHOTOMETER TEST RESULTS FOR SLIP-CAST MODELS MADE FROM GE 204 PARTICLE SIZE 2, 100% MONODISPERSE, WITH 6% COLLOIDAL SILICA SOLIDS*

Wavelength, μm	SN4-1 t = 0.25 cm (0.10 in.)			SN4-16, t = 0.25 cm (0.10 in.)			SN4-50, t = 0.51 cm (0.20 in.)			SN4-15, t = 0.51 cm (0.20 in.)			SN4-13, t = 0.76 cm (0.30 in.)			SN4-51, t = 0.76 cm (0.30 in.)		
	R, %	T, %	A, %	R, %	T, %	A, %	R, %	T, %	A, %	R, %	T, %	A, %	R, %	T, %	A, %	R, %	T, %	A, %
0.25	61.5	0.0	38.5	55.6	0.0	44.4	52.6	0.0	47.4	50.5	0.0	49.5	59.9	0.0	40.1	55.9	0.0	44.1
0.30	75.0	0.6	21.8	66.0	0.0	34.0	69.9	0.0	30.1	67.2	0.0	32.8	75.0	0.1	24.9	73.5	0.0	26.5
0.35	85.1	1.9	13.0	81.7	0.8	17.5	83.2	0.1	16.7	82.1	0.2	17.7	85.4	0.1	13.5	84.7	0.0	15.3
0.40	88.9	2.5	8.6	87.0	2.3	10.7	88.2	0.5	11.3	87.8	0.6	11.6	88.7	0.1	11.2	88.0	0.1	11.9
0.45	90.1	2.7	7.2	89.9	2.9	7.2	90.7	0.7	8.6	90.4	0.8	8.8	90.4	0.2	9.4	90.2	0.1	9.7
0.50	91.7	2.9	5.4	91.2	3.0	5.8	92.2	0.8	7.0	91.7	0.9	7.4	92.3	0.2	7.5	91.7	0.2	8.1
0.60	93.0	3.2	3.8	92.2	3.2	4.6	93.7	1.0	5.3	93.4	1.1	5.5	93.7	0.3	6.0	93.1	0.2	6.7
0.70	95.0	3.2	1.8	94.2	3.2	2.6	95.3	1.1	3.6	95.1	1.2	3.7	95.2	0.5	4.3	95.0	0.4	4.6
0.80	95.3	3.6	1.1	94.5	3.6	1.9	95.6	1.5	2.9	95.3	1.8	2.9	95.9	0.9	3.2	95.2	0.9	3.9
0.90	95.2	3.8	1.0	94.3	3.8	1.9	95.9	1.6	2.5	95.6	1.8	2.6	96.1	1.0	2.9	95.4	1.0	3.6
1.00	95.3	3.8	.9	94.5	3.9	1.6	95.9	1.6	2.5	95.7	1.8	2.5	96.2	1.0	2.8	95.5	1.0	3.5
1.20	95.2	3.8	1.0	94.7	3.9	1.4	95.8	1.6	2.6	95.5	1.8	2.7	96.0	0.9	3.1	95.4	0.9	3.7
1.40	95.2	3.8	1.0	94.7	3.9	1.4	95.6	1.6	2.8	95.5	1.8	2.7	95.9	1.0	3.1	95.4	1.0	3.6
1.60	95.6	4.1	.3	94.9	4.2	.9	96.0	1.8	2.2	96.1	1.9	2.0	96.3	1.1	2.6	95.7	1.0	3.3
1.80	95.8	4.0	.2	95.4	4.2	.4	96.4	1.7	1.9	96.2	1.9	1.9	96.6	1.0	2.4	96.0	1.0	3.0
1.90	95.8	3.9	.3	95.8	3.8	.4	96.7	1.7	1.6	96.5	1.7	1.8	96.5	0.8	2.7	96.3	0.8	2.9
2.00	95.8	3.9	.3	95.7	3.8	.5	96.6	1.3	2.1	96.5	1.6	1.9	96.5	0.7	2.8	96.3	0.7	3.0
2.10	95.5	2.5	2.0	95.0	3.3	1.7	95.7	0.9	3.4	95.5	1.1	3.4	95.3	0.1	4.6	95.4	0.1	4.5
2.20	95.1	2.5	2.4	94.8	2.6	2.6	94.7	0.1	5.2	94.7	0.3	5.0	94.5	0.1	5.4	94.8	0.1	5.1
2.40	96.0	2.4	1.6	95.4	2.0	2.6	95.4	0.0	4.6	95.4	0.1	4.5	94.6	0.1	5.3	95.4	0.1	4.5
2.50	95.2	0.3	4.5	94.6	0.1	5.3	95.1	0.0	4.9	94.8	0.1	5.1	94.6	0.1	5.3	94.9	0.0	5.1

*R = reflectance, T = transmittance, A = absorptance.

TABLE 14.- SPECTROPHOTOMETER TEST RESULTS FOR SLIP-CAST MODELS MADE FROM GE 204 PARTICLE SIZE 3, 100% MONODISPERSE, WITH 6% COLLOIDAL SILICA SOLIDS*

Wavelength, μm	SN7-20, t = 0.25 cm (0.10 in.)			SN7-18, t = 0.51 cm (0.20 in.)			SN7-17, t = 0.51 cm (0.20 in.)			SN7-19, t = 0.76 cm (0.30 in.)		
	R, %	T, %	A, %	R, %	T, %	A, %	R, %	T, %	A, %	R, %	T, %	A, %
0.25	63.8	0.0	36.2	63.2	0.0	36.8	65.3	0.0	34.7	62.9	0.0	37.1
0.30	73.2	0.0	26.8	71.1	0.0	28.9	77.8	0.0	22.2	72.8	0.0	27.2
0.35	86.6	0.4	13.0	85.1	0.0	14.9	86.6	0.0	13.4	85.4	0.0	14.6
0.40	90.0	1.5	8.5	89.7	0.5	9.8	90.3	0.5	9.2	90.1	0.2	9.7
0.45	91.8	1.7	6.5	92.2	0.6	7.2	91.9	0.6	7.5	92.0	0.3	7.7
0.50	93.2	1.8	5.0	93.6	0.8	5.6	93.7	0.8	5.5	93.8	0.4	5.8
0.60	94.3	2.0	3.7	94.5	1.0	5.5	95.3	1.0	3.7	94.5	0.4	5.1
0.70	96.0	2.1	1.9	96.2	1.0	4.5	96.6	1.0	2.4	96.4	0.4	3.2
0.80	96.1	2.4	1.5	96.6	1.3	2.1	96.6	1.2	2.2	96.6	0.7	2.7
0.90	96.3	2.6	1.1	96.6	1.5	1.9	96.7	1.4	1.9	96.6	0.8	2.6
1.00	96.2	2.7	1.1	96.6	1.5	1.9	96.8	1.5	1.7	97.3	0.9	1.8
1.20	96.1	2.7	1.2	96.3	1.5	2.2	96.6	1.5	1.9	96.6	0.9	2.5
1.40	96.2	2.7	1.1	96.3	1.5	2.2	96.6	1.4	2.0	96.3	0.8	2.9
1.60	96.6	2.8	.6	97.0	1.6	1.4	97.0	1.5	1.5	96.9	1.0	2.1
1.80	96.9	2.8	.3	97.0	1.5	1.5	97.3	1.5	1.2	96.8	0.9	2.3
1.90	97.4	2.9	.3	97.0	1.3	1.7	97.4	1.4	1.2	96.7	0.6	2.7
2.00	97.3	2.6	.1	96.8	1.3	1.9	97.2	1.2	1.6	96.5	0.5	3.0
2.10	96.6	2.3	1.1	95.8	0.8	3.4	96.2	0.8	3.0	95.3	0.1	4.6
2.20	96.4	1.5	2.1	94.9	0.2	4.9	95.4	0.2	4.4	94.2	0.1	5.7
2.40	97.0	1.1	1.9	95.8	0.2	4.0	96.1	0.1	3.8	94.2	0.1	5.7
2.50	96.7	0.3	3.0	95.8	0.2	4.0	96.1	0.1	3.8	94.2	0.1	5.7

*R = reflectance, T = transmittance, A = absorptance.

TABLE 15.- SPECTROPHOTOMETER TEST RESULTS FOR SLIP-CAST MODELS MADE FROM GE 204 PARTICLE SIZE 4, 100% MONODISPERSE, WITH 6% COLLOIDAL SILICA SOLIDS*

Wavelength, μm	SN10-24, t = 0.25 cm (0.10 in.)			SN10-53 t = 0.25 cm (0.10 in.)			SN10-52, t = 0.51 cm (0.20 in.)			SN10-22, t = 0.51 cm (0.20 in.)			SN10-21, t = 0.76 cm (0.30 in.)			SN10-54, t = 0.76 cm (0.30 in.)		
	R, %	T, %	A, %	R, %	T, %	A, %	R, %	T, %	A, %	R, %	T, %	A, %	R, %	T, %	A, %	R, %	T, %	A, %
0.25	64.1	0.0	35.9	66.2	0.0	33.8	67.4	0.0	32.6	62.8	0.0	37.2	62.3	0.0	37.7	67.2	0.0	32.8
0.30	76.3	0.0	23.7	75.1	0.0	24.9	76.3	0.1	23.6	75.1	0.0	24.9	73.7	0.1	26.2	75.9	0.0	24.1
0.35	85.5	0.3	14.2	86.0	0.2	13.8	86.2	0.1	13.7	85.9	0.0	14.1	86.1	0.1	13.8	88.1	0.0	11.9
0.40	89.2	1.1	9.7	89.1	1.0	9.9	90.1	0.2	9.7	90.2	0.2	9.6	90.4	0.1	9.5	90.0	0.1	9.9
0.45	91.2	1.2	7.6	91.2	1.1	7.7	92.5	0.2	7.3	92.0	0.4	7.6	92.3	0.1	7.6	91.9	0.1	8.0
0.50	92.8	1.2	6.0	92.7	1.1	6.2	93.8	0.3	5.9	93.5	0.4	6.1	93.9	0.1	6.0	93.4	0.1	6.5
0.60	93.9	1.3	4.8	94.0	1.2	4.8	94.7	0.4	4.9	95.0	0.5	4.5	94.8	0.1	5.1	94.5	0.1	5.4
0.70	95.2	1.3	3.5	95.7	1.3	3.0	96.6	0.4	3.0	96.2	0.7	3.1	96.6	0.2	3.2	96.3	0.1	3.6
0.80	95.5	1.8	2.7	96.2	1.6	2.2	96.7	0.8	2.5	96.7	0.9	2.4	96.7	0.3	3.0	96.5	0.2	3.3
0.90	95.6	1.9	2.5	96.2	1.7	2.1	96.9	0.9	2.2	96.7	0.9	2.4	96.7	0.4	2.9	96.6	0.4	3.0
1.00	94.7	2.0	3.3	96.2	1.8	2.0	96.8	0.9	2.3	96.9	0.9	2.2	96.9	0.4	2.7	96.5	0.4	3.1
1.20	95.7	1.9	2.4	96.2	1.8	2.0	96.6	0.9	2.5	96.7	0.9	2.4	96.5	0.4	3.1	96.5	0.4	3.1
1.40	95.8	1.9	2.3	96.2	1.8	2.0	96.8	0.9	2.3	96.5	0.9	2.6	96.4	0.4	3.2	96.4	0.4	3.2
1.60	96.1	2.1	1.8	96.4	2.0	1.6	97.2	0.8	2.0	97.0	1.0	2.0	96.8	0.5	2.7	96.7	0.4	2.9
1.80	96.4	2.1	1.5	96.7	2.0	1.3	97.4	0.7	1.9	97.2	0.8	2.0	96.8	0.3	2.9	97.0	0.3	2.7
1.90	97.0	2.0	1.6	96.7	2.0	1.3	97.4	0.7	1.9	97.2	0.8	2.0	96.7	0.2	3.1	97.0	0.2	2.8
2.00	96.7	1.7	1.6	96.7	1.7	1.6	97.4	0.5	2.1	97.0	0.6	2.4	96.5	0.1	3.4	96.8	0.1	3.1
2.10	96.1	1.4	2.5	96.1	1.3	2.6	96.5	0.1	3.4	95.9	0.3	3.8	95.5	0.1	4.4	95.9	0.1	4.1
2.20	95.5	0.8	3.7	95.7	0.7	3.6	95.9	0.1	3.4	95.1	0.0	4.9	94.5	0.1	5.4	95.4	0.0	4.6
2.40	96.8	0.1	3.1	96.1	0.2	3.7	96.1	0.1	3.8	95.5	0.0	4.5	94.9	0.1	5.0	95.7	0.0	4.3
2.50	95.9	0.1	4.0	95.9	0.1	4.0	95.9	0.1	4.0	95.2	0.0	4.8	94.9	0.1	5.0	95.5	0.0	4.5

*R = reflectance, T = transmittance, A = absorptance.

TABLE 16.- SPECTROPHOTOMETER TEST RESULTS FOR SLIP-CAST MODELS MADE FROM GE 204 PARTICLE SIZE 5, 100% MONODISPERSE, WITH 6% COLLOIDAL SILICA SOLIDS*

Wavelength, μm	SN15-25, t = 0.25 cm (0.10 in.)			SN15-27, t = 0.51 cm (0.20 in.)			SN15-55, t = 0.51 cm (0.20 in.)			SN15-26, t = 0.76 cm (0.30 in.)		
	R, %	T, %	A, %	R, %	T, %	A, %	R, %	T, %	A, %	R, %	T, %	A, %
0.25	69.0	0.0	31.0	69.6	0.0	30.4	69.3	0.0	30.7	69.7	0.0	30.3
0.30	77.8	0.0	22.2	79.3	0.0	20.7	79.2	0.0	20.8	78.9	0.0	21.1
0.35	87.6	0.0	12.4	87.8	0.0	12.2	88.5	0.0	11.5	86.9	0.0	13.1
0.40	91.0	0.1	8.9	90.8	0.2	9.2	90.7	0.1	9.2	90.4	0.0	9.6
0.45	92.3	1.1	6.6	92.6	0.3	7.1	92.6	0.2	7.2	92.5	0.0	7.5
0.50	94.1	1.2	4.7	94.1	0.4	5.5	93.9	0.3	5.8	93.9	0.0	6.1
0.60	95.0	1.3	3.7	95.4	0.4	4.2	95.1	0.4	4.5	95.3	0.0	4.7
0.70	96.7	1.4	1.9	96.8	0.4	2.8	96.7	0.4	2.9	96.6	0.1	3.3
0.80	96.9	1.7	1.4	97.0	0.8	2.2	96.8	0.7	2.5	96.9	0.4	2.7
0.90	96.8	1.8	1.4	97.1	1.0	1.9	97.0	0.9	2.1	97.2	0.5	2.3
1.00	96.9	1.9	1.2	97.2	1.0	1.8	97.1	0.9	2.0	97.1	0.5	2.4
1.20	96.8	1.9	1.3	97.0	1.0	2.0	97.0	0.9	2.1	96.8	0.5	2.7
1.40	96.8	1.9	1.3	96.6	1.0	2.4	96.8	0.9	2.3	96.8	0.4	2.8
1.60	97.3	2.1	.6	97.0	1.0	2.0	97.1	0.9	2.0	97.2	0.5	2.3
1.80	97.5	2.1	.4	97.2	1.0	1.8	97.3	0.9	1.8	97.1	0.4	2.5
1.90	97.7	1.9	.4	97.3	0.9	1.8	97.3	0.8	1.9	97.0	0.2	2.8
2.00	97.6	1.8	.6	97.2	0.6	2.2	97.2	0.6	2.2	96.8	0.1	3.1
2.10	96.9	1.5	1.6	96.3	0.3	3.4	96.3	0.3	3.4	95.9	0.0	4.1
2.20	96.7	0.8	2.5	95.7	0.3	4.0	95.7	0.3	4.0	95.1	0.0	4.9
2.40	96.8	0.4	2.8	95.9	0.2	3.9	96.0	0.2	3.8	95.3	0.0	4.7
2.50	96.6	0.2	3.2	95.8	0.2	4.0	95.8	0.2	4.0	95.1	0.0	4.9

*R = reflectance, T = transmittance, A = Absorptance.

TABLE 17.- SPECTROPHOTOMETER TEST RESULTS FOR SLIP-CAST MODELS MADE FROM PARTICLE SIZE 6, 100% MONODISPERSE, WITH 6% COLLOIDAL SILICA SOLIDS*

Wavelength, μm	SN60-12, t = 0.25 cm (0.10 in.)			SN60-10, t = 0.25 cm (0.10 in.)			SN60-56, t = 0.51 cm (0.20 in.)			SN60-8, t = 0.51 cm (0.20 in.)			SN60-7, t = 0.76 cm (0.30 in.)			SN60-57, t = 0.76 cm (0.30 in.)		
	R, %	T, %	A, %	R, %	T, %	A, %	R, %	T, %	A, %	R, %	T, %	A, %	R, %	T, %	A, %	R, %	T, %	A, %
0.25	72.9	0.0	27.1	72.5	0.0	27.5	73.2	0.0	26.8	72.6	0.0	27.4	72.4	0.0	27.6	72.0	0.0	28.0
0.30	80.6	0.0	19.4	80.4	0.0	19.6	79.3	0.0	20.7	80.4	0.0	19.6	81.3	0.0	18.7	80.4	0.0	19.6
0.35	89.9	0.1	10.0	89.6	0.0	10.4	89.7	0.0	10.3	88.9	0.0	11.1	89.6	0.0	10.4	89.3	0.0	10.7
0.40	91.7	0.5	7.8	91.5	0.1	8.4	91.4	0.0	8.6	91.5	0.0	8.5	91.0	0.0	9.0	91.5	0.0	8.5
0.45	93.6	0.6	5.8	93.0	0.3	6.7	93.4	0.0	6.6	93.2	0.0	6.8	92.6	0.0	7.4	93.3	0.0	6.7
0.50	94.6	0.7	4.7	94.3	0.5	5.2	94.7	0.0	5.3	94.8	0.0	5.2	94.3	0.0	5.7	94.5	0.0	5.5
0.60	96.1	0.8	3.1	95.4	0.6	4.0	95.6	0.0	4.4	95.4	0.0	4.6	95.3	0.0	4.7	95.6	0.0	4.4
0.70	97.4	1.0	1.6	97.1	0.7	2.2	97.1	0.1	2.8	97.2	0.2	2.6	96.8	0.1	3.1	97.2	2.1	2.7
0.80	97.4	1.2	1.4	97.2	0.8	2.0	97.5	0.2	2.3	97.4	0.4	2.2	97.1	0.2	2.7	97.3	0.1	2.7
0.90	97.5	1.3	1.2	97.4	1.0	1.6	97.6	0.4	2.0	97.7	0.5	1.8	97.0	0.2	2.8	97.5	0.2	2.3
1.00	97.4	1.3	1.3	97.4	1.0	1.6	97.7	0.4	1.9	97.6	0.5	1.9	97.3	0.2	2.5	97.5	0.2	2.3
1.20	97.5	1.3	1.2	97.1	1.0	1.9	97.3	0.4	2.3	97.3	0.5	2.2	97.1	0.2	2.7	97.4	0.2	2.4
1.40	97.5	1.3	1.2	97.4	1.0	1.6	97.3	0.4	2.3	97.4	0.5	2.1	96.9	0.2	2.9	97.3	0.2	2.5
1.60	97.8	1.5	.7	97.6	1.1	1.3	97.8	0.5	1.7	97.4	0.7	1.9	97.2	0.2	2.6	97.6	0.2	2.2
1.80	98.4	1.5	.1	98.0	1.0	1.0	98.0	0.3	1.7	98.0	0.6	1.4	97.3	0.1	2.6	98.0	0.2	1.8
1.90	98.6	1.4	.0	98.2	1.0	.8	98.2	0.2	1.6	98.2	0.4	1.4	97.2	0.0	2.8	98.2	0.1	1.7
2.00	98.5	1.2	.3	98.1	0.8	1.1	98.1	0.2	1.7	98.2	0.2	1.6	97.1	0.0	2.9	98.1	0.0	1.9
2.10	98.0	1.0	1.0	97.5	0.7	1.8	96.4	0.1	3.5	97.3	0.2	2.5	96.3	0.0	3.7	97.2	0.0	2.8
2.20	97.9	0.4	1.7	97.4	0.1	2.5	96.8	0.1	3.1	97.0	0.2	2.9	96.0	0.0	4.0	97.2	0.0	2.8
2.40	98.4	0.1	1.5	97.5	0.1	2.4	96.9	0.0	3.1	97.1	0.2	2.9	96.1	0.0	3.9	97.2	0.0	2.8
2.50	97.6	0.1	2.3	97.5	0.1	2.4	96.9	0.0	3.1	96.9	0.2	2.9	96.2	0.0	3.8	97.0	0.0	3.0

*R = reflectance, T = transmittance, A = absorptance.

Figure 28 shows the average reflectance from 0.25 to 2.5 μm for each of the five different particle-size configurations. These reflectances represent averages for all models, since there is no distinguishable change in reflectance for the different thicknesses of the 100% monodisperse configurations that were tested.

Similarly, figure 29 shows the average reflectance over the same spectral region for models made from Particle Size 6 and 0.51-cm (0.20-in.) thick models made from continuous-particle-size GE 204, both with and without colloidal silica. Note that the models prepared from 100% monodisperse Particle Size 6 have the highest reflectance, and this is significantly higher than that of both continuous-particle-size configurations.

Atomic absorption and flame emission analyses made of the 100% monodisperse test models after spectrophotometer testing revealed that the level of alkali-metal contamination was higher than anticipated. Assayed models made from Particle Sizes 2, 4, and 6 consistently had contamination on the order of 18.1 ppm of sodium and 19.3 ppm of potassium for the method of preparation described in Section III. This excess alkali metal may have been introduced in preparing the 100% monodisperse slips, most likely during the 30-minute rolling of the slips in the glass jars prior to casting. Since the jars were ordinary laboratory glassware, and therefore had relatively high levels of alkali metals, the abrasion of the silica particles against the glass walls could have introduced significant amounts of sodium and potassium.

Even with increased levels of alkali-metal contamination, the monodisperse particle-size slips gave a higher reflectance than the continuous-particle-size slips.

Figures 30 and 31 show average values of transmittance from 0.25 to 2.5 μm for 0.25-cm (0.10-in.) and 0.51-cm (0.20-in.) thick discs made from the continuous-particle-size slips, and the 100% monodisperse particle-size slips made from Particle Sizes 2, 4, and 6. In addition to having the highest reflectance, these figures show that the smallest-particle-size monodisperse silica also exhibited the lowest transmittance, especially at longer wavelengths. In addition, the 100% monodisperse configurations made from Particle Sizes 4 and 6 had a lower transmittance than the continuous-particle-size configuration.

c. 75/25% blend GE-204: The density of the 100% monodisperse slip cast configurations is relatively low, 1.35 g/cm^3 (84 lb/ft^3), compared to 1.95 g/cm^3 (122 lb/ft^3) for the continuous-particle-size configuration. This could be increased by increasing the solids content of the slips and/or by changing either the pH or the proportion of colloidal silica. However, a better way to increase the density is to select particles that will give closer packing in both the slip and the cast article. One way is to select a second particle size whose diameter is 1/4 to 1/5 that of the first particle size.

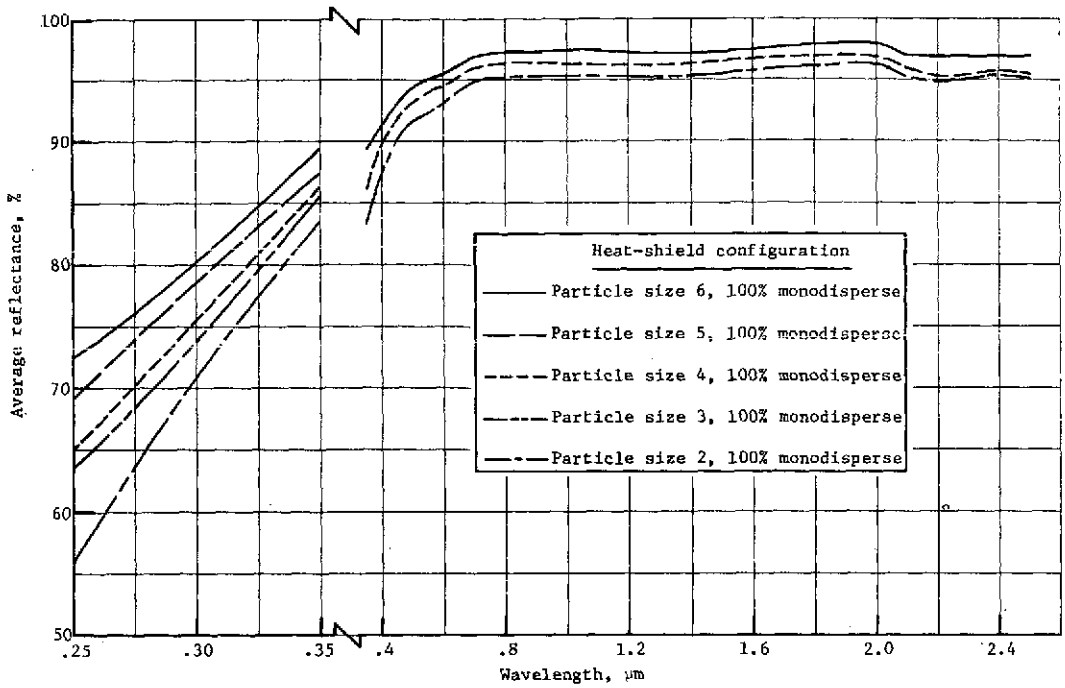

Figure 28.- Spectral reflectance of 100% monodisperse slip-cast configurations made from different particle sizes of GE 204 fused silica

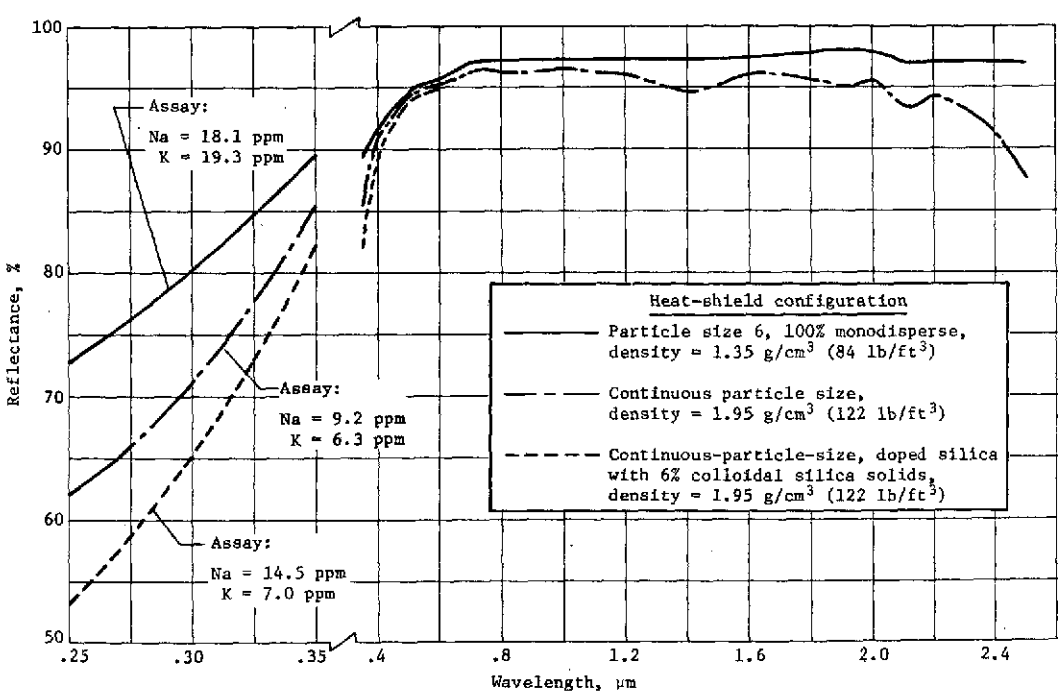

Figure 29.- Spectral reflectance of different slip-cast configurations made from GE 204 fused silica

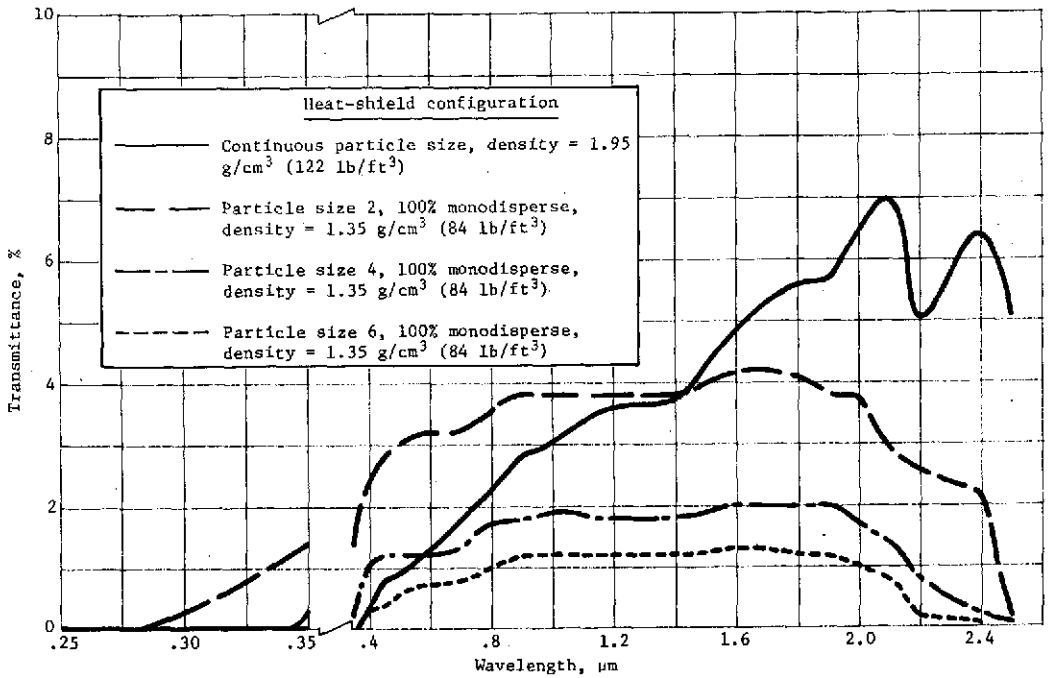

Figure 30.- Spectral transmittance of 0.25-cm (0.10-in.) thick models of different slip-cast configurations made from GE 204 fused silica

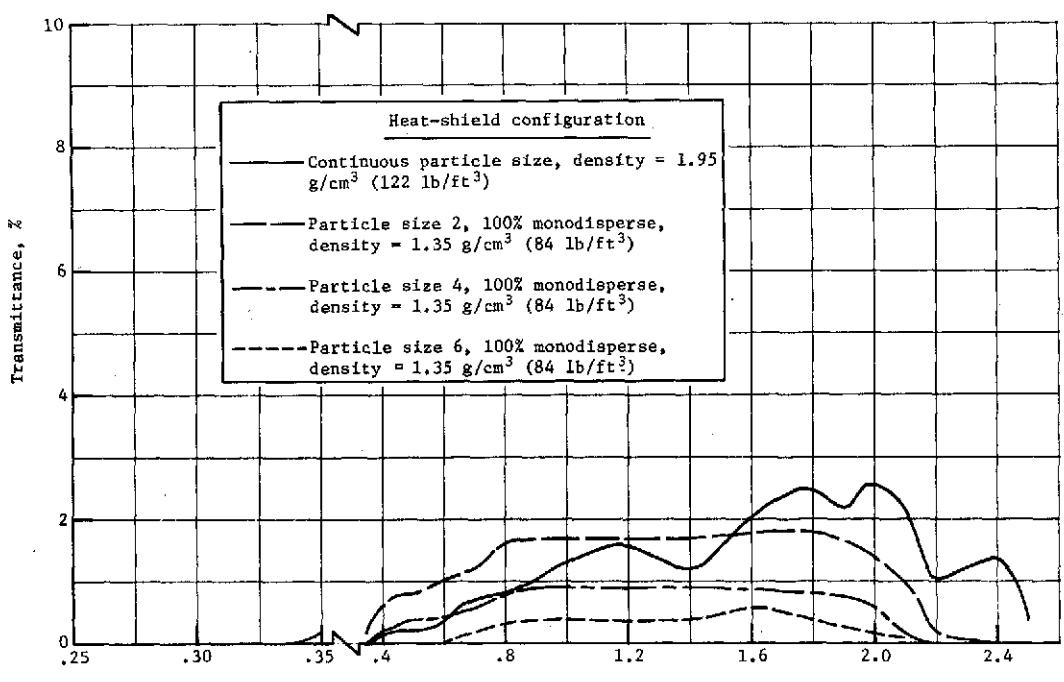

Figure 31.- Spectral transmittance of 0.51-cm (0.20-in.) thick models of different slip-cast configurations made from GE 204 fused silica

To implement this approach, two such particle sizes were blended using 75% (by weight) of the larger and 25% (by weight) of the smaller. The density of the resulting configurations was about 1.50 g/cm^3 (94 lb/ft^3).

Spectrophotometer test results for 75/25% blend, slip-cast configurations made from PS-2/PS-6, PS-4/PS-7, and PS-6/PS-8 are given in tables 18, 19, and 20, respectively.

TABLE 18.- SPECTROPHOTOMETER TEST RESULTS FOR SLIP-CAST MODELS MADE FROM PARTICLE SIZE 2, 75/25% BLEND, WITH 6% COLLOIDAL SILICA SOLIDS*

Wavelength, μm	SN4-76, t = 0.51 cm (0.20 in.)			SN4-77, t = 0.51 cm (0.20 in.)			SN4-78, t = 0.51 cm (0.20 in.)		
	R, %	T, %	A, %	R, %	T, %	A, %	R, %	T, %	A, %
0.25	66.4	0.0	33.6	67.0	0.0	33.0	67.0	0.0	33.0
0.30	75.4	0.1	24.5	75.7	0.0	24.3	76.0	0.0	24.0
0.35	85.7	0.1	14.2	85.4	0.0	14.6	86.3	0.0	13.7
0.40	90.0	0.2	9.8	90.3	0.2	9.5	90.0	0.3	9.7
0.45	92.3	0.2	7.5	92.3	0.3	7.4	91.4	0.3	8.3
0.50	93.5	0.3	6.2	93.6	0.3	6.1	93.1	0.3	6.6
0.60	94.7	0.3	5.0	95.0	0.4	4.6	94.4	0.5	5.1
0.70	96.5	0.4	3.1	96.6	0.7	2.7	95.8	0.7	3.5
0.80	96.5	0.7	2.8	96.9	0.9	2.2	96.1	0.9	3.0
0.90	96.7	0.8	2.5	96.8	0.8	2.4	96.3	0.9	2.8
1.00	96.6	0.9	2.5	96.7	0.8	2.5	96.2	0.9	2.9
1.20	96.5	0.9	2.6	96.6	0.9	2.5	96.4	0.9	2.7
1.40	96.5	0.8	2.7	96.6	0.8	2.6	96.7	0.8	2.5
1.60	96.9	0.7	2.4	96.7	0.9	2.4	96.8	1.1	2.1
1.80	97.0	0.7	2.3	96.9	0.7	2.4	97.1	1.1	1.8
1.90	97.1	0.8	2.1	97.1	0.8	2.1	97.4	1.1	1.5
2.00	97.0	0.6	2.4	97.0	0.6	2.4	97.0	1.1	1.9
2.10	96.4	0.2	3.4	96.3	0.4	3.3	95.9	0.9	3.2
2.20	95.9	0.1	4.0	95.7	0.1	4.2	94.9	0.5	4.6
2.40	96.2	0.1	3.7	96.2	0.0	3.8	95.6	0.5	3.9
2.50	96.0	0.1	3.9	95.9	0.0	4.1	95.5	0.3	4.2

*R = reflectance, T = transmittance, A = absorptance.

TABLE 19.- SPECTROPHOTOMETER TEST RESULTS FOR SLIP-CAST MODELS MADE FROM PARTICLE SIZE 4, 75/25% BLEND, WITH 6% COLLOIDAL SILICA SOLIDS*

Wavelength, μm	SN10-79, t = 0.51 cm (0.20 in.)			SN10-80, t = 0.51 cm (0.20 in.)			SN10-81, t = 0.51 cm (0.20 in.)		
	R, %	T, %	A, %	R, %	T, %	A, %	R, %	T, %	A, %
0.25	69.4	0.0	30.6	69.7	0.0	30.3	70.6	0.0	29.4
0.30	76.4	0.0	23.6	78.1	0.0	21.9	78.2	0.0	21.8
0.35	85.9	0.0	14.1	87.7	0.0	12.3	87.7	0.0	12.3
0.40	89.9	0.0	10.1	89.4	0.0	10.6	91.6	0.0	8.4
0.45	91.5	0.0	8.5	91.0	0.0	9.0	93.2	0.0	6.8
0.50	93.5	0.0	6.5	93.2	0.0	6.8	95.0	0.0	5.0
0.60	94.7	0.0	5.3	94.0	0.0	6.0	96.6	0.0	3.4
0.70	96.7	0.1	3.2	96.7	0.0	3.3	94.9	0.2	4.9
0.80	96.9	0.6	2.5	96.9	0.4	2.7	95.3	0.8	3.9
0.90	97.1	0.7	2.2	97.1	0.5	2.4	97.1	0.8	2.1
1.00	97.0	0.8	2.2	97.1	0.6	2.3	97.2	0.8	2.0
1.20	97.0	0.8	2.2	96.3	0.6	3.1	97.0	0.8	2.2
1.40	96.4	0.6	3.0	97.0	0.2	2.8	96.7	0.7	2.6
1.60	97.0	0.9	2.1	96.9	0.7	2.4	96.9	0.9	2.2
1.80	97.0	0.9	2.1	97.0	0.8	2.2	97.1	1.0	1.9
1.90	97.6	0.7	1.7	97.3	0.7	2.0	97.4	0.9	1.7
2.00	97.6	0.9	1.5	97.6	0.6	1.8	97.7	0.9	1.4
2.10	96.6	0.5	2.9	96.7	0.5	2.8	96.8	0.8	2.4
2.20	95.2	0.0	4.8	95.0	0.1	4.8	95.4	0.2	4.4
2.40	96.5	0.0	3.5	96.5	0.0	3.5	97.1	0.1	2.8
2.50	95.5	0.0	4.5	95.8	0.0	4.2	96.2	0.0	3.8

*R = reflectance, T = transmittance, A = absorptance.

TABLE 20.- SPECTROPHOTOMETER TEST RESULTS FOR SLIP-CAST MODELS MADE FROM PARTICLE SIZE 6, 75/25% BLEND, WITH 6% COLLOIDAL SILICA SOLIDS*

Wavelength, μm	SN60-84, t = 0.51 cm (0.20 in.)			SN60-85, t = 0.51 cm (0.20 in.)			SN60-86, t = 0.51 cm (0.20 in.)		
	R, %	T, %	A, %	R, %	T, %	A, %	R, %	T, %	A, %
0.25	71.1	0.0	28.9	72.2	0.0	27.8	71.6	0.0	28.4
0.30	79.3	0.0	20.7	79.7	0.0	20.3	79.6	0.0	20.4
0.35	89.0	0.0	11.0	88.8	0.0	11.2	88.9	0.0	11.1
0.40	91.7	0.0	8.3	91.3	0.0	8.7	91.6	0.0	8.4
0.45	93.6	0.0	6.4	93.2	0.0	6.8	93.4	0.0	6.6
0.50	95.0	0.0	5.0	94.6	0.0	5.4	94.7	0.0	5.3
0.60	95.9	0.0	4.1	95.8	0.0	4.2	95.9	0.0	4.1
0.70	97.5	0.1	2.4	97.4	0.1	2.5	97.4	0.0	2.6
0.80	97.7	0.2	2.1	97.5	0.2	2.3	97.7	0.2	2.1
0.90	98.0	0.4	1.6	97.6	0.4	2.0	97.8	0.3	1.9
1.00	98.0	0.4	1.6	98.1	0.4	1.5	98.0	0.4	1.6
1.20	97.9	0.4	1.7	98.0	0.4	1.6	97.8	0.4	1.8
1.40	97.8	0.5	1.7	97.8	0.5	1.7	97.8	0.5	1.7
1.60	98.0	0.4	1.6	98.0	0.5	1.5	98.1	0.4	1.5
1.80	98.5	0.3	1.2	98.2	0.4	1.4	98.4	0.3	1.3
1.90	98.7	0.2	1.1	98.3	0.2	1.5	98.5	0.2	1.3
2.00	98.6	0.0	1.4	98.2	0.0	1.8	98.4	0.0	1.6
2.10	98.0	0.0	2.0	97.6	0.0	2.4	97.8	0.0	2.2
2.20	97.7	0.0	2.3	97.4	0.0	2.6	97.6	0.0	2.4
2.40	97.6	0.0	2.4	97.2	0.0	2.8	97.5	0.0	2.5
2.50	97.5	0.0	2.5	97.2	0.0	2.8	97.5	0.0	2.5

*R = reflectance, T = transmittance, A = absorptance.

The same trend prevails for the blends as for the 100% monodisperse particle-size slips: The smallest particles produce the highest reflectance and the lowest transmittance.

Figure 32 shows the spectral reflectance for the three 75/25% blend configurations described in tables 18 through 20.

By comparing these values with those shown in figure 28 for the 100% monodisperse configurations, it can be seen that for a given particle size, e.g., PS-2, adding the smaller particles increases the reflectance. However, for the 75/25% blend configuration made from PS-6/PS-8, the reflectance is not significantly improved over that for the 100% monodisperse PS-6 configuration at near-UV wavelengths. This is probably caused by two opposing effects: Although using smaller particles may improve the scattering, it also increases the contamination. During classification, foreign particles abraded from the ball milling equipment are concentrated in the PS-8 particle fraction. Thus, while the PS-8 particles may improve scattering of the matrix, they can also absorb more radiation.

Figure 33 shows the spectral transmittance for the three 75/25% blend configurations and the continuous-particle-size configuration made from GE 204. As expected, the transmittance of the 75/25% blend configurations is lower than that for the 100% monodisperse configuration of the corresponding particle size. In addition, the transmittance of the blends is significantly lower than that for the continuous-particle-size configuration even though the latter material is 30% more dense.

d. Continuous-particle-size Suprasil: The reflectance of slip-cast fused silica is very dependent on the presence of impurities such as alkali-metal contaminants, especially in the UV region of the spectrum. As a result, we prepared a number of slip-cast configuration from Suprasil (Amersil, Inc.) to determine the increased reflectance that could be obtained from a higher-purity fused silica. The results of the spectrophotometer tests on this material are given in table 21, and are compared with those for the continuous-particle-size and Particle Size 6 100% monodisperse GE 204 fused silicas in figure 34. The Suprasil produced a reflectance of about 83% at 0.25 μm. This represents a substantial improvement over that obtained for the GE 204 configurations at UV wavelengths.

Subsequent atomic absorption and flame emission analyses of selected Suprasil samples revealed about 4.0 ppm of sodium and 3.1 ppm of potassium, or about half the amounts found in the GE 204 continuous-particle-size configuration.

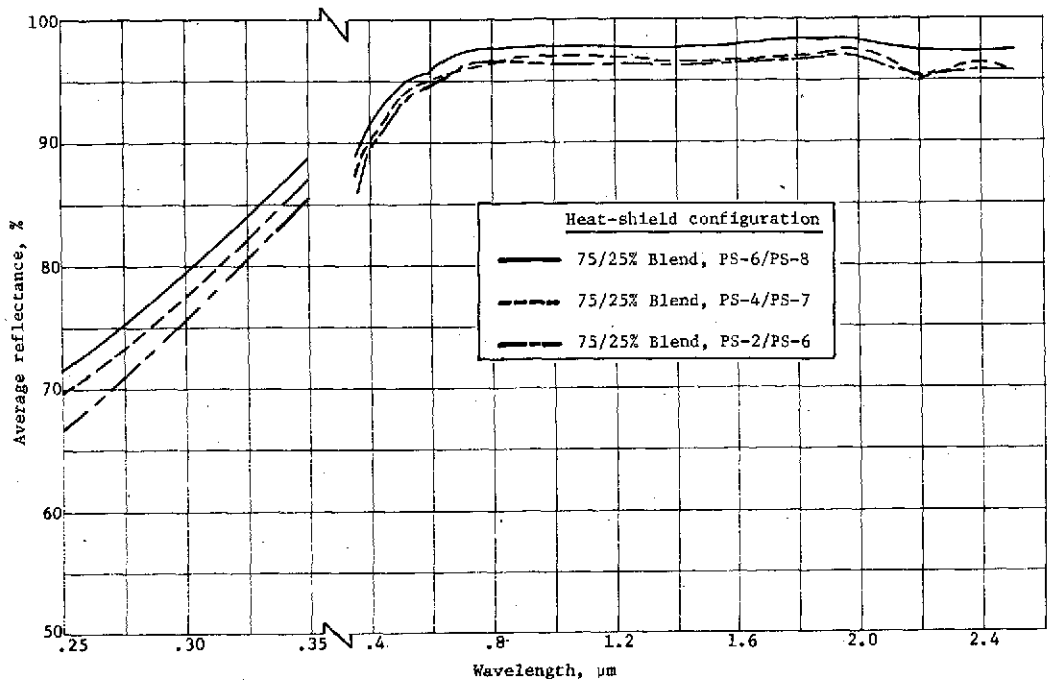

Figure 32.- Spectral reflectance of 75/25% blend, slip-cast configurations made from different particle sizes of GE 204 fused silica

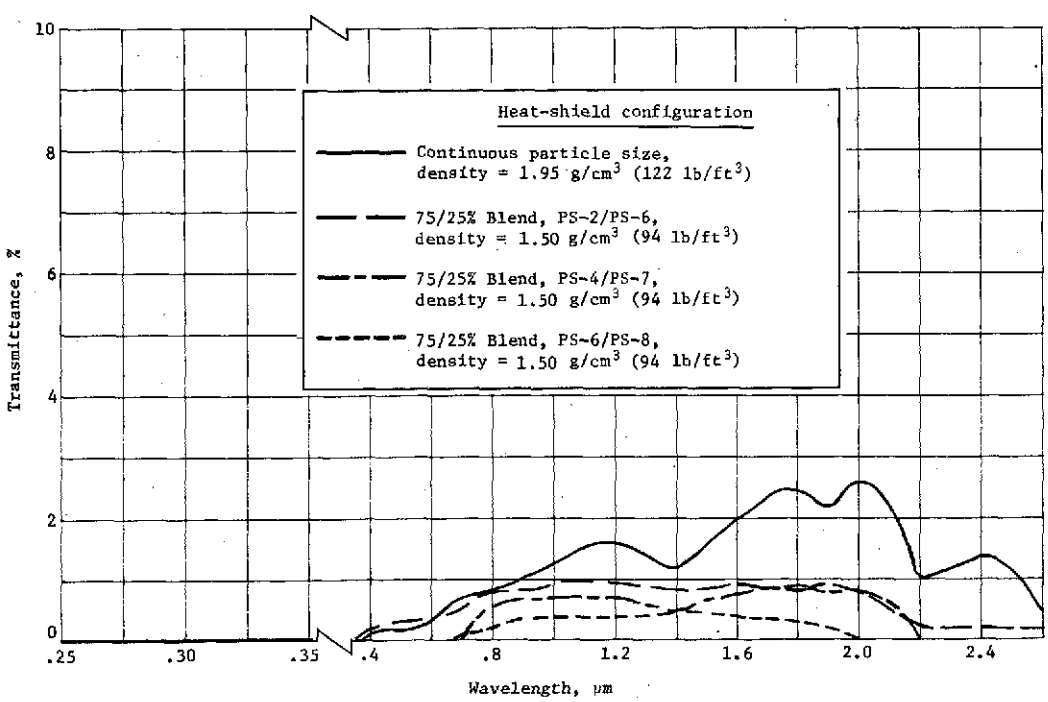

Figure 33.- Spectral transmittance of 0.51-cm (0.20-in.) thick models of different slip-cast configurations made from GE 204 fused silica

TABLE 21.- SPECTROPHOTOMETER TEST RESULTS FOR SLIP-CAST MODELS MADE FROM CONTINUOUS-PARTICLE-SIZE SUPRASIL SLIP*

Wavelength, μm	SNC-74, t = 0.25 cm (0.10 in.)			SNC-75, t = 0.25 cm (0.10 in.)			SNC-70, t = 0.51 cm (0.20 in.)			SNC-71, t = 0.51 cm (0.20 in.)			SNC-72, t = 0.51 cm (0.20 in.)			SNC-73, t = 0.51 cm (0.20 in.)		
	R, %	T, %	A, %	R, %	T, %	A, %	R, %	T, %	A, %	R, %	T, %	A, %	R, %	T, %	A, %	R, %	T, %	A, %
0.25	83.3	0.0	16.7	83.4	0.0	16.6	83.5	0.0	16.5	82.8	0.0	17.2	83.0	0.0	17.0	83.5	0.0	16.5
0.30	85.4	0.0	14.6	85.6	0.0	14.4	86.0	0.0	14.0	84.7	0.0	15.3	85.4	0.0	14.6	86.3	0.0	13.7
0.35	89.9	0.0	10.1	90.1	0.0	9.9	90.2	0.0	9.8	88.9	0.0	11.1	90.4	0.0	9.6	90.5	0.0	9.5
0.40	91.0	0.2	8.8	91.2	0.2	8.6	91.2	0.3	8.5	90.1	0.0	9.9	91.9	0.1	8.0	90.8	0.2	9.0
0.45	92.1	0.8	7.1	92.4	0.7	6.9	92.7	0.3	7.0	93.5	0.0	6.5	92.7	0.3	7.0	93.5	0.2	6.3
0.50	93.1	1.1	5.8	93.2	1.2	5.6	93.6	0.7	5.7	95.0	0.1	5.1	94.4	0.6	5.0	95.0	0.6	4.4
0.60	94.2	1.2	4.6	94.4	1.2	4.4	95.7	0.8	3.5	96.0	0.5	3.5	95.7	0.8	3.5	95.9	0.7	3.4
0.70	96.4	1.5	2.1	96.6	1.5	1.9	96.5	1.1	2.4	96.3	0.8	2.9	96.7	1.0	2.3	96.6	0.9	2.5
0.80	96.1	2.0	1.9	96.4	1.9	1.7	96.5	1.3	2.2	96.3	1.1	2.6	96.5	1.5	2.0	96.5	1.3	2.2
0.90	95.9	2.4	1.7	96.0	2.5	1.5	96.2	1.6	2.2	96.0	1.5	2.5	96.2	1.5	2.3	96.2	1.5	2.3
1.00	95.4	2.8	1.8	95.6	2.7	1.7	96.0	1.8	2.2	96.0	1.8	2.2	96.2	1.9	1.9	96.2	1.8	2.0
1.20	94.8	3.7	1.5	95.0	3.6	1.4	95.4	2.3	2.3	95.5	2.0	2.5	95.8	2.5	1.7	95.6	2.4	2.0
1.40	92.8	4.2	3.0	93.0	4.3	2.7	93.0	2.0	5.0	93.0	1.8	5.2	93.2	2.1	4.7	93.2	2.0	4.8
1.60	93.3	6.0	.7	93.5	5.9	.6	94.6	3.6	1.8	94.8	3.4	1.8	94.8	3.9	1.3	94.6	3.5	1.9
1.80	92.0	7.0	1.0	92.5	7.0	.5	93.7	4.2	2.1	93.7	3.8	2.5	93.7	4.5	1.8	93.8	3.9	2.3
1.90	91.0	7.3	1.7	91.3	7.0	1.7	91.9	3.8	4.3	92.0	3.5	4.5	92.1	4.0	3.9	92.1	3.6	4.3
2.00	91.3	8.5	.2	91.4	8.4	.2	92.6	4.8	2.6	92.8	4.3	2.9	92.7	5.1	2.2	92.8	4.7	2.5
2.10	88.1	8.4	3.5	88.2	8.3	3.5	90.3	4.4	5.3	90.5	3.9	5.6	90.4	4.8	4.8	90.5	4.4	5.1
2.20	84.7	7.5	7.8	84.9	7.6	7.5	85.2	3.0	11.8	85.3	3.6	11.1	85.4	3.3	11.3	85.4	3.3	11.3
2.40	84.2	9.5	6.3	84.2	9.4	6.4	86.1	4.3	9.6	86.3	3.6	10.1	86.3	4.5	9.2	86.3	4.2	9.5
2.50	80.9	7.7	11.4	81.3	7.4	11.3	81.0	2.8	16.2	81.1	2.0	16.9	81.0	3.2	15.8	81.1	2.8	16.1

*R = reflectance, T = transmittance, A = absorptance.

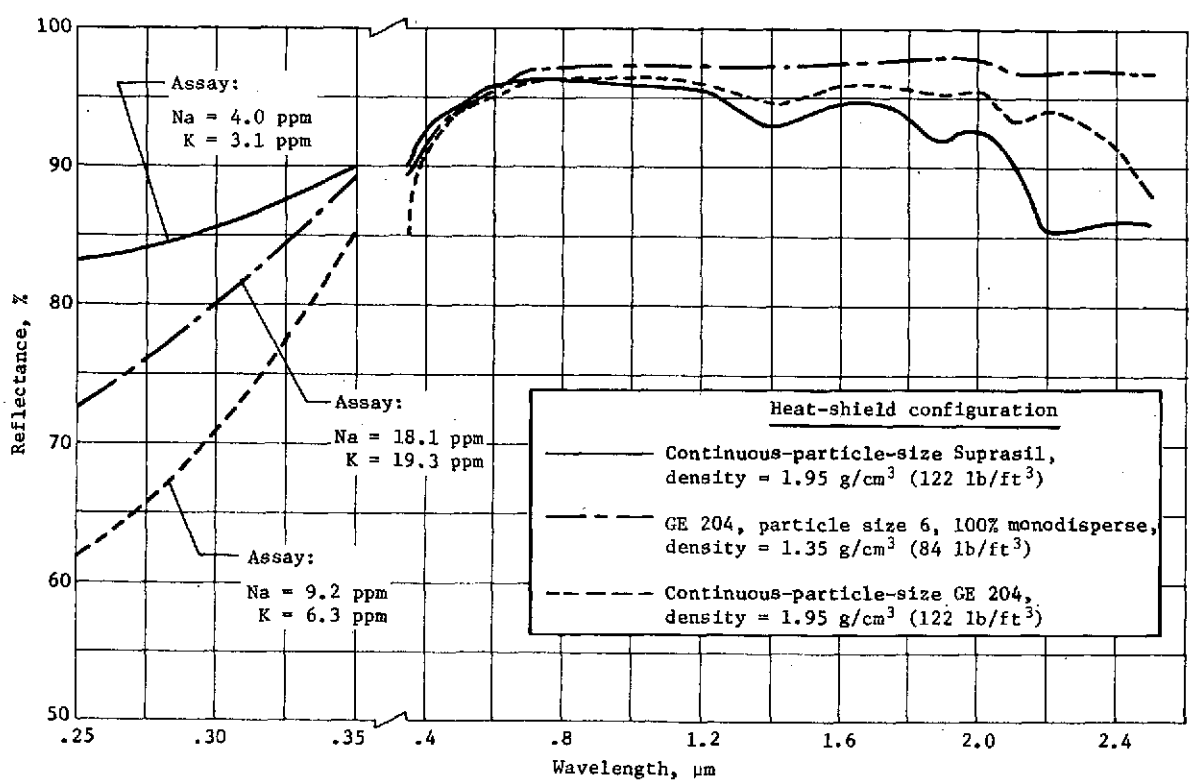

Figure 34.- Spectral reflectance of the slip-cast configuration made from Suprasil synthetic fused silica compared with the curves for slip-cast configurations made from GE 204 fused silica

Based on the results observed in this contract, a logical next step in a reflective heat-shield development program would be to determine the reflectance for 100% monodisperse configurations and 75/25% blend configurations made from Suprasil.

2. Flexural strength tests.

a. Continuous-particle-size GE 204: Table 22 shows the results of the mechanical property tests on the continuous-particle-size GE 204. The slip-cast models used in these tests were fired for 4 hours at 1478°K (2200°F) and had a density of 1.93 g/cm^3 (120 lb/ft^3).

TABLE 22.- MECHANICAL PROPERTIES OF SLIP-CAST MODELS MADE FROM CONTINUOUS-PARTICLE-SIZE SLIP, FIRED 4 hr AT 1478°K

Model number	Density		Modulus of rupture		Modulus of elasticity	
	g/cm^3	lb/ft^3	MN/m^2	$lb/in.^2$	GN/m^2	$lb/in.^2$
FNC-34-1	1.93	120	39.6	5.75×10^3	29.2	4.24×10^6
FNC-34-2	1.94	121	35.0	5.07	27.1	3.93
FNC-34-3	1.91	119	37.4	5.43	27.8	4.04
FNC-34-4	1.94	121	37.6	5.46	28.7	4.16
FNC-34-5	1.94	121	27.2	3.95	28.4	4.12
FNC-35-1	1.93	120	39.6	5.75	30.6	4.44
FNC-35-2	1.92	120	33.0	4.78	25.3	3.66
FNC-35-3	1.92	120	37.6	5.45	27.3	3.96
FNC-35-4	1.95	122	34.2	4.96	29.2	4.24
FNC-35-5	1.93	120	36.1	5.23	29.8	4.32
FNC-35-6	1.93	120	31.2	4.53	27.6	4.00
Average	1.93	120	35.3	5.12	28.3	4.10

As shown above, the average modulus of rupture was 35.3 MN/m^2 (5120 $lb/in.^2$); and the average modulus of elasticity, 28.3 GN/m^2 (4.10×10^6 $lb/in.^2$).

b. 100% monodisperse GE 204: Mechanical property tests were performed on three slip-cast configurations made using 100% monodisperse particle sizes: PS-2, PS-4, and PS-6. The results of these tests are given in tables 23, 24, and 25. All of these configurations were fired for 5 hours at 1533°K (2300°F).

The PS-2 (20- to 40-μm-diameter) configuration had an average density of 1.38 g/cm^3 (86.3 lb/ft^3), a rupture modulus of 16.2 MN/m^2 (2360 $lb/in.^2$), and a modulus of elasticity of 19.0 GN/m^2 (2.76×10^6 $lb/in.^2$). The PS-4 (10- to 21-μm-diameter) configuration had an average density of 1.37 g/cm^3 (85.4 lb/ft^3), a rupture modulus of 17.9 MN/m^2 (2590 $lb/in.^2$), and a modulus of elasticity of 22.6 GN/m^2 (3.28×10^6 $lb/in.^2$). The PS-6 (5- to 11-μm-diameter) configuration had an average density of 1.35 g/cm^3 (84.5 lb/ft^3), a rupture modulus of 14.6 MN/m^2 (2120 $lb/in.^2$), and a modulus of elasticity of 17.1 GN/m^2 (2.48×10^6 $lb/in.^2$).

Note that the 5-hr, 1533°K firing schedule used in this program is not necessarily the optimum firing schedule for these configurations, and that the mechanical properties vary according to the firing schedule. A subsequent SEM examination of the PS-6 configuration, for instance, indicated that a firing time of less than 5 hours may be better for this particular particle size. (See the appendix for these SEM photographs.) This may explain why this sample had a lower modulus of rupture.

c. 75/25% blend GE 204: As mentioned earlier, the 75/25% blend configurations were studied as a means of increasing the density of monodisperse particle size, slip-cast fused silica. A higher density reduces the surface recession during entry and results in better mechanical strength.

Four 75/25% blend configurations were tested: PS-2/PS-6, PS-3/PS-7, PS-4/PS-7, and PS-5/PS-8. The first three configurations were fired for 5 hours at 1533°K (2300°F); the fourth configuration was fired for 4 hours at 1533°K (2300°F). Again, these firing schedules are not necessarily optimum.

Tables 26, 27, and 28 are the test results for the PS-2/PS-6, PS-3/PS-7, and PS-4/PS-7 configurations, respectively.

Note that the PS-2/PS-6 material exhibited the best properties--a rupture modulus of 23.6 MN/m^2 (3430 $lb/in.^2$), and a modulus of elasticity of 32.3 GN/m^2 (4.68×10^6 $lb/in.^2$). For a low-density fused silica--1.50 g/cm^3 (93.8 lb/ft^3)--this material has good mechanical strength and stiffness. Its properties compare favorably with those of higher-density, continuous-particle-size materials.

The test results for the PS-5/PS-8 75/25% blend configuration are given in table 29.

TABLE 23.- MECHANICAL PROPERTIES OF SLIP-CAST MODELS MADE FROM PARTICLE SIZE 2, 100% MONODISPERSE, FIRED 5 hr AT 1533°K

Model number	Density		Modulus of rupture		Modulus of elasticity	
	g/cm^3	lb/ft^3	MN/m^2	$lb/in.^2$	GN/m^2	$lb/in.^2$
FN4-54-1	1.37	85.5	17.0	2.46×10^3	19.3	2.80×10^6
FN4-54-2	1.40	87.4	16.3	2.36	18.6	2.70
FN4-54-3	1.38	86.2	14.9	2.16	19.0	2.76
FN4-54-4	1.38	86.2	13.6	1.97	17.4	2.52
FN4-54-5	1.38	86.2	19.4	2.82	20.8	3.02
Average	1.38	86.3	16.2	2.36	19.0	2.76

TABLE 24.- MECHANICAL PROPERTIES OF SLIP-CAST MODELS MADE FROM PARTICLE SIZE 4, 100% MONODISPERSE, FIRED 5 hr AT 1533°K

Model number	Density		Modulus of rupture		Modulus of elasticity	
	g/cm^3	lb/ft^3	MN/m^2	$lb/in.^2$	GN/m^2	$lb/in.^2$
FN10-55-1	1.37	85.5	18.5	2.68×10^3	22.1	3.20×10^6
FN10-55-2	1.36	84.9	20.1	2.91	25.4	3.69
FN10-55-3	1.38	86.2	18.1	2.62	23.2	3.37
FN10-55-4	1.37	85.5	12.9	1.87	18.7	2.71
FN10-55-5	1.36	84.9	19.8	2.87	23.6	3.42
Average	1.37	85.4	17.9	2.59	22.6	3.28

TABLE 25.- MECHANICAL PROPERTIES OF SLIP-CAST MODELS MADE FROM PARTICLE SIZE 6, 100% MONODISPERSE, FIRED 5 hr AT 1533°K

Model number	Density		Modulus of rupture		Modulus of elasticity	
	g/cm^3	lb/ft^3	MN/m^2	$lb/in.^2$	GN/m^2	$lb/in.^2$
FN60-46-1	1.37	85.5	14.0	2.03×10^3	16.0	2.32×10^6
FN60-46-2	1.33	83.0	14.1	2.05	15.5	2.25
FN60-46-3	1.36	84.9	15.3	2.22	17.5	2.54
FN60-46-4	1.35	84.3	13.0	1.88	17.8	2.50
FN60-46-5	1.36	84.9	16.7	2.42	19.4	2.81
Average	1.35	84.5	14.6	2.12	17.1	2.48

TABLE 26.- MECHANICAL PROPERTIES OF SLIP-CAST MODELS MADE FROM PARTICLE SIZE 2, 75/25% BLEND, FIRED 5 hr AT 1533°K

Model number	Density		Modulus of rupture		Modulus of elasticity	
	g/cm^3	lb/ft^3	MN/m^2	$lb/in.^2$	GN/m^2	$lb/in.^2$
FN4-60-1	1.46	91.1	23.7	3.44×10^3	32.6	4.72×10^6
FN4-60-2	1.52	94.9	23.2	3.36	27.1	3.93
FN4-60-3	1.49	93.0	22.4	3.25	31.7	4.60
FN4-60-4	1.55	96.8	21.5	3.12	37.5	5.44
FN4-60-5	1.49	93.0	27.4	3.98	32.8	4.76
Average	1.50	93.8	23.6	3.43	32.3	4.68

TABLE 27.- MECHANICAL PROPERTIES OF SLIP-CAST MODELS MADE FROM PARTICLE SIZE 3, 75/25% BLEND, FIRED 5 hr AT 1533°K

Model number	Density		Modulus of rupture		Modulus of elasticity	
	g/cm^3	lb/ft^3	MN/m^2	$lb/in.^2$	GN/m^2	$lb/in.^2$
FN7-61-1	1.56	97.4	20.5	2.97×10^3	28.7	4.16×10^6
FN7-61-2	1.57	98.0	19.0	2.76	30.3	4.40
FN7-61-3	1.55	96.8	20.6	2.99	32.3	4.68
FN7-61-4	1.56	97.4	23.6	3.42	36.4	5.28
FN7-61-5	1.56	97.4	22.1	3.21	35.0	5.08
Average	1.56	97.4	21.2	3.07	32.6	4.72

TABLE 28.- MECHANICAL PROPERTIES OF SLIP-CAST MODELS MADE FROM PARTICLE SIZE 4, 75/25% BLEND, FIRED 5 hr AT 1533°K

Model number	Density		Modulus of rupture		Modulus of elasticity	
	g/cm^3	lb/ft^3	MN/m^2	$lb/in.^2$	GN/m^2	$lb/in.^2$
FN10-57-1	1.60	99.9	19.4	2.82×10^3	32.6	4.72×10^6
FN10-57-2	1.55	96.8	19.0	2.76	30.6	4.44
FN10-57-3	1.56	97.4	20.0	2.90	32.0	4.64
FN10-57-4	1.59	99.3	21.8	3.16	37.5	5.44
FN10-57-5	1.59	99.3	19.9	2.89	32.8	4.76
Average	1.58	98.5	20.0	2.91	33.1	4.80

TABLE 29.- MECHANICAL PROPERTIES OF SLIP-CAST MODELS MADE FROM PARTICLE SIZE 5, 75/25% BLEND, FIRED 4 hr AT 1533°K

Model number	Density		Modulus of rupture		Modulus of elasticity	
	g/cm^3	lb/ft^3	MN/m^2	$lb/in.^2$	GN/m^2	$lb/in.^2$
FN15-62-1	1.57	98.0	22.2	3.22×10^3	35.3	5.12×10^6
FN15-62-2	1.57	98.0	18.4	2.67	26.6	3.85
FN15-62-3	1.57	98.0	23.3	3.38	36.1	5.24
FN15-62-4	1.56	97.4	21.1	3.06	36.1	5.24
FN15-62-5	1.56	97.4	16.3	2.37	24.5	3.55
Average	1.57	98.0	20.3	2.97	31.7	4.60

3. High-intensity-radiation tests.

a. Continuous-particle-size GE 204: Table 30 gives the results of the xenon-arc lamp test for the continuous-particle-size GE 204 slip-cast configuration. These tests were basically conducted to compare to the 100% monodisperse and 75/25% blend configurations. The test results were consistent under the incident radiation fluxes of 1050 W/cm^2 (928 Btu/ft^2-sec).

Note that the xenon arc-lamp spectrum contains considerably more radiation at the longer-wavelength visible and IR regions, where fused silica has a higher transmittance, than the anticipated outer-planet-entry shock layer radiation. Thus, the fused silica configurations will transmit more of the xenon arc lamp radiation. Other than this, it is difficult to directly relate the transmittance of the test spectrum to that of the entry spectrum.

b. 100% monodisperse GE 204: Table 31 shows the results of exposing the GE 204 100% monodisperse configurations to a high-intensity xenon arc-lamp radiation of 1190 to 1270 W/cm^2 (1050 to 1120 Btu/ft^2-sec). These tests corroborated the results of the spectrophotometer tests: that is, for a given density and thickness, models made from smaller particle sizes had a lower transmittance.

TABLE 30.- XENON ARC-LAMP TEST RESULTS FOR CONTINUOUS-PARTICLE-SIZE, SLIP-CAST GE 204

Model number	Composition	Thickness		Incident flux		Transmittance, %	Average transmittance, %
		cm	in.	W/cm^2	Btu/ft^2-sec		
DNC-77	Continuous particle size	0.76	0.30	1050	928	0.26	0.25
DNC-78	Continuous particle size	0.76	0.30	1050	928	0.24	
DNC-79	Continuous particle size	0.51	0.20	1050	928	0.58	0.57
DNC-80	Continuous particle size	0.51	0.20	1050	928	0.56	
DNC-81	Continuous particle size	0.25	0.10	1050	928	1.42	1.41
DNC-82	Continuous particle size	0.25	0.10	1050	928	1.40	

TABLE 31.- XENON ARC-LAMP TEST RESULTS FOR THE 100% MONODISPERSE, SLIP-CAST CONFIGURATIONS*

Model number	Composition	Incident flux		Transmittance, %	Average transmittance, %
		W/cm^2	Btu/ft^2-sec		
DN4-55	100% PS-2	1270	1120	0.826	0.845
DN4-56	100% PS-2	1270	1120	0.844	
DN4-57	100% PS-2	1270	1120	0.864	
DN7-110	100% PS-3	1190	1050	0.565	0.570
DN7-111	100% PS-3	1190	1050	0.580	
DN7-112	100% PS-3	1190	1050	0.565	
DN10-46	100% PS-4	1270	1120	0.494	0.456
DN10-44	100% PS-4	1270	1120	0.419	
DN10-123	100% PS-4	1190	1050	0.455	
DN15-117	100% PS-5	1190	1050	0.333	0.329
DN15-118	100% PS-5	1190	1050	0.339	
DN15-119	100% PS-5	1190	1050	0.315	
DN60-1	100% PS-6	1270	1120	0.160	0.152
DN60-3	100% PS-6	1270	1120	0.160	
DN60-4	100% PS-6	1270	1120	0.136	

*All Models 0.51 cm (0.20 in.) Thick.

c. 75/25% blend GE 204: Table 32 summarizes the irradiation results for the GE 204 75/25% blend configurations. Of all the different slip-cast materials tested, the PS-6/PS-8 configuration exhibited the lowest transmittance, 0.135%, for a 0.51-cm (0.20-in.) thick model.

TABLE 32.- XENON ARC-LAMP TEST RESULTS FOR THE 75/25% BLEND, SLIP-CAST CONFIGURATIONS*

Model number	Composition	Incident flux		Transmittance, %	Average transmittance, %
		W/cm^2	Btu/ft^2-sec		
DN4-125	75% PS-2, 25% PS-6	1190	1050	0.507	
DN4-126	75% PS-2, 25% PS-6	1190	1050	0.521	0.514
DN4-127	75% PS-2, 25% PS-6	1190	1050	0.515	
DN7-90	75% PS-3, 25% PS-7	1190	1050	0.434	
DN7-91	75% PS-3, 25% PS-7	1190	1050	0.451	0.442
DN7-142	75% PS-3, 25% PS-7	1190	1050	0.441	
DN10-95	75% PS-4, 25% PS-7	1190	1050	0.300	
DN10-130	75% PS-4, 25% PS-7	1190	1050	0.300	0.301
DN10-131	75% PS-4, 25% PS-7	1190	1050	0.302	
DN15-136	75% PS-5, 25% PS-8	1190	1050	0.239	
DN15-137	75% PS-5, 25% PS-8	1190	1050	0.241	0.245
DN15-138	75% PS-5, 25% PS-8	1190	1050	0.255	
DN60-101	75% PS-6, 25% PS-8	1190	1050	0.135	
DN60-100	75% PS-6, 25% PS-8	1190	1050	0.135	0.135
DN60-145	75% PS-6, 25% PS-8	1190	1050	0.134	

*All models 0.51 cm (0.20 in.) thick.

4. Thermal conductivity tests.- The thermal conductivity of the continuous-particle-size, slip-cast, fused-silica configuration was determined by the guarded hot-plate method. This configuration had a density of 1.95 g/cm^3 (122 lb/ft^3). At 436°K (324°F), k was found to be 0.269 J/m-s-°K (0.155 Btu/ft-hr-°F); at 569°K (565°F), it was 0.386 J/m-s-°K (0.224 Btu/ft-hr-°F).

B. Foamed-Slip Configuration Testing

To study the effect of reduced density on reflectance, we attempted to produce lower-density, foamed-slip configurations from the continuous-particle-size slips and the monodisperse slips. The preparation of the foamed versions was originally planned before we found that the 100% monodisperse and 75/25% blend configurations had considerably lower densities than regular, continuous-particle-size, slip-cast fused silica. (The advantage of a density lower than 1.95 g/cm^3 (120 lb/ft^3) for regular, slip-cast fused silica is a significantly reduced thermal conductivity.)

Because the 100% monodisperse configuration had a density of 1.35 g/cm^3 (84.5 lb/ft^3) we decided to try foamed configurations to achieve a density lower than this. Using continuous-particle-size slips, we successfully produced two foamed configurations with densities of 1.18 g/cm^3 (73.7 lb/ft^3) and 0.980 g/cm^3 (61.2 lb/ft^3), respectively. However, we were unable to produce low-density foam configurations using the 100% monodisperse slips.

All the foamed, 100%-monodisperse-slip configurations contained a myriad of small hairline cracks. Extensive efforts to overcome this cracking problem were not undertaken, primarily because our initial attempts showed that fused-silica configurations with densities much lower than 1.35 g/cm^3 (84.5 lb/ft^3) would be impractical for an outer-planet-entry heat shield due to their high surface recessions. Subsequent optical tests were conducted on the 100% monodisperse foam configuration, but the cracking problem precluded mechanical tests.

A further problem encountered with the foam configuration prepared from 100% monodisperse slip was that it required 16% (by weight) of colloidal silica solids, which, according to the level of purity for the presently available low-sodium collidal silica, introduced about 16 ppm of sodium into the final configuration.

1. Spectrophotometer tests.

a. Continuous-particle-size GE 204: As mentioned above, foamed-slip configurations with two different densities were prepared from the continuous-particle-size slip. The higher-density version was 1.18 g/cm^3 (73.7 lb/ft^3); the lower-density version, 0.980 g/cm^3 (61.2 lb/ft^3). Spectrophotometer test results for these configurations are given in tables 33 and 34.

TABLE 33.- SPECTROPHOTOMETER TEST RESULTS FOR FOAMED-SLIP MODELS MADE FROM CONTINUOUS-PARTICLE-SIZE SLIP, DENSITY = 1.18 g/cm^3 (73.7 lb/ft^3)*

Wavelength, μm	SNC-103, t = 0.51 cm (0.20 in.)			SNC-104, t = 0.51 cm (0.20 in.)			SNC-105, t = 0.51 cm (0.20 in.)		
	R, %	T, %	A, %	R, %	T, %	A, %	R, %	T, %	A, %
0.25	50.0	0.0	50.0	54.5	0.0	45.5	50.8	0.0	49.2
0.30	60.2	0.0	39.8	62.1	0.0	37.9	60.5	0.0	39.5
0.35	77.5	0.2	22.3	80.0	0.1	19.9	78.2	0.2	21.6
0.40	83.7	0.4	15.9	84.1	0.4	15.5	83.8	0.5	15.7
0.45	88.0	0.5	11.5	88.0	0.6	11.4	88.2	0.5	11.3
0.50	92.0	0.6	7.4	92.1	0.6	7.3	92.1	0.6	7.3
0.60	93.8	1.1	5.1	93.9	1.2	4.9	93.9	1.2	4.9
0.70	94.1	1.4	4.5	94.3	1.5	4.2	94.1	1.4	4.5
0.80	94.2	1.9	3.9	94.4	2.0	3.6	94.1	1.9	4.0
0.90	94.4	2.0	3.6	94.5	2.0	3.5	94.4	2.1	3.5
1.00	94.4	2.1	3.5	94.7	2.0	3.3	94.5	2.2	3.3
1.20	93.8	2.2	4.0	94.0	2.1	3.9	93.8	2.2	4.0
1.40	93.7	2.0	4.3	93.9	2.0	4.1	93.6	2.0	4.4
1.60	94.1	2.3	3.6	94.3	2.4	3.3	94.4	2.5	3.1
1.80	93.8	2.9	3.3	94.0	3.0	3.0	94.2	3.0	2.8
1.90	93.0	2.8	4.2	93.5	2.9	3.6	93.7	3.0	3.3
2.00	92.5	2.8	4.7	93.1	2.9	4.0	92.8	3.0	4.2
2.10	91.0	2.7	6.3	92.1	2.8	5.1	91.7	2.8	5.5
2.20	92.0	2.6	5.4	92.9	2.7	4.4	92.5	2.6	4.9
2.40	90.0	2.2	7.8	90.8	2.3	6.9	91.0	2.1	6.9
2.50	84.6	2.1	13.3	85.1	2.2	12.7	87.1	2.1	10.8

*R = reflectance, T = transmittance, A = absorptance.

TABLE 34.- SPECTROPHOTOMETER TEST RESULTS FOR FOAMED-SLIP MODELS MADE FROM CONTINUOUS-PARTICLE-SIZE SLIP, DENSITY ≈ 0.980 g/cm^3 (61.2 lb/ft^3)*

Wavelength, μm	SNC-109, t = 0.51 cm (0.20 in.)			SNC-110, t = 0.51 cm (0.20 in.)			SNC-111, t = 0.51 cm (0.20 in.)		
	R, %	T, %	A, %	R, %	T, %	A, %	R, %	T, %	A, %
0.25	51.3	0.0	48.7	51.3	0.0	48.7	50.2	0.0	49.8
0.30	60.3	0.0	39.7	60.7	0.0	39.3	60.0	0.0	40.0
0.35	78.1	0.2	21.7	78.0	0.2	21.8	77.2	0.2	22.6
0.40	84.0	0.4	15.6	84.2	0.5	15.3	83.3	0.4	16.3
0.45	87.9	0.6	11.5	88.8	0.6	10.6	87.0	0.6	12.4
0.50	92.0	0.6	7.4	92.4	0.6	7.0	88.5	0.6	10.9
0.60	93.8	1.1	5.1	94.2	1.2	4.6	93.3	1.1	5.6
0.70	94.0	1.4	4.6	94.5	1.5	4.0	93.2	1.5	5.3
0.80	94.0	1.8	4.2	94.8	1.9	3.3	93.5	1.9	4.6
0.90	94.3	2.2	3.5	94.9	2.1	3.0	94.0	2.0	4.0
1.00	94.3	2.3	3.4	94.9	2.0	3.1	94.0	2.0	4.0
1.20	94.1	2.2	3.7	94.2	2.2	3.6	93.8	2.2	4.0
1.40	93.8	2.0	4.2	94.0	2.0	4.0	93.6	2.0	4.4
1.60	94.2	2.4	3.4	94.5	2.4	3.1	93.9	2.4	3.7
1.80	93.8	2.9	3.3	94.2	2.9	2.9	93.5	3.0	3.5
1.90	93.0	2.9	4.1	93.5	3.0	3.5	93.1	2.8	4.1
2.00	92.6	2.8	4.6	93.1	2.9	4.0	92.6	2.9	4.5
2.10	90.9	2.8	6.3	91.6	2.7	5.7	90.6	2.8	6.6
2.20	91.9	2.6	5.5	92.5	2.6	4.9	91.6	2.6	5.8
2.40	90.5	2.1	7.4	90.6	2.3	7.1	90.4	2.3	7.3
2.50	86.0	2.0	12.0	85.2	2.1	12.7	84.0	2.1	13.9

*R = reflectance, T = transmittance, A = absorptance.

As shown in these tables, essentially no difference in optical performance was detected between these two configurations. Their reflectance was lower than that of the continuous-particle-size, slip-cast configuration, primarily because of the 10% (by weight) colloidal silica solids needed to foam the material.

b. 100% Monodisperse GE 204: Table 35 gives the spectrophotometer test results for the 100% monodisperse foamed-slip configuration. Particle Size 6 was used in this configuration because these 5- to 11-μm particles gave the highest reflectance and lowest transmittance when used in the slip-cast configuration.

The test results showed that, although this configuration contains 16% (by weight) of colloidal silica solids, its reflectance is higher than that of the continuous-particle-size foamed slip, which contains only 10% (by weight) of colloidal silica solids.

2. Flexure tests.- Flexural tests were conducted only on the continuous-particle-size, foamed-slip configuration: Because of cracking, the 100% monodisperse, foamed-slip configuration was not tested.

Table 36 gives the results for the 1.18-g/cm^3 (73.9-lb/ft^3) version. This configuration had an average rupture modulus of 10.2 MN/m^2 (1470 lb/in.^{2}) and an average modulus of elasticity of 20.7 GN/m^2 (3.00 x 10^6 lb/in.^{2}). Table 37 gives the results for the 0.980-g/cm^3 (61.2-lb/ft^3) version. This configuration had an average rupture modulus of 7.66 MN/m^2 (1110 lb/in.^{2}) and an average modulus of elasticity of 19.9 GN/m^2 (2.89 x 10^6 lb/in.^{2}).

3. Xenon arc-lamp tests.- Table 38 gives the results of the high-intensity-radiation tests for all three foamed-slip configurations. The 100% monodisperse configuration made from Particle Size 6 had a noticeably lower transmittance than both of the continuous-particle-size configurations, consistent with the performance of this particle size for the slip-cast configurations.

C. Pressure-Sintered Configuration Testing

Pressure-sintered configurations were prepared from four separate batches of 100% monodisperse material, Particle Sizes 2, 4, 5, and 6. The fabrication method for these configurations posed several scaleup problems. Compared with the relative ease of fabricating the slip-cast configuration, which was selected as the primary silica reflecting heat-shield configuration, it probably would be much more difficult to fabricate a full-size, pressure-sintered heat shield. As a result, we were unable to

TABLE 35.- SPECTROPHOTOMETER TEST RESULTS FOR FOAMED-SLIP MODELS MADE FROM PARTICLE SIZE 6, 100% MONODISPERSE, DENSITY = 1.10 g/cm^3 (68.7 lb/ft^3)*

Wavelength, μm	SN60-115, t = 0.51 cm (0.20 in.)			SN60-116, t = 0.51 cm (0.20 in.)			SN60-118, t = 0.51 cm (0.20 in.)		
	R, %	T, %	A, %	R, %	T, %	A, %	R, %	T, %	A, %
0.25	61.0	0.0	39.0	58.0	0.0	42.0	63.5	0.0	36.5
0.30	70.1	0.0	29.9	70.0	0.0	30.0	70.5	0.0	29.5
0.35	83.5	0.0	16.5	83.8	0.0	16.2	84.5	0.0	15.5
0.40	89.0	0.0	11.0	89.1	0.0	10.9	89.0	0.0	11.0
0.45	91.5	0.1	8.4	91.4	0.1	8.5	91.8	0.1	8.1
0.50	93.5	0.1	6.4	93.6	0.1	6.3	93.1	0.1	6.8
0.60	94.5	0.4	5.1	94.3	0.5	5.2	94.2	0.4	5.4
0.70	95.0	0.7	4.3	94.7	0.8	4.5	94.7	0.8	4.5
0.80	95.6	0.9	3.5	95.0	1.0	4.0	95.0	1.0	4.0
0.90	95.6	1.0	3.4	95.0	1.1	3.9	95.1	1.0	3.9
1.00	95.8	1.1	3.1	95.1	1.2	3.7	95.2	1.1	3.7
1.20	95.6	1.1	3.3	95.1	1.3	3.6	95.1	1.2	3.7
1.40	95.4	1.2	3.4	95.1	1.2	3.7	95.0	1.2	3.8
1.60	95.6	1.2	3.2	95.1	1.3	3.6	94.9	1.2	3.9
1.80	95.5	1.1	3.4	95.0	1.2	3.8	94.9	1.1	4.0
1.90	95.5	1.0	3.5	95.0	1.1	3.9	94.8	1.0	4.2
2.00	95.3	1.0	3.7	95.0	1.1	3.9	94.8	1.1	4.1
2.10	94.9	0.8	4.3	94.7	0.9	4.4	94.5	0.8	4.7
2.20	94.9	0.7	4.4	94.1	0.3	5.6	93.9	0.5	5.6
2.40	94.8	0.0	5.2	94.1	0.0	5.9	93.7	0.0	6.3
2.50	94.6	0.0	5.4	94.0	0.0	6.0	93.4	0.0	6.6

*R = reflectance, T = transmittance, A = absorptance.

TABLE 36.- MECHANICAL PROPERTIES OF FOAMED-SLIP MODELS MADE FROM CONTINUOUS-PARTICLE-SIZE SLIP, HIGHER-DENSITY FOAM, FIRED 4 hr AT 1478°K

Model number	Density		Modulus of rupture		Modulus of elasticity	
	g/cm^3	lb/ft^3	MN/m^2	$lb/in.^2$	GN/m^2	$lb/in.^2$
FNC-63-1	1.12	69.9	9.45	1.37×10^3	20.1	2.91×10^6
FNC-63-2	1.18	73.7	10.0	1.45	20.6	2.98
FNC-63-3	1.21	75.5	11.0	1.60	21.6	3.13
FNC-63-4	1.19	74.3	10.3	1.50	20.6	2.99
FNC-63-5	1.22	76.2	10.0	1.45	20.6	2.99
Average	1.18	73.9	10.2	1.47	20.7	3.00

TABLE 37.- MECHANICAL PROPERTIES OF FOAMED-SLIP MODELS MADE FROM CONTINUOUS-PARTICLE-SIZE SLIP, LOWER-DENSITY FOAM, FIRED 4 hr AT 1478°K

Model number	Density		Modulus of rupture		Modulus of elasticity	
	g/cm^3	lb/ft^3	MN/m^2	$lb/in.^2$	GN/m^2	$lb/in.^2$
FNC-64-1	0.976	60.9	6.66	0.966×10^3	18.2	2.64×10^6
FNC-64-2	0.988	61.7	10.0	1.45	24.7	3.59
FNC-64-3	0.985	61.5	8.27	1.20	18.2	2.65
FNC-64-4	0.974	60.8	6.33	0.918	19.3	2.80
FNC-64-5	0.977	61.0	7.03	1.02	19.0	2.76
Average	0.980	61.2	7.66	1.11	19.9	2.89

TABLE 38.- XENON ARC-LAMP TEST RESULTS FOR FOAMED-SLIP CONFIGURATIONS MADE FROM CONTINUOUS-PARTICLE-SIZE SLIP AND FOR 100% MONODISPERSE SLIP MADE FROM PARTICLE SIZE 6

Model number	Composition	Density		Incident flux		Transmittance, %	Average transmittance, %
		g/cm^3	lb/ft^3	W/cm^2	Btu/ft^2-sec		
DNC-148	Continuous particle size	1.18	73.7	1190	1050	1.12	1.16
DNC-149	Continuous particle size	1.18	73.7	1190	1050	1.18	
DNC-150	Continuous particle size	1.18	73.7	1190	1050	1.17	
DNC-155	Continuous particle size	0.98	61.2	1190	1050	1.55	1.45
DNC-156	Continuous particle size	0.98	61.2	1190	1050	1.42	
DNC-157	Continuous particle size	0.98	61.2	1190	1050	1.47	
DNC-161	100% monodisperse PS-6	1.10	68.7	1190	1050	.612	.590
DNC-162	100% monodisperse PS-6	1.10	68.7	1190	1050	.555	
DNC-163	100% monodisperse PS-6	1.10	68.7	1190	1050	.597	

devote much effort to optimizing the pressure-sintered fused silica. The samples produced for testing were too dense because most of the scattering voids were eliminated--either by pressing the model at pressures that were too high, or sintering it under conditions that were too severe.

1. Spectrophotometer tests.- The test results for the pressure-sintered configurations prepared from Particle Sizes 2, 4, 5, and 6 are given in tables 39 through 43.

Two different densities were achieved using Particle Size 6; table 43 gives the results for the lower-density configuration. Actually, the different processing parameters produced only a very slight difference in density: 2.09 g/cm^3 (130 lb/ft^3) for the higher-density version, and 2.07 g/cm^3 (129 lb/ft^3) for the lower-density version.

Except for the samples made from Particle Sizes 2 and 5, the samples ranged from highly translucent to transparent. The negative values for absorptance shown in some of the tables are due to experimental error: For the reflectance measurements made with the incident beam 0.26 rad (15 deg) off normal, these very dense materials reflected some radiation specularly at the front surface.

2. Flexure tests.- The flexure test results for the pressure sintered configurations are given in tables 44 through 48. The highest modulus of rupture, 31.3 MN/m^2 (4540 $lb/in.^2$), was achieved for the higher-density version of Particle Size 6, as shown in table 47.

3. Xenon arc-lamp tests.- The xenon arc-lamp test results for the pressure-sintered configurations are given in table 49. The lowest transmittance, about 1.66%, was obtained for Particle Size 2. This configuration was underfired, however, and had very poor mechanical strength.

TABLE 39.- SPECTROPHOTOMETER TEST RESULTS FOR PRESSURE-SINTERED MODELS MADE FROM PARTICLE SIZE 2*

Wavelength, μm	SPS4-88, t = 0.51 cm (0.20 in.)			SPS4-89, t = 0.51 cm (0.20 in.)			SPS4-90, t = 0.51 cm (0.20 in.)		
	R, %	T, %	A, %	R, %	T, %	A, %	R, %	T, %	A, %
0.25	55.5	0.0	44.5	55.8	0.0	44.2	53.0	0.0	47.0
0.30	65.9	0.0	34.1	66.5	0.0	33.5	66.2	0.0	33.8
0.35	78.8	0.1	21.1	79.2	0.0	20.8	80.0	0.0	20.0
0.40	80.7	0.4	18.9	81.1	0.2	18.7	82.1	0.2	17.7
0.45	83.0	1.1	15.9	83.4	1.0	15.6	84.0	0.9	15.1
0.50	85.0	1.3	13.7	85.2	1.1	13.7	85.4	1.0	13.6
0.60	86.7	1.6	11.7	86.7	1.5	11.8	86.8	1.4	11.8
0.70	89.0	1.8	9.2	88.8	1.8	9.4	89.2	1.9	8.9
0.80	90.4	2.7	6.9	90.3	2.6	7.1	90.7	2.5	6.8
0.90	90.3	2.8	6.9	90.3	2.6	7.1	90.6	2.7	6.7
1.00	90.2	2.8	7.0	90.1	2.6	7.3	90.7	2.7	6.6
1.20	90.2	2.8	7.0	89.7	2.7	7.6	89.7	2.7	7.6
1.40	90.1	3.1	6.8	89.7	3.0	7.3	89.4	3.0	7.6
1.60	90.1	3.1	6.8	89.4	3.0	7.6	89.3	3.0	7.7
1.80	89.8	3.0	7.2	89.3	3.2	7.5	89.4	3.1	7.5
1.90	89.7	3.0	7.3	89.3	3.2	7.5	89.3	3.2	7.5
2.00	89.5	3.0	7.5	89.3	3.3	7.4	89.2	3.3	7.5
2.10	89.1	3.1	7.8	89.0	3.4	7.6	89.2	3.3	7.5
2.20	89.0	3.2	7.8	89.0	3.5	7.5	89.1	3.4	7.5
2.40	88.9	3.0	8.1	89.1	3.3	7.6	88.9	3.2	7.9
2.50	88.5	2.7	8.8	88.7	2.9	8.4	88.8	3.0	8.2

*R = reflectance, T = transmittance, A = absorptance.

TABLE 40.- SPECTROPHOTOMETER TEST RESULTS FOR PRESSURE-SINTERED MODELS MADE FROM PARTICLE SIZE 4*

Wavelength, μm	SPS10-91, t = 0.51 cm (0.20 in.)			SPS10-92, t = 0.51 cm (0.20 in.)			SPS10-93, t = 0.51 cm (0.20 in.)		
	R, %	T, %	A, %	R, %	T, %	A, %	R, %	T, %	A, %
0.25	26.4	2.2	71.4	28.0	0.0	72.0	23.6	0.0	76.4
0.30	41.1	1.4	57.5	47.4	0.0	52.6	40.4	0.9	58.7
0.35	64.2	13.4	22.4	70.8	7.8	21.4	64.4	11.9	23.7
0.40	63.9	12.7	23.4	72.5	7.4	20.1	63.8	13.5	22.7
0.45	63.7	13.9	22.4	75.5	8.2	16.3	65.1	14.5	20.4
0.50	65.4	14.8	19.8	76.6	9.6	13.8	66.5	15.8	17.7
0.60	70.0	17.5	12.5	80.9	11.7	7.4	73.0	18.9	8.1
0.70	73.5	19.1	7.4	79.6	13.5	6.9	72.6	20.3	7.1
0.80	74.6	21.1	4.3	80.7	15.2	4.1	74.5	22.5	3.0
0.90	74.5	22.3	3.2	80.4	16.3	3.3	74.4	23.8	1.8
1.00	73.6	23.2	3.2	80.1	16.8	3.1	73.7	24.6	1.7
1.20	72.2	24.5	3.3	78.7	17.8	3.5	72.2	25.9	1.9
1.40	72.2	26.7	1.1	78.5	19.5	2.0	71.9	28.0	.1
1.60	71.9	28.1	.0	78.3	20.5	1.2	71.6	29.3	-.9
1.80	71.4	30.1	-1.5	77.9	21.9	.2	70.8	31.1	-1.9
1.90	72.9	31.7	-3.9	78.2	23.0	-1.2	71.7	32.7	-4.4
2.00	72.4	32.8	-5.2	78.3	23.9	-2.2	72.0	33.8	-5.8
2.10	71.9	33.2	-5.1	78.0	24.3	-2.3	71.3	34.3	-5.6
2.20	70.7	33.9	-4.6	77.5	25.0	-2.5	70.1	35.0	-5.1
2.40	69.2	36.7	-5.9	76.5	26.8	-3.3	68.3	37.5	-5.8
2.50	69.4	37.6	-7.0	78.0	27.4	-5.4	69.0	38.7	-7.7

*R = reflectance, T = transmittance, A = absorptance.

TABLE 41.- SPECTROPHOTOMETER TEST RESULTS FOR PRESSURE-SINTERED MODELS MADE FROM PARTICLE SIZE 5*

Wavelength, μm	SPS15-94, t = 0.51 cm (0.20 in.)			SPS15-95, t = 0.51 cm (0.20 in.)			SPS15-96, t = 0.51 cm (0.20 in.)		
	R, %	T, %	A, %	R, %	T, %	A, %	R, %	T, %	A, %
0.25	59.3	0.0	40.7	57.7	0.0	42.3	55.9	0.0	44.1
0.30	69.1	0.0	30.9	67.9	0.0	32.1	66.6	0.0	33.4
0.35	81.0	0.0	19.0	80.8	0.0	19.2	79.3	0.0	20.7
0.40	84.4	0.0	15.6	82.0	0.3	17.7	81.2	0.3	18.5
0.45	86.6	0.1	13.3	85.0	0.5	14.5	83.5	1.1	15.4
0.50	88.8	0.1	11.1	87.2	0.7	12.1	85.3	1.2	13.5
0.60	91.1	0.2	8.7	89.0	0.8	10.2	86.8	1.6	11.6
0.70	93.1	0.4	6.5	91.0	1.2	7.8	88.8	1.9	9.3
0.80	93.8	0.7	5.5	92.1	1.6	6.3	90.2	2.7	7.1
0.90	93.9	0.9	5.2	92.1	1.8	6.1	90.2	2.8	7.0
1.00	93.9	0.9	5.2	93.0	1.9	5.1	90.0	2.8	7.2
1.20	93.7	0.9	5.4	93.0	1.9	5.1	89.6	2.9	7.5
1.40	93.6	0.9	5.5	92.0	1.9	6.1	89.6	3.1	7.3
1.60	93.6	1.0	5.4	91.0	2.1	6.9	89.3	3.4	7.3
1.80	93.5	1.1	5.4	91.0	2.2	6.8	89.2	3.5	7.3
1.90	93.5	1.1	5.4	90.0	2.2	7.8	89.3	3.4	7.3
2.00	93.6	1.1	5.3	91.0	2.1	6.9	89.4	3.5	7.1
2.10	93.5	1.1	5.4	90.0	2.0	8.0	89.1	3.7	7.2
2.20	93.5	1.2	5.3	90.0	1.9	8.1	89.1	3.8	7.1
2.40	93.7	1.0	5.3	90.0	1.9	8.1	89.2	3.6	7.2
2.50	93.4	0.8	5.8	90.0	1.9	8.1	88.8	3.1	8.1

*R = reflectance, T = transmittance, A = absorptance.

TABLE 42.- SPECTROPHOTOMETER TEST RESULTS FOR PRESSURE-SINTERED MODELS MADE FROM PARTICLE SIZE 6 [Higher-Density Configuration, Pressed at 2.8 GN/m^2 (46 000 $lb/in.^2$)]*

Wavelength, μm	SPS60-97, t = 0.51 cm (0.20 in.)			SPS60-98, t = 0.51 cm (0.20 in.)			SPS60-99, t = 0.51 cm (0.20 in.)		
	R, %	T, %	A, %	R, %	T, %	A, %	R, %	T, %	A, %
0.25	26.3	0.0	73.7	23.4	0.0	76.6	25.6	0.0	74.4
0.30	38.1	0.0	61.9	36.5	0.0	63.5	38.4	0.0	61.6
0.35	65.9	7.1	27.0	64.5	7.4	28.1	65.8	10.5	23.7
0.40	65.6	7.6	26.8	62.6	8.2	29.2	63.7	7.8	28.5
0.45	68.0	10.6	21.4	66.0	12.0	22.0	68.9	11.7	19.4
0.50	68.0	11.8	20.2	68.5	13.0	18.5	70.9	12.7	16.4
0.60	73.2	13.1	13.7	70.9	14.3	14.8	73.5	13.9	12.6
0.70	74.8	14.4	10.8	72.8	15.8	11.4	74.5	15.4	10.1
0.80	76.2	16.5	7.3	74.8	18.1	7.1	76.0	17.7	6.3
0.90	75.9	17.3	6.8	74.6	19.4	6.0	75.8	18.8	5.4
1.00	75.6	18.3	6.1	74.3	20.4	5.3	75.6	19.8	4.6
1.20	74.8	20.0	5.2	73.7	22.0	4.3	75.0	21.5	3.5
1.40	74.5	21.8	3.7	73.6	24.0	2.4	74.6	23.5	1.9
1.60	74.1	23.2	2.7	73.3	25.5	1.2	74.4	24.9	.7
1.80	73.3	25.0	1.7	72.5	27.3	.2	73.5	26.7	-.2
1.90	73.9	26.3	-.2	73.4	28.8	-2.2	74.1	28.2	-2.3
2.00	74.1	27.3	-1.4	73.5	30.0	-3.5	74.2	29.3	-3.5
2.10	73.5	27.9	-1.4	72.9	30.3	-3.2	73.6	29.9	-3.5
2.20	72.5	28.8	-1.3	72.1	31.2	-3.3	72.6	30.7	-3.3
2.40	71.0	30.8	-1.8	70.6	33.8	-4.4	71.2	33.2	-4.4
2.50	71.6	32.1	-3.7	71.0	35.1	-6.1	71.5	34.2	-5.7

*R = reflectance, T = transmittance, A = absorptance.

TABLE 43.- SPECTROPHOTOMETER TEST RESULTS FOR PRESSURE-SINTERED MODELS MADE FROM PARTICLE SIZE 6 [Lower-Density Configuration, Pressed at 2.1 GN/m^2 (30 000 lb/in.^{2})]*

Wavelength, μm	SPS60-100, t = 0.51 cm (0.20 in.)			SPS60-101, t = 0.51 cm (0.20 in.)			SPS60-102, t = 0.51 cm (0.20 in.)		
	R, %	T, %	A, %	R, %	T, %	A, %	R, %	T, %	A, %
0.25	15.4	0.0	84.6	16.9	0.0	83.1	16.0	0.0	84.0
0.30	28.8	0.5	71.2	29.4	0.9	69.7	31.0	0.5	68.5
0.35	61.8	14.6	23.6	62.0	14.0	24.0	62.2	14.2	23.6
0.40	59.2	13.8	27.0	59.7	13.5	26.8	59.2	13.2	27.6
0.45	63.3	16.9	19.8	63.0	16.4	20.6	64.2	16.2	19.6
0.50	66.2	18.6	15.2	66.1	17.6	16.3	66.2	17.0	16.8
0.60	70.1	19.7	10.2	70.2	18.5	11.3	70.2	18.9	10.9
0.70	71.0	20.8	8.2	71.4	19.7	8.9	70.9	19.9	9.2
0.80	73.8	23.2	3.0	74.0	21.8	4.2	73.8	22.4	3.8
0.90	74.4	24.2	1.4	74.6	22.9	2.5	74.2	23.4	2.4
1.00	74.2	24.9	.9	74.4	23.4	2.2	74.0	24.2	1.8
1.20	73.4	26.2	.4	73.6	24.7	1.7	73.4	25.3	1.3
1.40	73.4	27.7	-1.1	73.8	26.1	.1	73.4	27.0	-.4
1.60	73.6	28.8	-2.4	73.6	27.2	-.9	73.3	28.0	-1.3
1.80	72.7	30.2	-2.9	72.7	28.6	-1.3	72.4	29.5	-1.9
1.90	73.3	31.7	-3.0	73.5	30.0	-3.5	73.1	30.9	-4.0
2.00	73.5	32.6	-6.1	73.7	30.8	-4.5	73.2	31.8	-5.0
2.10	72.7	33.0	-5.7	72.9	31.1	-4.0	72.6	32.1	-4.7
2.20	71.7	33.5	-5.2	72.1	31.8	-3.9	71.5	32.8	-4.3
2.40	69.8	36.1	-5.9	70.5	34.0	-4.5	61.8	35.0	-4.8
2.50	70.5	37.2	-7.7	71.0	35.0	-6.0	70.4	36.1	-6.5

*R = reflectance, T = transmittance, A = absorptance.

TABLE 44.- MECHANICAL PROPERTIES OF PRESSURE-SINTERED MODELS MADE FROM PARTICLE SIZE 2, PRESSED AT 0.317 GN/m^2 (4.6×10^4 $lb/in.^2$), AND FIRED 20 hr AT 1333°K (1940°F)

Model number	Density		Modulus of rupture		Modulus of elasticity	
	g/cm^3	lb/ft^3	MN/m^2	$lb/in.^2$	GN/m^2	$lb/in.^2$
FPS4-011	1.90	119	8.27	1.20×10^3	57.2	8.28×10^6
FPS4-012	1.87	117	7.79	1.13	64.8	9.40
FPS4-013	1.92	120	7.24	1.05	65.6	9.52
Average	1.90	119	7.77	1.13	62.4	9.08

TABLE 45.- MECHANICAL PROPERTIES OF PRESSURE-SINTERED MODELS MADE FROM PARTICLE SIZE 4, PRESSED AT 0.317 GN/m^2 (4.6×10^4 $lb/in.^2$), AND FIRED 18 hr AT 1438°K (2128°F)

Model number	Density		Modulus of rupture		Modulus of elasticity	
	g/cm^3	lb/ft^3	MN/m^2	$lb/in.^2$	GN/m^2	$lb/in.^2$
FPS10-031	2.13	133	17.8	2.58×10^3	43.6	6.32×10^6
FPS10-032	2.14	134	16.3	2.37	58.0	8.40
FPS10-033	2.13	133	*	*	*	*
Average	2.13	133	17.0	2.48	50.8	7.36
*Invalid data; model failed prematurely.						

TABLE 46.- MECHANICAL PROPERTIES OF PRESSURE-SINTERED MODELS MADE FROM PARTICLE SIZE 5, PRESSED AT 0.317 GN/m^2 (4.6×10^4 $lb/in.^2$), AND FIRED 18 hr AT 1393°K (2047°F)

Model number	Density		Modulus of rupture		Modulus of elasticity	
	g/cm^3	lb/ft^3	MN/m^2	$lb/in.^2$	GN/m^2	$lb/in.^2$
FPS15-043	2.14	134	9.65	1.40×10^3	70.4	10.2×10^6
FPS15-044	2.14	134	11.0	1.59	70.0	10.2
FPS15-045	2.15	134	8.27	1.20	70.8	10.3
Average	2.14	134	9.64	1.40	70.4	10.2

TABLE 47.- MECHANICAL PROPERTIES OF PRESSURE-SINTERED MODELS MADE FROM PARTICLE SIZE 6, HIGHER-DENSITY CONFIGURATION, PRESSED AT 0.317 GN/m^2 (4.6 x 10^4 lb/in.^{2}), AND FIRED 8 hr AT 1440°K (2146°F) AND 16 hr AT 1333°K (1940°F)

Model number	Density		Modulus of rupture		Modulus of elasticity	
	g/cm^3	lb/ft^3	MN/m^2	lb/in.^{2}	GN/m^2	lb/in.^{2}
FPS60-051	2.09	130	32.5	4.72 x 10^3	66.4	9.60 x 10^6
FPS60-053	2.08	130	31.2	4.52	63.6	9.24
FPS60-054	2.09	130	30.1	4.37	66.0	9.04
Average	2.09	130	31.3	4.54	64.0	9.28

TABLE 48.- MECHANICAL PROPERTIES OF PRESSURE-SINTERED MODELS MADE FROM PARTICLE SIZE 5, LOWER-DENSITY CONFIGURATION, PRESSED AT 0.207 GN/m^2 (3.0 x 10^4 lb/in.^{2}), AND FIRED 16 hr AT 1523°K (2281°F)

Model number	Density		Modulus of rupture		Modulus of elasticity	
	g/cm^3	lb/ft^3	MN/m^2	lb/in.^{2}	GN/m^2	lb/in.^{2}
FPS60-055	2.07	129	29.6	4.30 x 10^3	60.4	8.76 x 10^6
FPS60-056	2.07	129	26.3	3.81	59.6	8.64
FPS60-057	2.07	129	*	*	*	*
Average	2.07	129	28.0	4.06	60.0	8.68

*Invalid data; model failed prematurely.

TABLE 49.- XENON ARC-LAMP TEST RESULTS FOR PRESSURE-SINTERED CONFIGURATIONS MADE FROM VARIOUS PARTICLE SIZES [All Models 0.51 cm (0.20 in.) Thick]

Model number	Composition	Preparation*	Incident flux		Transmittance, %	Average transmittance, %
			W/cm^2	Btu/ft^2-sec		
DPS4-88	100% PS-2	A	1070	944	1.65	1.66
DPS4-89	100% PS-2	A	1070	944	1.68	
DPS4-90	100% PS-2	A	1070	944	1.66	
DPS10-91	100% PS-4	B	1070	944	21.4	18.8
DPS10-92	100% PS-4	B	1070	944	14.0	
DPS10-93	100% PS-4	B	1070	944	21.0	
DPS15-94	100% PS-5	C	1020	901	2.51	9.50
DPS15-95	100% PS-5	C	1020	901	9.80	
DPS15-96	100% PS-5	C	1020	901	16.2	
DPS60-97	100% PS-6	D	1110	975	20.8	20.1
DPS60-98	100% PS-6	D	1110	975	19.5	
DPS60-99	100% PS-6	D	1110	975	20.0	
DPS60-100	100% PS-6	E	1100	971	20.1	19.0
DPS60-101	100% PS-6	E	1100	971	18.4	
DPS60-102	100% PS-6	E	1100	971	18.4	

*Preparations:

A = Pressed at 0.317 GN/m^2 (4.6×10^4 $lb/in.^2$), fired 20 hours at 1333°K (1940°F)
B = Pressed at 0.317 GN/m^2 (4.6×10^4 $lb/in.^2$), fired 18 hours at 1438°K (2128°F)
C = Pressed at 0.317 GN/m^2 (4.6×10^4 $lb/in.^2$), fired 18 hours at 1393°K (2047°F)
D = Pressed at 0.317 GN/m^2 (4.6×10^4 $lb/in.^2$), fired 8 hours at 1448°K (2146°F) then 16 hours at 1333°K (1940°F)
E = Pressed at 0.207 GN/m^2 (3.0×10^4 $lb/in.^2$), fired 16 hours at 1523°K (2281°F).

V. FULL-SIZE HEAT SHIELD FABRICATION AND ATTACHMENT

A. FUSED-SILICA HEAT SHIELD FABRICATION

1. Slip preparation.- Various high-purity grades of synthetic and natural fused silica are commercially available (e.g., Amersil, Inc.; Dynasil, Inc.; and General Electric) in a variety of geometric forms such as rods, discs, ribbons, and tubes. After extensive quality control tests on each lot of these raw, fused silicas, as discussed in a following section, the materials would be crushed in a jaw crusher mill or other suitable crushing apparatus.

The jaw lining material should be sufficiently hard and able to be readily and completely removed by physical or chemical means. Iron jaws are frequently used because iron contamination is easily removed magnetically or by dissolution in a mineral acid, preferably hydrochloric. Alumina jaws can also be used, but alumina is difficult to remove from fused silica. (It has not yet been determined whether alumina is a detrimental impurity in a silica reflecting heat shield. As discussed in Section II, aluminum cations have been found to be capable of counteracting the detrimental effect of alkali metals in a silica matrix.) In addition, high-purity fused silica jaws might also be used to crush the material, but such jaws would probably need frequent replacing due to rapid wear.

To comminute the crushed and purified cullet for preparing the 75/25% blend configurations, fluid-energy milling is the recommended method. (Fluid-energy milling has been discussed in Section III.)

One advantage of the fluid-energy mill is that it can produce optimum-sized particles with a minimum of wasted material (i.e., particles that have been milled too fine). The alternative would be ball milling, but this produces a very wide size distribution of particles (ref. fig. 18) and a large amount of waste material. Since this study indicates that synthetic fused silica is the best material to use in a reflecting heat shield, and since this material is expensive [from $440 to $880 per kilogram ($200 to $400 per pound) in small quantities], waste material should be minimized.

The second, and most important reason for using fluid-energy milling, is that it produces a noncontaminated, fused-silica powder. The entire inside surface of the mill and the collecting apparatus can be made from, or lined with, very-high-purity, slip-cast silica. [If a mill is lined with polyurethane, then the organic contamination from this lining could be burned out by heating the silica powder in a furnace at 1313°K (1000°F).]

After being comminuted, the fluid-energy-milled particles must be further classified to segregate the small amounts of fines and oversized particles that inevitably result from any milling process. Three classification techniques appear feasible: air classification, using an air classifier such as the Donaldson A12 or B18 models; elutriation in aqueous media, using a Babcock-Schultz elutriator; or sedimentation in aqueous media, using a larger-scale version of the technique shown in figure 17. Each of these methods gives satisfactory classification; however, from the standpoint of production economics, air classification appears to be the best method at this time.

The slip can be prepared using basically the same procedure outlined in Section III, but with larger proportions. One difference is that the slip will be prepared in polyethylene or polypropylene containers, rather than glass, to eliminate contamination by alkali silicates. The slip will then be rolled for a suitable time to provide thorough mixing while minimizing further particle-size reduction and will be evacuated before being cast to remove trapped air.

2. Casting.- Fused-silica radomes made from continuous-particle-size slips have used the type of mold shown in figure 35. After the plaster mold is filled with slip, the system is pressurized to increase the drainage rate. After a sufficient time to build up a specific wall thickness, the mold is depressurized and inverted, and the excess slip is poured out, leaving behind a radome shell.

Casting a thick-walled radome without pressurization requires a long fabrication period. Long times are detrimental because the larger particles settle out of the slip and the wall thickness becomes nonuniform from top to bottom. The relationship between the wall thickness and casting time at different pressures is shown in figure 36.

A fused-silica heat shield for an outer-planet probe will require a thickness of at least 2.5 cm (1.0 in.). Note in figure 36 that casting such a thickness, even at a pressure of 0.414 MN/m^2 (60 $lb/in.^2$), will take longer than 2 hours. Thus, segregation of particles in the slip will be an important problem, and the cast heat shield could possess considerable variation with respect to its mechanical properties.

A convenient and valuable aspect of slip casting using 100% monodisperse and 75/25% blend slips is that the drain times are significantly reduced. With such materials the drainage time is measured in minutes rather than hours, even at ambient pressure. Thus, there is little particle separation. Because of this rapid drainage rate, the type of casting described above--where the excess slip is removed after a given time, leaving behind a cast shell--is neither practical nor necessary.

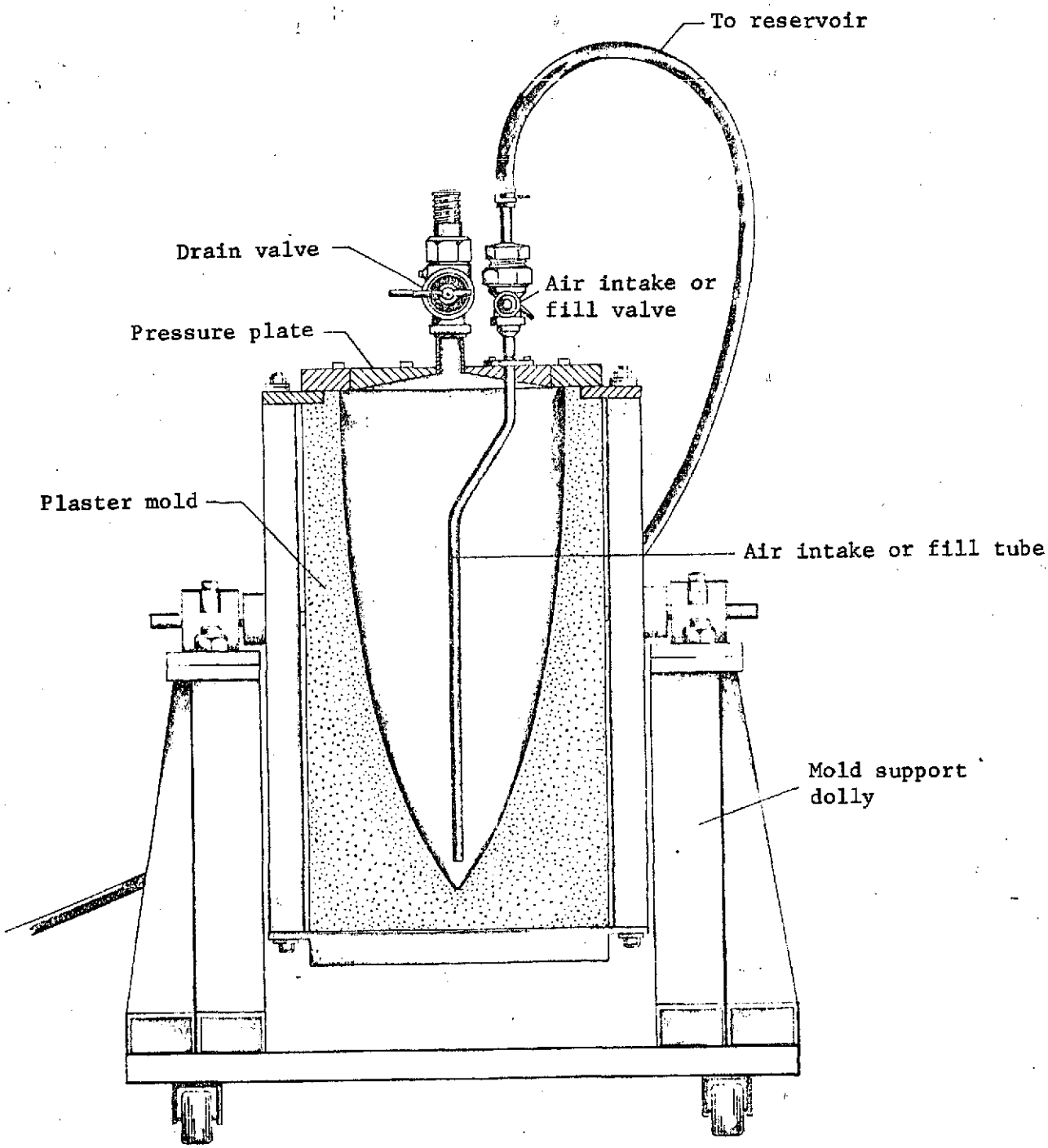

Figure 35.- Pressure-casting setup for slip-casting the fused-silica radome (ref. 22)

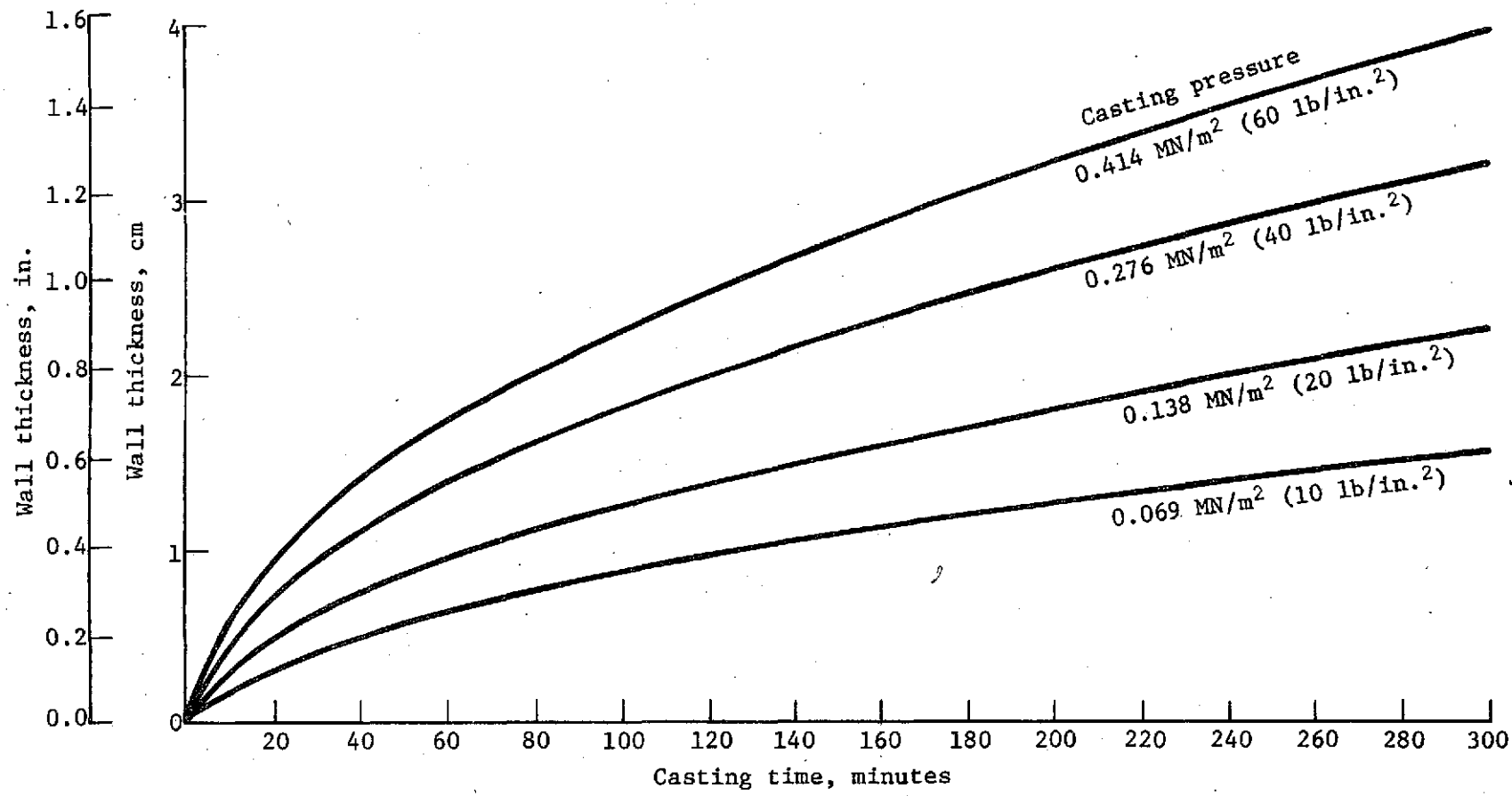

Figure 36.- Cast wall thickness vs. casting time at different pressures for continuous-particle-size, slip-cast fused silica (ref. 21)

Figure 37 shows a preliminary mold designed for casting an 89-cm (35-in.) diameter, 2.5-cm (1.0-in.) thick, fused-silica heat shield from 75/25% blend slips. This is the approximate size and shape of a single-piece heat shield for an outer-planet probe.

The mold is made from plaster, has two pieces, and is supported by an aluminum structure. The top piece has eight reservoirs or fill holes, each approximately 5.1 cm (2.0 in.) in diameter and 7.6 cm (3.0 in.) deep. The slip is simultaneously poured into four of these holes and the remaining four are used as air vents. Once the mold is full, all the reservoirs are filled to allow for shrinkage during draining (the shrinkage for these slips is much less than for the continuous-particle-size slips). After a sufficient time for drying, the entire mold and supporting structure is inverted and the mold is opened, and the cast silica piece is then separated from the male portion of the mold. Afterward, the heat shield is allowed to dry further before being fired.

The cast article should have enough green strength to be handled before and during firing. If not, it can be supported in a fused-silica mandrel that has essentially the same shape as the female portion of the plaster mold.

The inside surfaces of the plaster mold are coated with ammonium alginate or soluble starch before casting the article to prevent the fused silica from adhering to the mold.

3. Quality control.- The work performed under the present program indicates that the raw materials used to produce a silica heat shield must be carefully inspected and tested for impurities and contamination. In addition, extensive testing will be necessary at various stages in the production cycle to determine which steps, if any, are introducing impurities, and to what degree.

The following tests should be performed on the as-received silica materials:

1) Atomic absorption, flame-emission analyses;

2) Visible and UV transmission analyses;

3) X-ray diffraction analyses.

a. Atomic absorption and flame emission analyses: These tests are conducted to determine the concentration of detrimental impurities such as Li, Na, K, Mg, Ca, and Fe. The randomly selected pieces of cullet are cleaned in a dilute hydrofluoric acid solution (10%) and dried. Then they are completely dissolved in hydrofluoric acid and the solution is tested on the spectrophotometer against standard solutions.

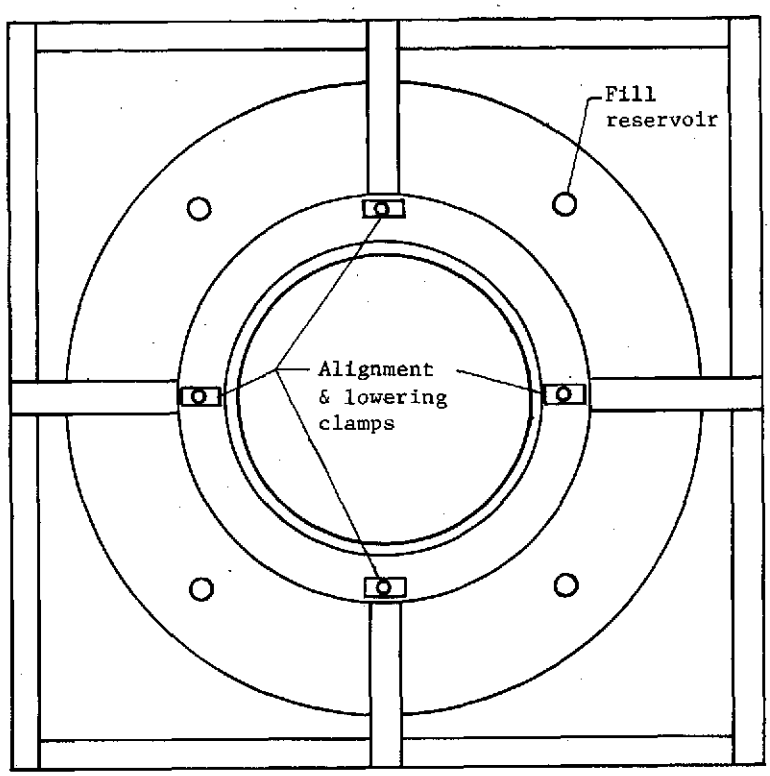

a) Top view

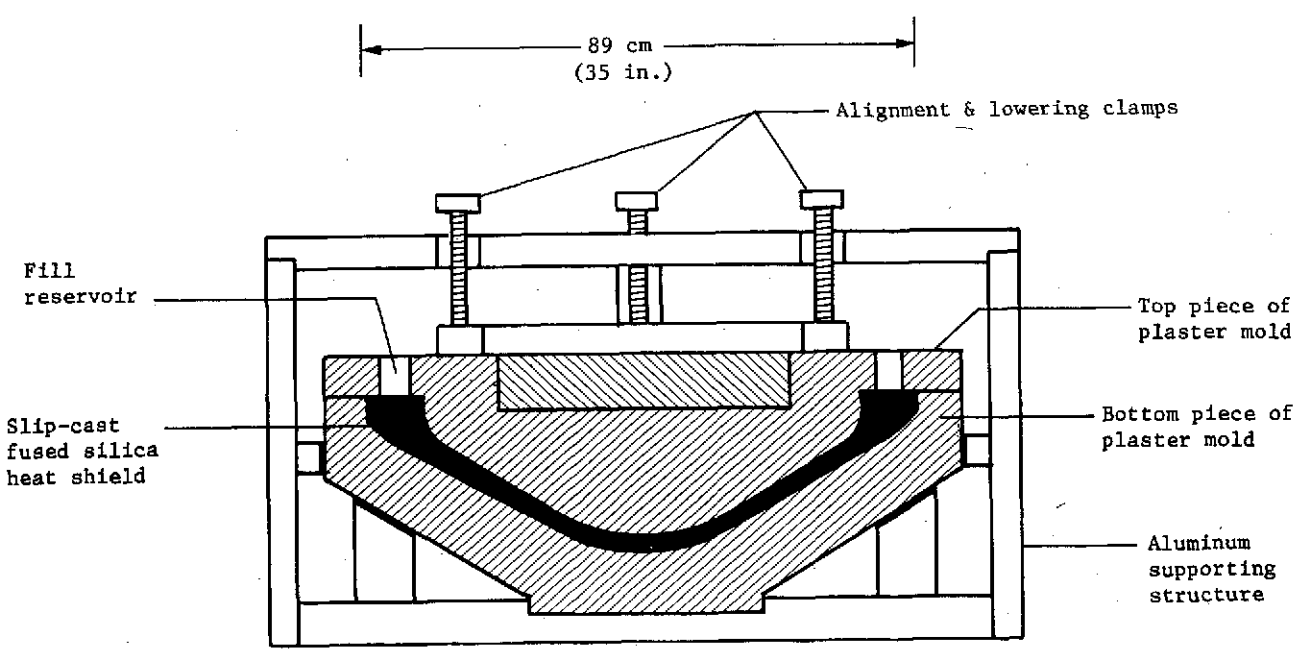

b) Cross-section view

Figure 37.- Two-piece plaster mold for slip-casting a single-unit, fused-silica heat shield for an outer-planet probe

b. Visible and UV transmission analyses: The relationship and positioning of the impurity in the matrix influences the degree of attenuation by absorption. Also, reduced species such as Si^{+3} and Si^{+2} are absorbing chromophores. Randomly selected pieces of cullet with a known thickness are cleaned and tested to determine their spectral transmittance and, thus, absorptance. The results are compared against nominal specification curves.

c. X-ray diffraction analyses: The presence of cristobalite and other crystalline forms of silicon dioxide in fused silica is undesirable and strongly affects properties such as the thermal expansion and thermal shock resistance. X-ray diffraction analyses are performed to determine the material's degree of crystallinity.

When preparing the fused-silica slips, various samples should be subjected to atomic absorption and flame emission analyses at various stages in the production process to check whether impurities are being introduced. The processing steps should then be modified as required to eliminate contamination.

The logical times for testing are as follows:

1) After crushing and postcleaning the fused-silica material with hydrochloric acid;

2) After fluid-energy milling;

3) After classifying the material;

4) After preparing the slip and rolling it in the plastic containers;

5) After casting, drying, and firing the finished article;

6) After machining the final configuration.

B. Fused-Silica Heat Shield Attachment

The following section discusses the attachment of a fused-silica reflecting heat shield in terms of the baseline configuration for the Mariner Jupiter-Uranus entry probe. The forebody of this probe is a 1.05-rad (60°) half-angle cone with an 89-cm (35-in.) base diameter (ref. 24); the ratio of the nose radius-to-base radius is taken as 0.5, and the probe has a hemispherical afterbody. The probe weight has been estimated to be 108 kg (239 lb) (ref. 24). The silica heat shield would cover the entire conical forebody.

Slip-cast fused silica is the most promising reflective heat shield material for outer-planet missions (ref. 25). Typical properties of a fused-silica material made from 75/25% blend slips are given in table 50.

TABLE 50.- TYPICAL PROPERTIES OF AN EFFICIENT, FUSED-SILICA, REFLECTING HEAT SHIELD

Density, g/cm^3 (lb/ft^3)	1.5 (93.6)
Porosity, %	31
Flexural strength, MN/m^2 ($lb/in.^2$)	20.7 (3000)
Flexural modulus, GN/m^2 ($lb/in.^2$)	32.4 (4.7×10^6)
Coefficient of thermal expansion,* cm/cm/°K (in./in./°F)	0.9×10^{-6} (0.5×10^{-6})
Thermal conductivity at 435°K (324°F), J/m-s-°K (Btu/hr-ft-°F)	0.268 (0.155)
Poisson's ratio*	0.17
Young's modulus/shear modulus*	2.3
Specific heat,* J/kg-°K (Btu/lb-°F)	753 (0.18)

*From reference 23.

The surface area of the conical forebody (neglecting the hemispherical nose radius) is:

$$A = \pi rs$$

where:

r = base radius = 44.5 cm (17.5 in.)

s = slant height = 51.3 cm (20.2 in.)

A = 7160 cm^2 (1110 $in.^2$).

Assuming a silica thickness of 2.54 cm (1.00 in.), the forebody would have a volume of 18 190 cm^3 (1110 $in.^3$). Based on a density of 1.5 g/cc (94 lb/ft^3), the silica heat shield would weigh 27.2 kg (60 lb).

During entry into the Uranus atmosphere at an entry angle of -0.87 rad (-50°), the heat shield can be subjected to a dynamic pressure of 1.01 MN/m^2 (10 atm), or 50% of the stagnation pressure, and to a peak deceleration force of 750 g (ref. 26). At an entry angle of -0.70 rad (-40°), which represents the nominal entry attitude, the dynamic pressure would be approximately 0.527 MN/m^2 (5.2 atm) and the peak deceleration would be 390 g (ref. 24).

Critical dynamic forces for spacecraft are generally associated with the acoustic noise generated during ascent. A typical acoustic criterion for the Titan III launch vehicle is an overall random noise of 150 dB, with a peak at 2000 Hz for 1 minute of total exposure. However, the resulting "g" loads are substantially less than those associated with entry.

Figure 38 shows the net forces on the heat shield during entry. At an entry angle of -0.87 rad (-50°), the pressure force of 0.630 MN (141 500 lb) is partially offset by the heat shield inertia force of 0.200 MN (45 000 lb), yielding a net force of 0.430 MN (96 500 lb). At an entry angle of -0.70 rad (-40°), the net compressive force on the heat shield is 0.222 MN (50 100 lb).

In the following paragraphs, attachment configurations and stresses will be discussed for a nominal -0.70 rad (-40°) entry.

The structural behavior of slip-cast fused silica, like that of other ceramics, is governed by the brittle nature of the material. When designing with a brittle material, the following principles must be recognized:

1) The fracture strength is defined statistically;

2) A high degree of scatter can be associated with mechanical properties;

3) Brittle materials are stronger in compression than in tension;

4) The average strength decreases as the specimen size increases;

5) Strength increases with temperature;

6) The materials are sensitive to mechanical shock;

7) Components exhibit a high degree of notch sensitivity.

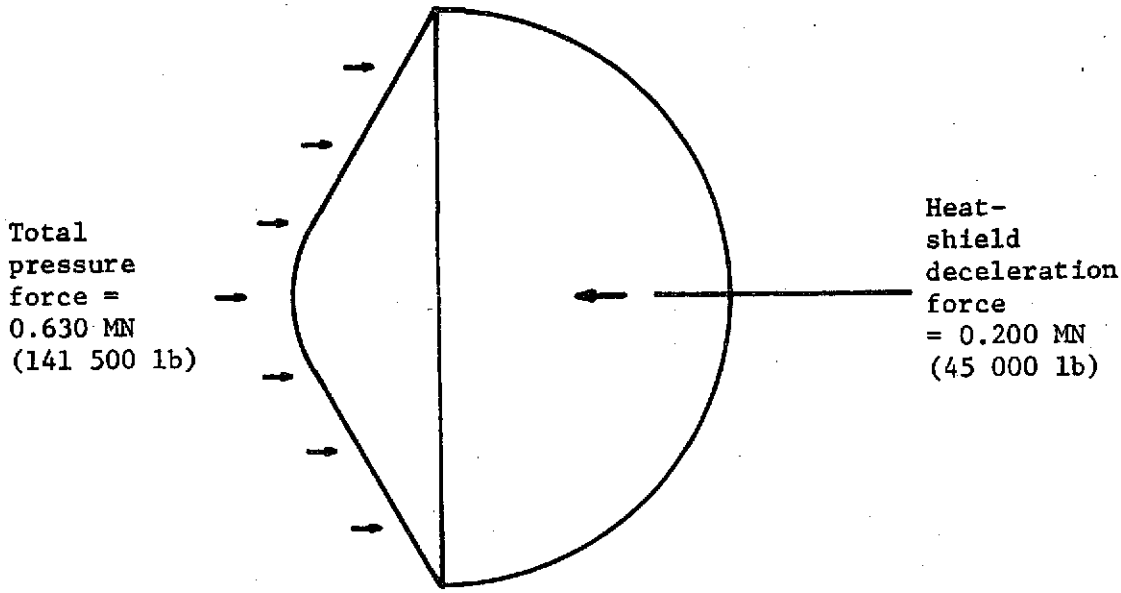

Net force on heat shield = 0.630 - 0.200 = 0.430 MN
(141 500 - 45 000 = 96 500 lb)

a) Entry angle = -0.87 rad (-50°)

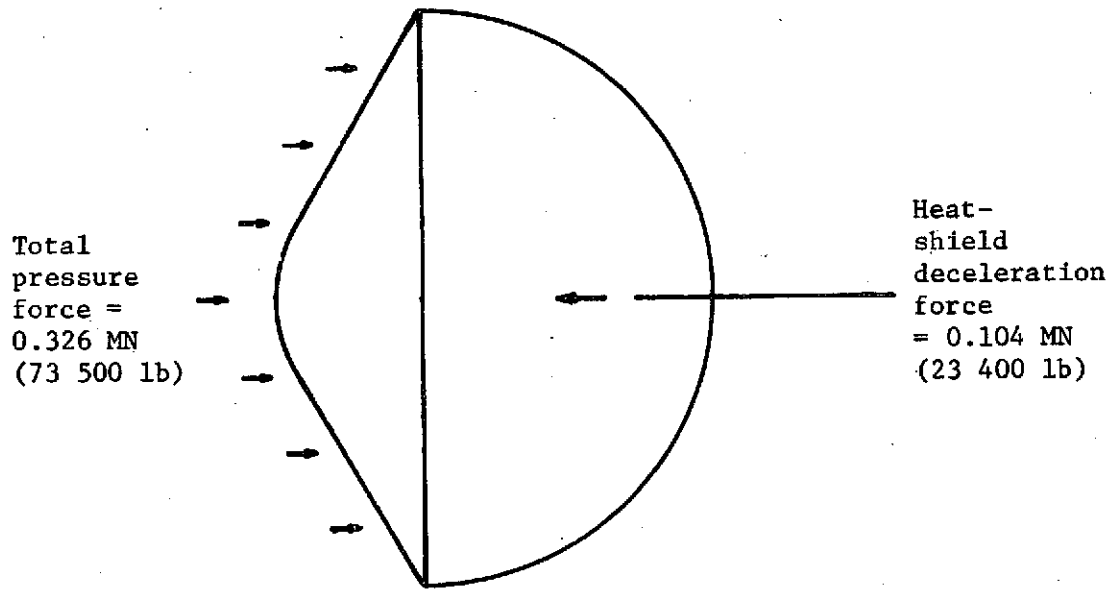

Net force on heat shield = 0.326 - 0.104 = 0.223 MN
(73 500 - 23 400 = 50 100 lb)

b) Entry angle = -0.70 rad (-40°)

Figure 38.- Net forces on conical-forebody heat shield for Uranus entry

Brittle behavior denotes the absence of yielding. When a local stress reaches the limit of the material's capability, a fracture will result. Therefore, attachment design requires that:

1) Nonredundant attachments, which permit an accurate determination of loads, must be used;

2) Any alignment during assembly must be avoided, since misfits, which introduce a high local stress, can cause a failure;

3) Proper account must be taken of all stress raisers due to section changes, discontinuities, locally applied loads, etc;

4) Joints between ceramic and metallic support structures must account for thermal expansion differences;

5) Restraint of thermal distortions must be minimized;

6) The design-allowable strength must be based on a desired probability of survival under given loading conditions.

The high loads encountered during entry, along with the moderate strength of slip-cast fused silica, rules out point attachments such as pin connections, since the resulting stresses would be too high. Consequently, a continuous attachment must be used over a large area of the silica heat shield to reduce the attachment stresses to acceptable values. A direct ceramic-to-metal attachment, via bolts, clamps, or snap ring devices, is not recommended because a slight misalignment of the mating surfaces can overload a local portion of the silica heat shield. Instead, the preferred method is to bond the shield to a metal structure through an elastomeric rubber pad. This attachment would be limited to a maximum temperature of 523° to 573°K (482° to 572°F). The rubber pad would:

1) Compensate for misalignments between mating ceramic and metallic surfaces;

2) Compensate for differential expansion between the ceramic and metal;

3) Allow thermal distortion of the silica heat shield due to temperature gradients;

4) Attenuate dynamic loads and shock loads via damping.

If temperature resistance to 573°K (572°F) as well as flexibility at low temperatures is required, then a silicone rubber pad must be used. The required pad stiffness, thickness, and strength must be determined as part of a detail design. The strength and temperature resistance of the bonding agent must be similar to that of the rubber pad. If a liquid adhesive system is used, care must be taken to prevent the adhesive from penetrating into the porous, slip-cast silica and interfering with the reflective and scattering properties of the silica heat shield.

The bond between the metallic structure and the silica heat shield (through an elastomeric pad) can be made in two ways:

1) By using a metal base ring;

2) By making a continuous attachment between the silica backface and a metallic backup structure.

Figure 39 shows a representative base-ring attachment method. For a compression load of 0.222 MN (50 100 lb), the compression stress in the rubber pad would be 2.29 MN/m^2 (332 $lb/in.^2$). The thermal coefficient of expansion of the rubber pad can be on the order of 25×10^{-5} cm/cm/°K (45×10^{-5} in./in./°F). Therefore, care must be taken to preserve the integrity of the bond and to prevent introducing stresses into the ceramic.

Note that in this type of design the metal ring is thermally isolated from the silica heat shield by the rubber pad, so its expansion coefficient may not be critical. Candidate materials for the ring are aluminum ($\alpha = 23.9 \times 10^{-6}/°K$), titanium ($\alpha = 8.5 \times 10^{-6}/°K$), and beryllium ($\alpha = 13.3 \times 10^{-6}/°K$).

Bending stresses due to entry loads in a 2.54-cm (1.00-in.) thick silica shell have been calculated to be less than 3.45 MN/m^2 (500 $lb/in.^2$). Shear stresses at the 31-cm (12.25-in.) radius (see fig. 39) will be approximately 1.91 MN/m^2 (277 $lb/in.^2$). Stresses of these magnitudes can be accommodated by a slip-cast, fused-silica heat shield. In addition, if the temperature at the bond-line rises above its permissible limit after the occurrence of significant heating and loading, a secondary mechanical attachment can be incorporated, as shown in figure 40. The metal channel fits loosely around the silica lip to permit unrestrained thermal expansion, and a layer of silica cloth and/or felt between the metallic member and the silica lip acts as a cushioning material. The metallic member would support the silica heat shield during the final stages of descent.

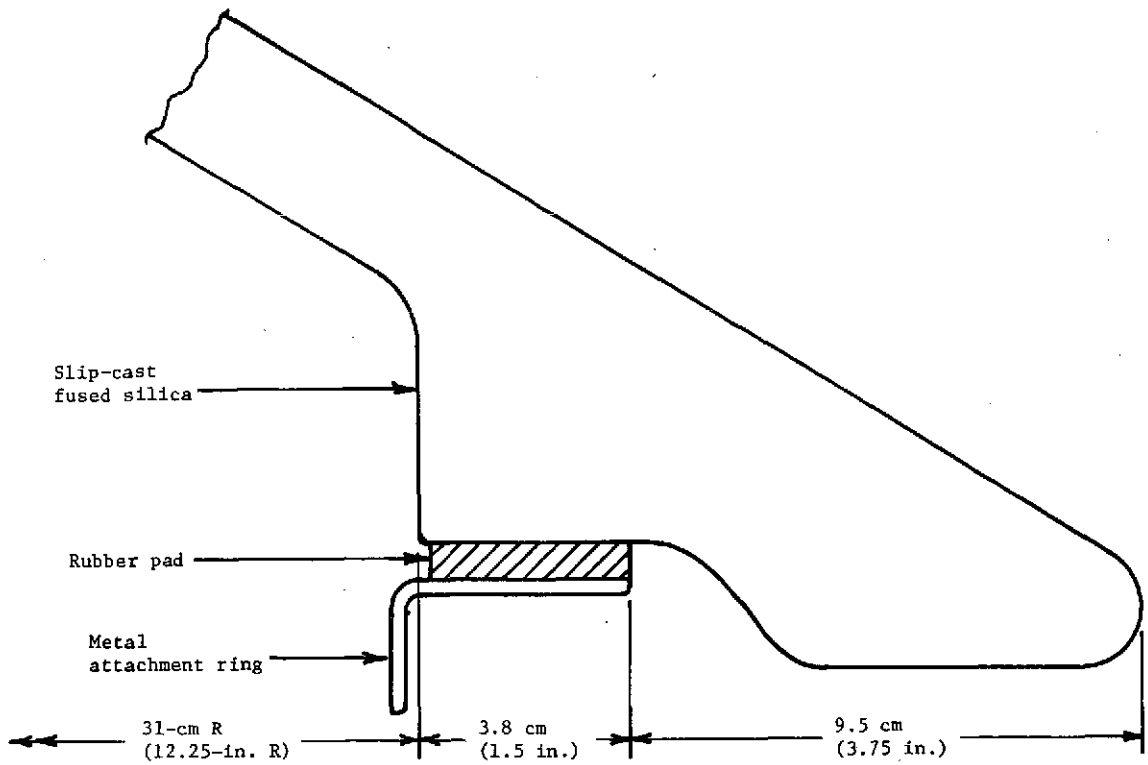

Base ring attachment for slip-cast fused silica heat shield

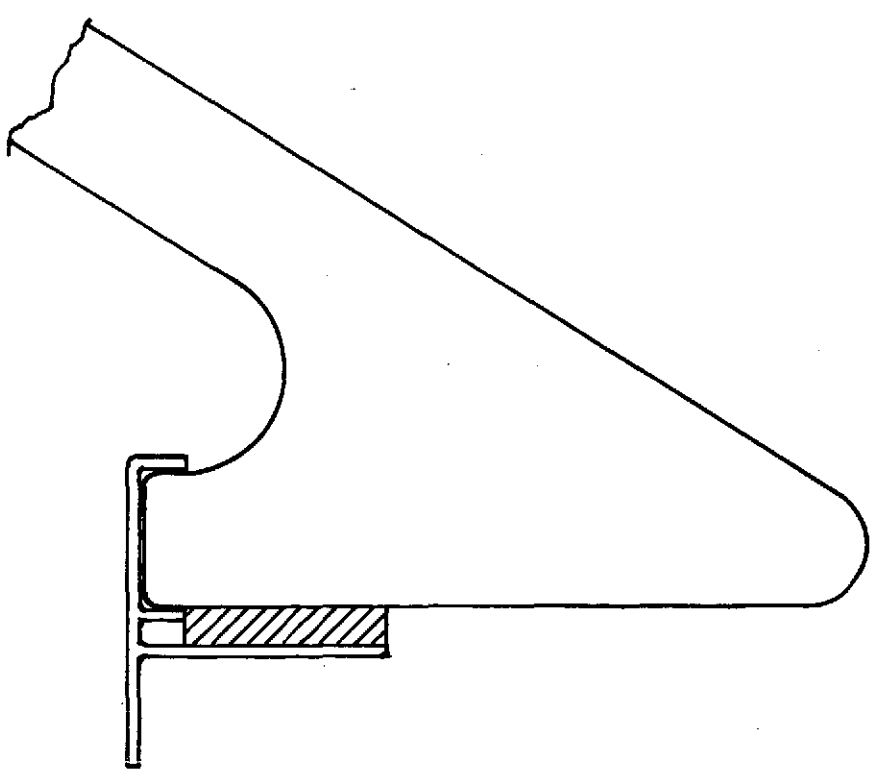

Figure 40.- Bonded base ring attachment with secondary mechanical retainer

The continuous attachment of a fused-silica heat shield to a metallic backup structure though a rubber pad provides a much greater attachment area than the base ring design. In this design the rubber pad must withstand a compressive stress of 0.269 MN/m^2 (39 $lb/in.^2$) and a shear stress of 0.155 MN/m^2 (22.5 $lb/in.^2$). These stresses can be accommodated by using a silicone sponge like that used as a strain isolator for the silica RSI thermal protection panels on the Space Shuttle. A secondary mechanical attachment, to retain the heat shield if the bondline overheats after the period of significant heating and loading, can also be incorporated into a continuous, bonded-attachment design.

A one-piece reflecting heat shield is preferred since the effects of joints on its reflection characteristics are unknown. However, a one-piece, fused-silica heat shield will be subjected to severe thermal gradients and, even with its low coefficient of thermal expansion and its low modulus of elasticity, significant thermal stresses may be generated. If these stresses exceed the strength of the fused-silica ceramic, then the heat shield must be made in sections, and attached by bonding each section through a strain isolator to a metallic backup structure.

As shown in figure 41, heat shield sections can be made in the following patterns:

1) A nose cap and a series of concentric rings;

2) A nose cap and a series of trapezoidal segments;

3) A series of tiles, approximately 15 by 15 cm (6 by 6 in.).

The optimum pattern would depend on thermal stresses, producibility, and the aerodynamics of the gaps and joints.

A damaged heat shield made from tiles can be repaired by replacing the damaged tile. Repairing a one-piece heat shield may depend on the nature of the damage, but could involve replacing the entire unit. Methods such as coring out and recasting damaged areas in a one-piece heat shield do not appear feasible at this time.

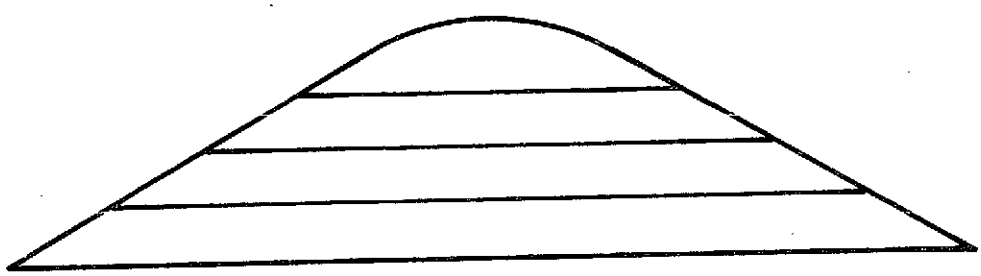

a) Nose cap and concentric rings

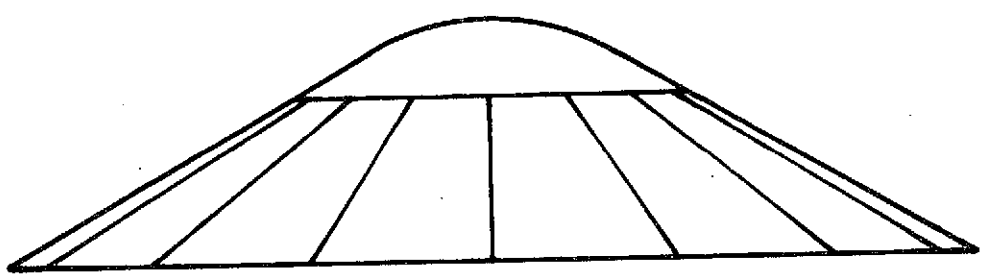

b) Nose cap and trapezoidal segments

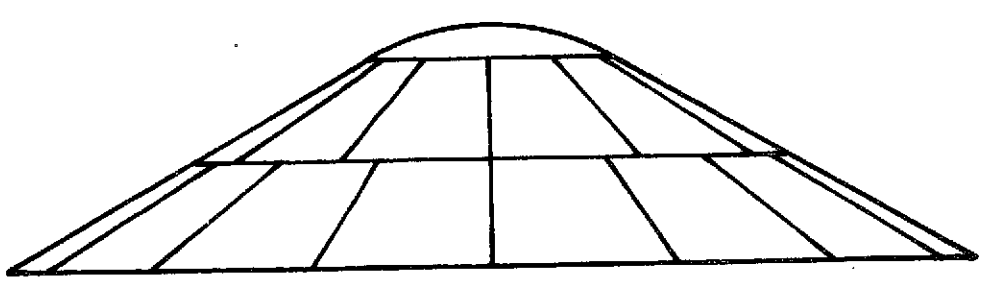

c) Trapezoidal tiles

Figure 41.- Section configurations for slip-cast silica heat shield

VI. CONCLUSIONS AND RECOMMENDATIONS

A. Summary of Program Results

The purpose of this program was to develop a high-purity, fused-silica heat shield to reflect shock-layer radiation and shield against the severe convective heating environment encountered during probe entries into outer-planet atmospheres. During the contract we also conducted theoretical investigations of the parameters that influence the optical, thermal and mechanical performance of fused silica. Three configurations of silica-bonded silica were fabricated and tested to ascertain their relative merits. These configurations were slip-cast, foamed-slip, and pressure-sintered fused silica. On the basis of these tests, we selected a preferred configuration and began to optimize the configuration and develop suitable processing techniques. Finally, we studied fabrication methods for a full-size heat shield and considered various alternatives for attaching the selected configuration.

Computer analyses using MSAP showed that in the absence of strong absorption, fused-silica particles ranging up to 28.8 μm in diameter produced higher reflectance than particles as small as 3.50 μm in diameter. However, in the presence of strong absorption--for instance, at high temperatures [e.g., 1773°K (2731°F)] or at impurity levels higher than GE 151, or both--the smaller particles produced higher reflectance. The analysis also showed that the reflectance increased with number of voids.

Relative to the predicted Saturn-entry shock-layer radiation, MSAP showed that the optimum reflectance for a fused-silica heat shield at 1773°K (2731°F) could be achieved by using 5- to 10-μm-diameter voids and a total void content of 20 to 30% by volume.

Of the three silica-bonded silica configurations studied, slip-cast fused silica proved to be the best configuration for a reflecting heat shield. It exhibited excellent radiation-scattering performance (i.e., high reflectivity) and was easy to fabricate. The low density of the foamed slip material is undesirable and would result in high surface recession during an outer-planet entry. Pressure-sintered fused silica is impractical because its fabrication is substantially more complex than slip-casting.

Of the various slip-cast configurations investigated, the ones prepared from the 75/25% blend slips performed the best (i.e., highest reflectance, lowest transmittance). Both the 100% monodisperse and 75/25% blend slips produced a better reflector, with noticeably reduced transmittance, than the continuous-particle-size slips generally used in slip-casting. In the 100% monodisperse configurations 5- to 11-μm-diameter particles gave higher reflectance and lower transmittance than the larger particles that were studied.

For the 75/25% blend slip-cast silicas, the configurations with 75% (by weight) of 5- to 11-μm-diameter particles gave the best performance. (Smaller particles may produce still higher reflectance, but can pose processing difficulties, and were not studied in this program.)

The 100% monodisperse and 75/25% blend configurations were less dense [1.35 g/cm^3 (84.5 lb/ft^3) and 1.50 g/cm^3 (93.8 lb/ft^3), respectively] than the slip-cast configurations made from continuous-particle-size slip [1.95 g/cm^3 (120 lb/ft^3)]. However, the higher reflectance and lower transmittance of the monodisperse configurations outweigh any increase in surface recession that might result from lower density. The mechanical strength of monodisperse, slip-cast silicas is lower than that of the continuous-particle-size, slip-cast silicas. However, the monodisperse materials have sufficient strength for an outer-planet heat shield.

For the slip-cast fused silicas, the higher-purity materials--especially materials with lower levels of alkali metals--produced the highest reflectance. The highest-purity fused silica that is commercially available is a synthetic, usually prepared by the vapor-phase hydrolysis of silicon tetrachloride. This is the preferred material for a reflecting heat shield. However, processing techniques that introduce impurities can easily nullify the benefits gained from using a synthetic fused silica. Therefore, noncontaminating processing techniques are essential in fabricating an optimum, fused silica reflecting heat shield.

Slip-cast materials made from 100% monodisperse fused-silica powders were more difficult to produce than the 75/25% blend configurations, due to casting problems that resulted in a large number of cracked billets. Since the monodisperse blends were easier to process, retained many of the advantageous optical characteristics of the 100% monodisperse material and had better mechanical properties than the 100% monodisperse material, the monodisperse blend configuration is recommended for silica reflective heat shields.

The fabrication of the 75/25% blends requires the use of colloidal silica. Presently available experimental low-sodium colloidal silicas contain sodium levels as high as 100 ppm of solids. At a proportion of 6% colloidal silica solids, an additional 6 ppm of sodium contamination is introduced into the final configuration by the colloidal silica. Lower-sodium colloidal silicas are desired, and these can be prepared by ion-exchange chromatography.

The monodisperse blend configurations have not been fully optimized. Their densities can be increased, within limits, by casting them at hydronium ion concentrations other than pH = 5.0, and/or by using larger quantities of colloidal silica. Their density, strength, and scattering properties can also be improved

by changing the proportion of the small-diameter component, the particle size of the small-diameter component, or both. Also, a small-particle-size third component could be added to the blend to improve performance. Firing schedules for the different particle blends have not been fully optimized; processing optimization should also improve the mechanical strength.

The full-scale fabrication of a slip-cast, fused-silica heat shield from continuous-particle-size slip presents some important technical problems. A thickness of 2.5 cm (1.0 in.) or more is required, and the time needed to drain the continuous-particle-size slip causes separation of heavier particles. This separation results in a nonuniform wall thickness and composition.

For the particle sizes studied under this program, slip cast articles made from monodisperse slips drain in minutes, as opposed to hours for the continuous-particle-size slips. Thus, particle separation does not occur and a more uniform part results.

B. Recommendations for Future Work

Based on these studies, two primary areas relating to slip-cast, fused-silica heat shield technology should be pursued:

1) Optimizing a reflecting heat shield material made from blends of monodisperse particle sizes;

2) Developing a conical, fused-silica reflecting heat shield to meet the requirements of a Uranus probe and other outer-planet probes.

As stated in the previous section, slip casting is the recommended method for producing a fused-silica heat shield. The tests conducted to date have shown that the 75/25% blend slips give the best performance. They exhibit a higher reflectance and lower transmittance than the continuous-particle-size slips, while possessing good strength. They also have a higher density, better mechanical strength, and better optical performance than the 100% monodisperse configurations. However, the blend configurations tested in this program can probably be further optimized, and the following tasks are recommended along this line:

1) Preparation of high-purity colloidal silica containing sodium contamination well below the level of present low-sodium sols ($\sim$88 ppm of solids) by ion-exchange chromatography;

2) Investigation of blending different monodisperse particles other than those used in the present configurations, where the radius of the 25%-component particles is 20 to 25% of that of the 75%-component particles;

3) Investigation of different blending proportions, other than 75% of the larger component and 25% of the smaller component;

4) Further investigation of different firing schedules to determine the optimum processing for monodisperse blend configurations;

5) Further investigations of the effects of pH and colloidal silica proportions on density, strength, and optical properties;

6) Investigations of the performance of slip-cast monodisperse blends made from high-purity synthetic fused silicas such as Suprasil.

Samples should be fabricated incorporating the above materials and processing variations, and their optical and mechanical properties should be evaluated.

Development problems associated with a full-size silica reflective heat shield fall into the areas of thermal design, structural design, attachment, fabrication scaleup, and quality assurance. To identify these problems and their solutions, a program of designing, analyzing, fabricating, inspecting and testing a silica heat shield should be conducted. The heat shield configuration should be the 1.05-rad (60-deg) half-angle cone baselined for the Jupiter-Uranus probe.

The development program would involve the following tasks:

1) Define the design environment and establish design criteria for a reflective heat shield for a Uranus entry probe. The environment should include convective and radiant heating pulses and heat flux distribution, dynamic pressure, aerodynamic shear, entry deceleration, and ascent dynamics;

2) Conduct heat-transfer analyses for three points on the conical forebody (stagnation point, cone edge, intermediate point) and establish heat-shield thickness requirements for each point;

3) Calculate temperature gradients through the thickness of the silica heat shield and along the meridian line from the stagnation point to the cone edge. Calculate thermal stresses in the silica heat shield resulting from these gradients;

4) Design the heat shield attachment details and calculate temperatures and stresses for the attachment area;

5) Develop a fabrication plan for fabricating a full-size, high-purity reflecting heat shield. The fabrication plan should include cleanliness requirements as well as provisions for inspecting the heat shield without contamination;

6) Fabricate and inspect two conical, 89-cm (35-in.) diameter heat shields using the procedures spelled out in the fabrication plan. Attach the heat shield to a suitable metallic structure;

7) Develop a test plan for the two conical heat shields. The tests to be considered should include structural loading, dynamic testing, cold soak, and quartz-lamp radiant heating. Identify instrumentation requirements for each of these tests;

8) Conduct structural and dynamic tests on one of the conical heat shields and cold soak and radiant heat (heat-transfer and thermal stress) tests on the second heat shield in accordance with the test plan;

9) Conduct a posttest analysis of the heat shields and provide failure analyses as required. Calculate attachment stresses, temperatures, and thermal stresses for the test conditions. Correlate these with strain gage, accelerometer, and thermocouple data and compare them with the corresponding stresses and temperatures predicted for the flight environment.

Martin Marietta Corporation
Denver Division
Denver, Colorado, August 14, 1974

VII. REFERENCES

1. Nicolet, W. E.: *Analytical Study of the Heating and Associated Heat Shielding Requirements for Outer-Planet Missions.* Third Monthly Progress Report, NASA-ARC Contract NAS2-7235, Aerotherm Project 7072, Jan. 1973.

2. Congdon, W. M.: Investigation of Reflecting Heat-Shield Materials for Outer-Planet Missions. Paper No. 74-702. Presented at AIAA/ASME 1974 Thermophysics and Heat Transfer Conference, Boston, Mass., July 15-17, 1974.

3. Coyle, T. D.: Silica Introduction. Vol. 18 of *Encyclopedia of Chemical Technology.* 2nd ed., John Wiley & Sons, Inc., 1969, pp. 46-61.

4. Schick, H. L.: A Thermodynamic Analysis of the High-Temperature Vaporization Properties of Silica. *Chem. Rev.*, vol. 60, 1960, pp. 331-362.

5. Dumbaugh, W. H.; and Schultz, P. C.: Vitreous Silica. Vol. 18 of *Encyclopedia of Chemical Technology.* 2nd ed., John Wiley & Sons, Inc., 1969, pp. 72-105.

6. Sigel, G. H., Jr.: Vacuum Ultraviolet Absorption in Alkali-Doped Fused Silica and Silicate Glasses. *J. Phys. Chem. Sol.*, vol. 32, 1971, pp. 2373-2383.

7. Lell, E.; Kreidl, N. J.; and Hensler, J. R.: Vol. 4-Radiation Effects in Quartz, Silica, and Glasses. *Progress in Ceramic Sciences*, J. E. Burke, ed., Pergamon Press, 1966, pp. 1-93.

8. Beder, E. C.; Bass, C. D.; and Shackleford, W. L.: Transmissivity and Absorption of Fused Quartz Between 0.22μ and 3.5μ, from Room Temperature to 1500°C. *Appl. Opt.*, vol. 10, no. 10, October 1971, pp. 2263-2268.

9. Anon.: *Fused-Quartz Catalog.* Form Q15. Tech. Data Booklet from General Electric Co., Lamp Glass Department, Willoughby, Ohio, Dec. 1969.

10. DeWitt, D. P.: *Handbook of the Optical, Thermal, and Mechanical Properties of Six Polycrystalline Dielectric Materials.* TPRC Rpt. 19. Prepared by Purdue University for NASA-Ames Research Center under Contract NAS2-6802, September 1972.

11. Anon.: *Fused Amorphous Silica.* Applied Space Technology Regional Advancement, Kansas City, Mo.

12. Anon.: *Glasrock.* Tech. Data Sheet from Glasrock Products, Inc., Atlanta, Ga.

13. Fleming, J. D.: Slip Casting of Fused Silica. *Cer. Bull.*, vol. 40, no. 12, 1961.

14. Anon.: *Silfrax.* Tech. Data Sheet from Fused Silica Products, Refractories and Electronics Div., Carborundum Co., Niagara Falls, N.Y.

15. Jaworski, W.; and Nagler, R. G.: *A Parametric Analysis of Venus Entry Heat-Shield Requirements.* Tech. Rpt. 32-1468, NASA-Jet Propulsion Laboratory, April 1970, p. 13.

16. Kingery, W. D.: Vol. 2-The Thermal Conductivity of Ceramic Dielectrics. *Progress in Ceramic Science*, J. E. Burke, ed., Pergamon Press, 1962, pp. 181-235.

17. Russell, H. W.: Principles of Heat Flow in Porous Insulators. *J. Am. Cer. Soc.*, vol. 18, 1935, p. 1.

18. Loeb, A. L.: Thermal Conductivity: Ch. VIII-A Theory of Thermal Conductivity of Porous Materials. *J. Am. Cer. Soc.*, vol. 37, no. 2, Feb. 1954, p. 96.

19. Gardon, R.: The Emissivity of Transparent Materials. *J. Am. Cer. Soc.*, vol. 39, no. 8, Aug. 1956, p. 278.

20. Ryshkewitch, E.: *Oxide Ceramics, Physical Chemistry, and Technology.* Academic Press (New York), 1960.

21. Harris, J. N.; and Welsh, E. A.: *Fused-Silica Design Manual.* Vol. 1, Rpt. for Contract N00017-72-C-4434, May 1973.

22. Walton, J. D.; and Poulos, N. E.: *Slip-Cast Fused Silica.* Tech. Doc. Rpt. ML-TDR-64-195, October 1964.

23. Lynch, J. F.; Ruderer, C. G.; and Duckworth, W. H.: *Engineering Properties of Ceramics: Data Book to Guide Materials Selection for Structural Applications.* Rpt. AFML-TR-66-52, June 1966.

24. Cowan, W. D.: Outer Planet Probe Design. Paper presented at the Outer-Planet Probe Technology Workshop, NASA-Ames Research Center, May 21-23, 1974.

25. Congdon, W. M.: High-Purity Silica Reflecting Heat Shield Development. Paper presented at the Outer-Planet Probe Technology Workshop, NASA-Ames Research Center, May 21-23, 1974.

26. Mezines, S. A.: Carbon-Phenolic Heat Shields for Outer-Planet Probes. Paper presented at the Outer-Planet Probe Technology Workshop, NASA-Ames Research Center, May 21-23, 1974.

APPENDIX

SCANNING ELECTRON MICROSCOPE PHOTOGRAPHS OF DIFFERENT SLIP-CAST CONFIGURATIONS

Figures 42, 43, and 44 compare the surfaces of samples prepared from Particle Sizes 2, 4, and 6 under magnification using a scanning electron microscope (SEM). Note that in each of these photographs the distance between hash marks is 30 μm. Each of the samples was fired at 1478°K (2200°F) for 4 hours. The difference in particle size and the relative degree of surface roughness between samples is quite apparent. In addition, a visual inspection and comparison of the particles to the 30-μm hash marks in each photograph corroborates the results of the Stokes' law size-determination tests, which were given by figure 18 in Section III. Particle Size 2 is about 20 to 40 μm, 4 is about 10 to 21 μm, and 6 is about 5 to 11 μm in diameter.

In figures 45 and 46, the surface of a slip-cast silica sample prepared from a continuous-particle-size slip is shown under two different magnifications. (Figure 18 in Section III showed the approximate size distribution for a continuous-particle-size slip as determined by the Stokes' law method.) These photographs reveal a surface that is covered with fused-silica "dust." The larger particles are mostly obscured due to the dust collected on their faces. In addition, the spaces between the larger particles are packed with the smaller particles, eliminating the larger interparticle voids.

Figures 45 and 46 show a continuous-particle-size surface that lacks the uniform array of scattering voids revealed by the monodisperse-particle-size surfaces in figures 42 through 44. This explains why the monodisperse-particle-size samples give higher reflectances than the continuous-particle-size samples, as discussed in Section IV.

Figure 47 is an SEM photograph of a sample made from Particle Size 6. Figures 46 and 47 show the large differences in the particle sizes and void sizes between the two samples (the distance between the hash marks in these figures is 3 μm).

Figures 48, 49, and 50 compare at the same magnification the surfaces of slip-cast, fused-silica samples all made from Particle Size 2 but fired under different conditions. Figure 48 shows a surface fired 4 hours at 1478°K (2200°F). Note that the necking between particles is slight and the sintering is incomplete. Figure 49 shows a surface fired for 4 hours at 1533°K (2300°F). The particles have become more rounded (minimizing the surface area and, thus, the surface free energy), and the necking

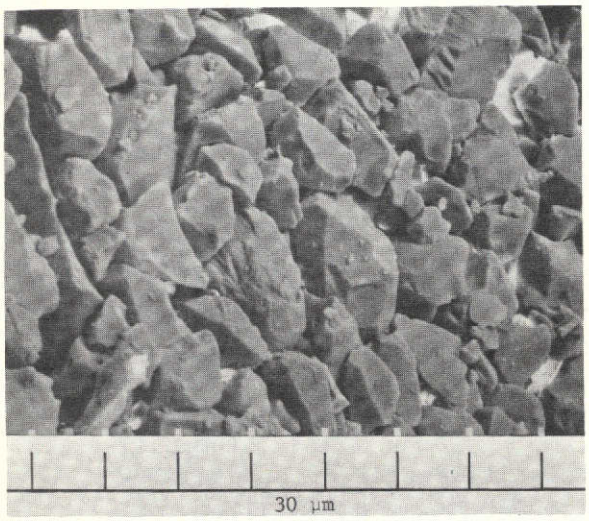

Figure 42.- SEM photograph of 100% monodisperse configuration, particle size 2 (20 to 40 µm), fired 4 hr at 1478°K (2200°F)

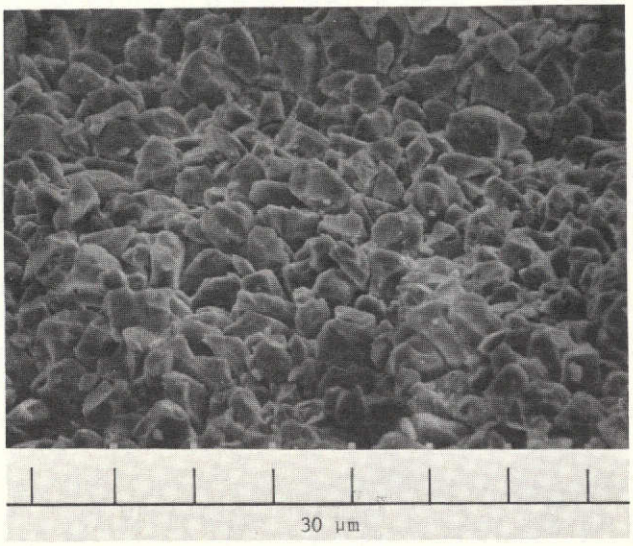

Figure 43.- SEM photograph of 100% monodisperse configuration, particle size 4 (10 to 21 µm), fired 4 hr at 1478°K (2200°F)

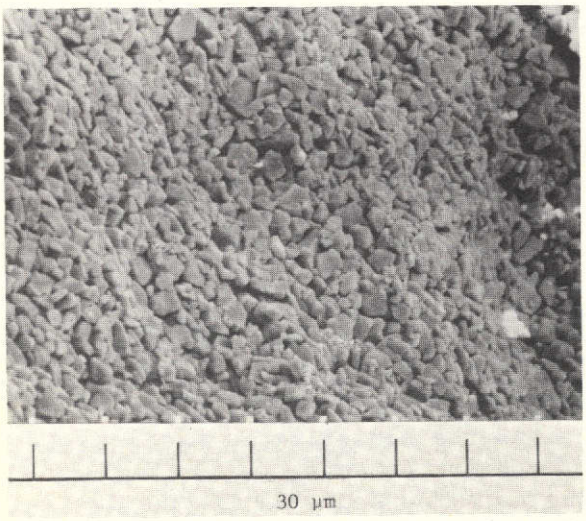

Figure 44.- SEM photograph of 100% monodisperse configuration, particle size 6 (5 to 11 µm), fired 4 hr at 1478°K (2200°F)

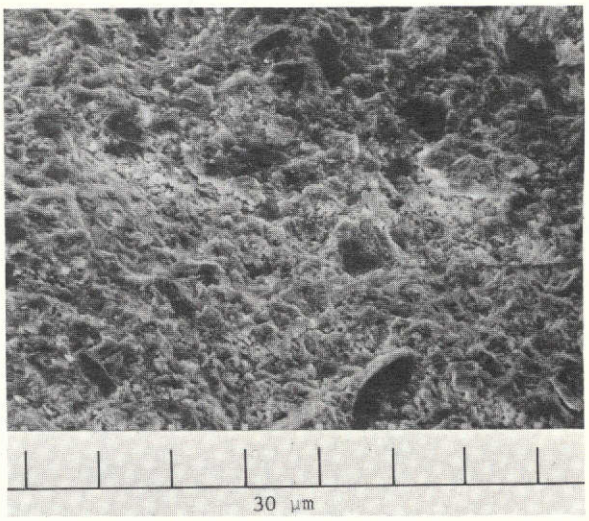

Figure 45.- SEM photograph of continuous-particle-size configuration, fired 4 hr at 1478°K (2200°F)

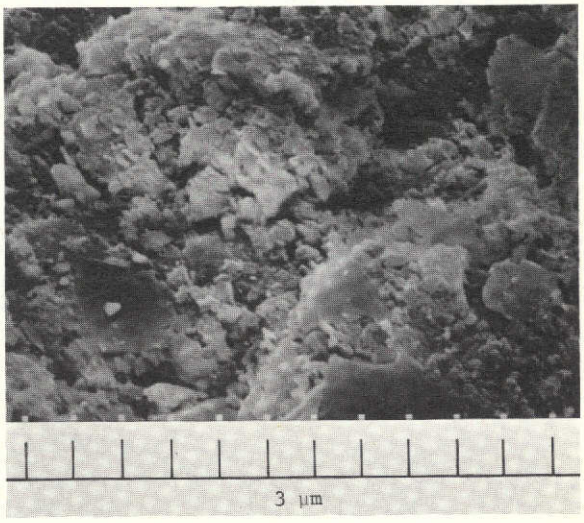

Figure 46.- SEM photograph of continuous-particle-size configuration, fired 4 hr at 1478°K (2200°F)

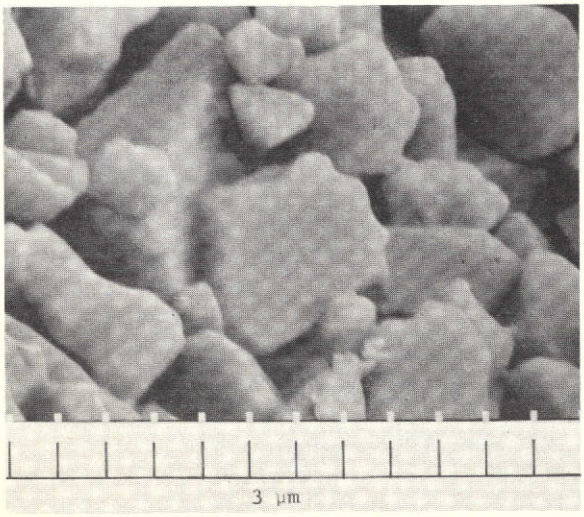

Figure 47.- SEM photograph of 100% monodisperse configuration, particle size 6 (5 to 11 μm), fired 4 hr at 1478°K (2200°F)

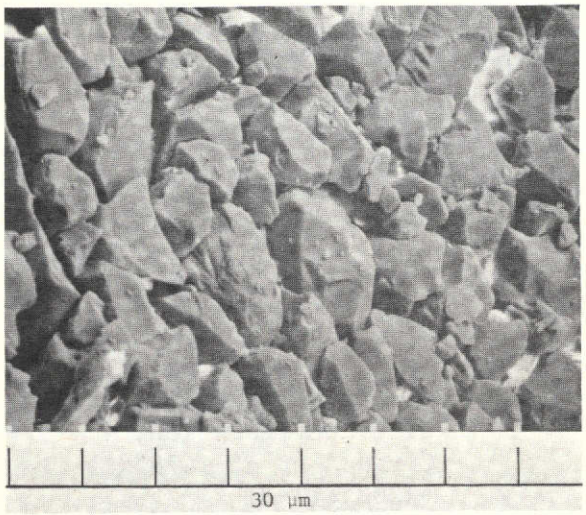

Figure 48.- SEM photograph of 100% monodisperse configuration, particle size 2 (20 to 40 μm), fired 4 hr at 1478°K (2200°F)

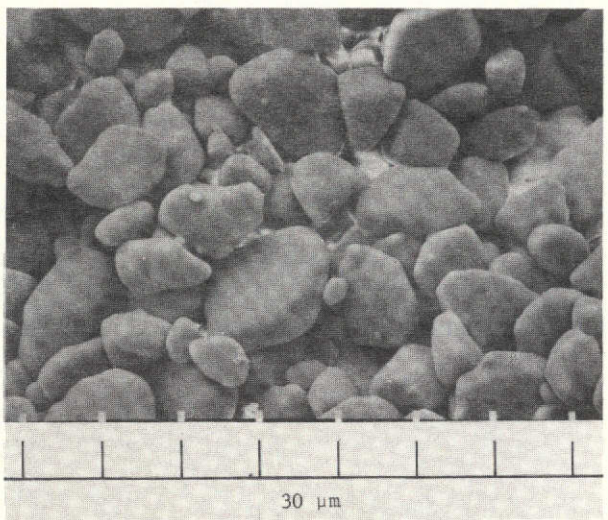

Figure 49.- SEM photograph of 100% monodisperse configuration, particle size 2 (20 to 40 μm), fired 4 hr at 1533°K (2300°F)

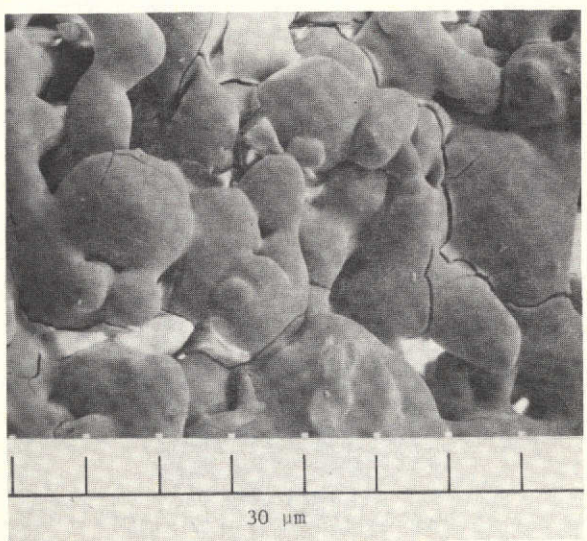

Figure 50.- SEM photograph of 100% monodisperse configuration, particle size 2 (20 to 40 μm), fired 4 hr at 1589°F (2400°F)

between particles is considerably greater. This is a sample that has undergone a large increase in strength and integrity due to firing. Figure 50 shows a Particle Size 6 surface that is overfired. This sample was sintered 4 hours at 1589°K (2400°F). The particles have coalesced to form larger particles, causing shrinkage of the part and leading to loss of scattering and bulk vitrification. The cracking shown in this photograph may have been caused by the formation of cristobalite.

Figures 51 through 53 are similar to figures 48 through 50 except that the samples were prepared from Particle Size 6 instead of 2. The surface shown in figure 51 was fired 4 hours at 1478°K (2200°F); the surface in figure 52 was fired 4 hours at 1533°K (2300°F); and the surface in figure 53 was fired 4 hours at 1589°K (2400°F).

Note that the sample in figure 51 is underfired: the necking between particles is very slight. In contrast, the sample in figure 53 is overfired: the coalescence of particles is almost complete. The slip-cast, fused-silica surface shown in figure 52 is sufficiently fired and, perhaps, even a little overfired. The diameters of the necks that have grown between particles are almost as large as the particles themselves, and some of the particles have almost completely coalesced.

It is interesting to compare figure 49 with figure 52, and figure 50 with figure 53. The 20- to 40-μm particles in figure 49 are fused noticeably less than the 5- to 11-μm particles in figure 52, even though both were fired 4 hours at 1533°K (2300°F). This confirms the general rule that, under identical firing schedules, smaller particles of the same material fuse more rapidly than larger particles. This fact is demonstrated even more clearly by comparing figure 50 with figure 53. In figure 53 the 5- to 11-μm particles have coalesced almost entirely, forming an optically smooth surface, whereas in figure 50, one can still distinguish individual particles and the surface is optically very rough. Both surfaces were fired 4 hours at 1589°K (2400°F).

Figures 54, 55, and 56 provide closeups of samples made from Particle Sizes 2, 4, and 6, respectively. Each of the samples has been fired 4 hours at 1533°K (2300°F). The necking between the 20- to 40-μm particles, which was difficult to see in figure 48 is more easily seen in figure 54. The necking between the 10- to 21-μm particles in figure 55 is slightly greater than for the larger particles in figure 54. And in figure 56, as mentioned earlier, some of the particles have almost completely coalesced.

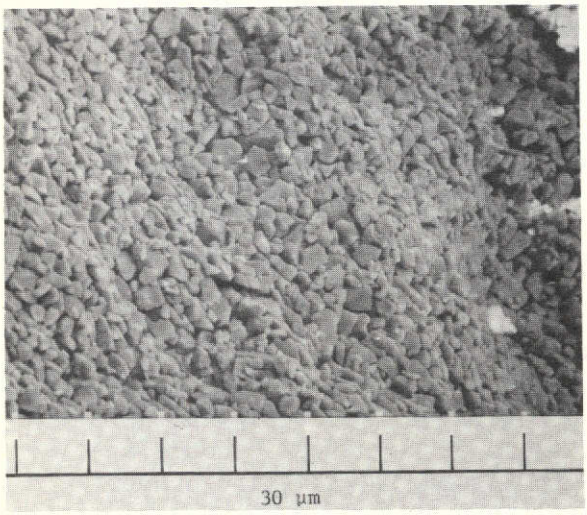

Figure 51.- SEM photograph of 100% monodisperse configuration, particle size 6 (5 to 11 µm), fired 4 hr at 1478°K (2200°F)

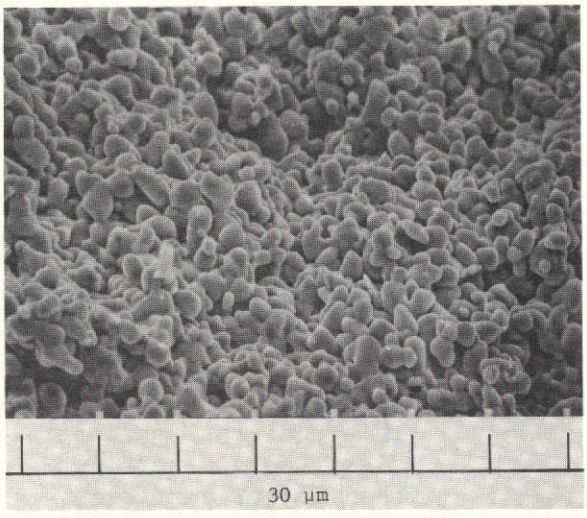

Figure 52.- SEM photograph of 100% monodisperse configuration, particle size 6 (5 to 11 µm), fired 4 hr at 1533°K (2300°F)

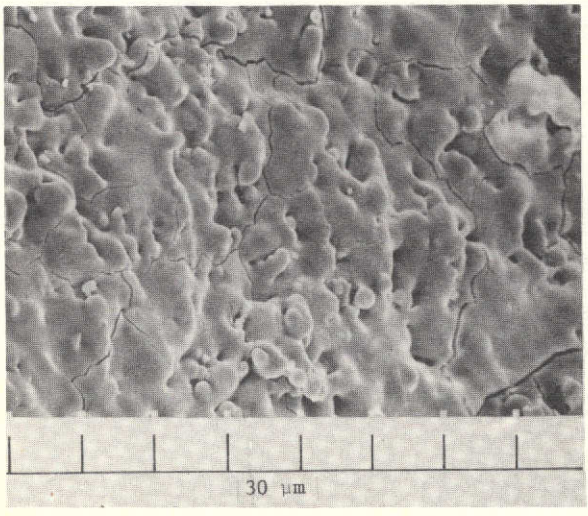

Figure 53.- SEM photograph of 100% monodisperse configuration, particle size 6 (5 to 11 µm), fired 4 hr at 1589°K (2400°F)

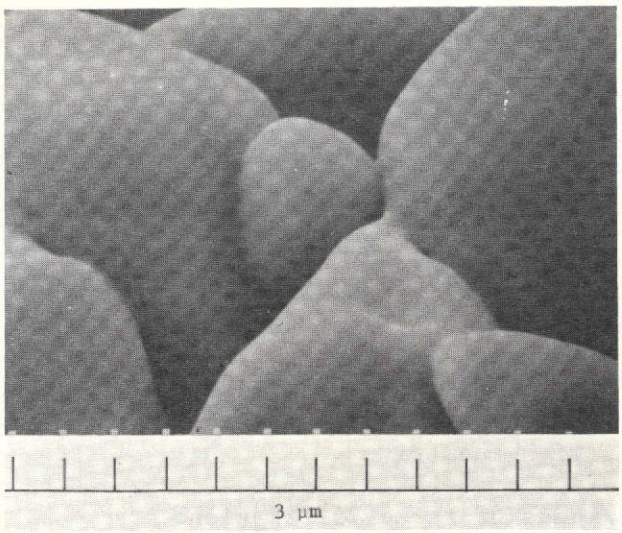

Figure 54.- SEM photograph of 100% monodisperse configuration, particle size 2 (20 to 40 μm), fired 4 hr at 1533°K (2300°F)

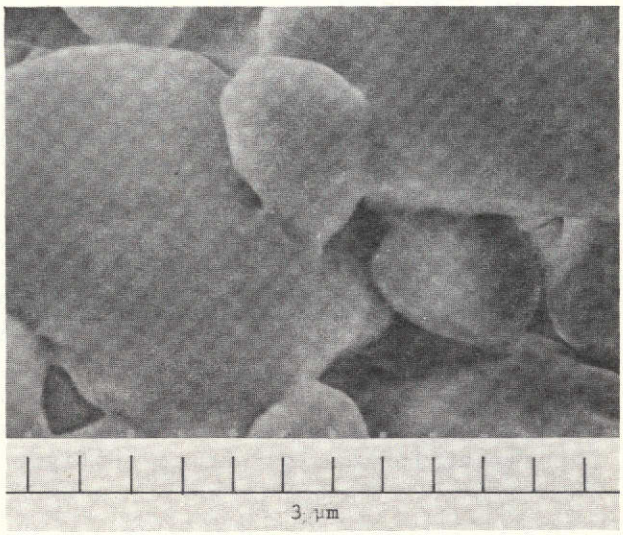

Figure 55.- SEM photograph of 100% monodisperse configuration, particle size 4 (10 to 21 μm), fired 4 hr at 1533°K (2300°F)

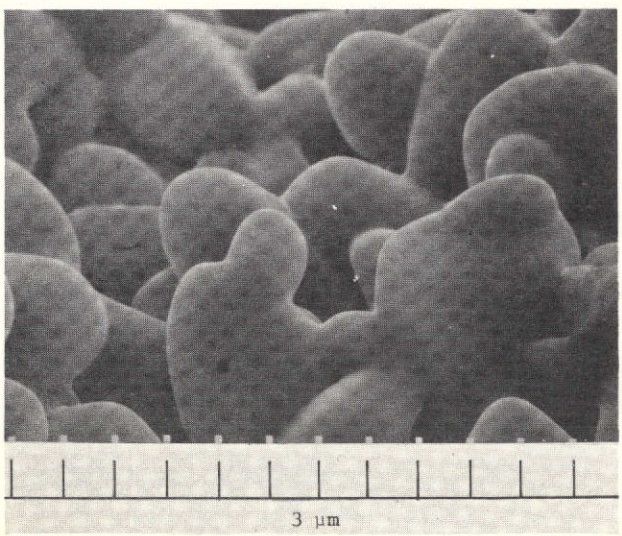

Figure 56.- SEM photograph of 100% monodisperse configuration, particle size 6 (5 to 11 μm), fired 4 hr at 1533°K (2300°F)

APPENDIX

As shown by figure 13 in Section II, optimum firing schedules for a continuous-particle-size, fused-silica configuration are 1 hour at 1533°K (2300°F), 4 hours at 1478°K (2200°F), and a range of values between these. In view of the above discussion, where it was shown that all the monodisperse configurations require more severe firing conditions to produce sufficient necking between particles, there is the indication that in these continuous-particle-size configurations the fine fused-silica dust is "cementing" the larger particles (those larger than ∿5 μm) together, rather than the larger particles fusing with themselves.

Figures 57 through 59 show the surfaces of three 75/25% blend configurations prepared from different particle sizes. The slip-cast configuration shown in figure 57 contains 75% (by weight) of PS-2 and 25% of PS-6, and was fired 5 hours at 1533°K (2300°F). The configuration in figure 58 contains 75% PS-4 and 25% PS-7, and was fired 4 hours at 1478°K (2200°F). Figure 18 shows a surface made from 75% PS-6 and 25% PS-8 that was fired 4 hours at 1478°K (2200°F).

Note that the voids in these 75/25% blend configurations are noticeably smaller than those for the corresponding 100% monodisperse configurations made from the larger-particle-size component. At the same time, the voids are not filled up by the very small particles, which is the case in the continuous-particle-size configurations. The fact that the voids are reduced explains why the 75/25% blends have a higher reflectance than the 100% monodisperse configurations.

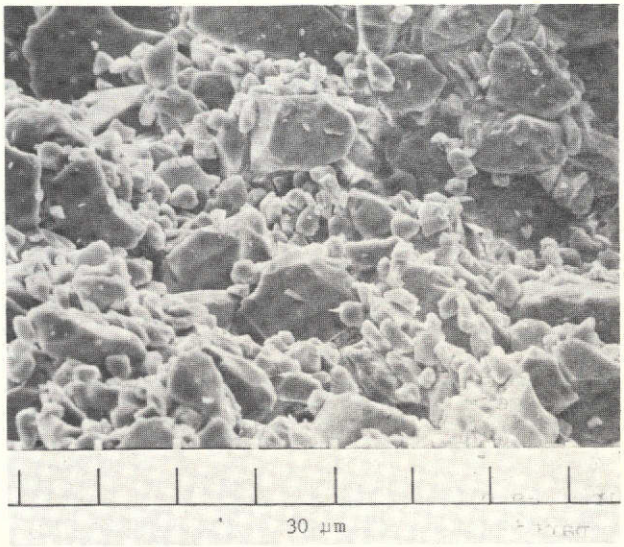

Figure 57.- SEM photograph of 75/25% blend configuration, 75% particle size 2 (20 to 40 µm), 25% particle size 6 (5 to 11 µm), fired 5 hr at 1533°K (2300°F)

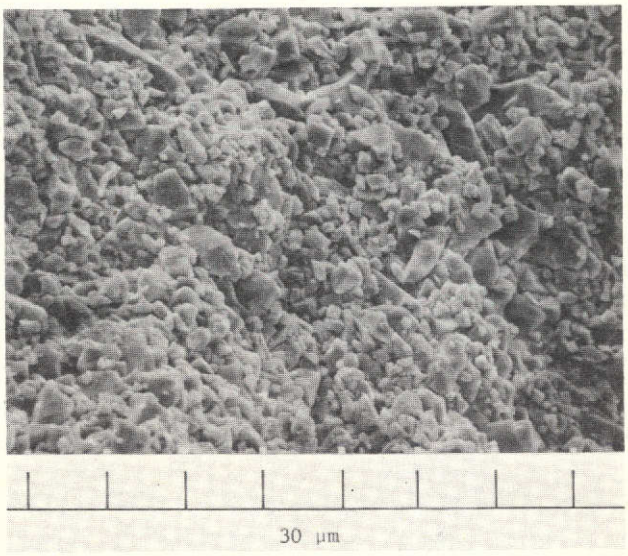

Figure 58.- SEM photograph of 75/25% blend configuration, 75% particle size 4 (10 to 21 µm), 25% particle size 7, fired 4 hr at 1478°K (2200°F)

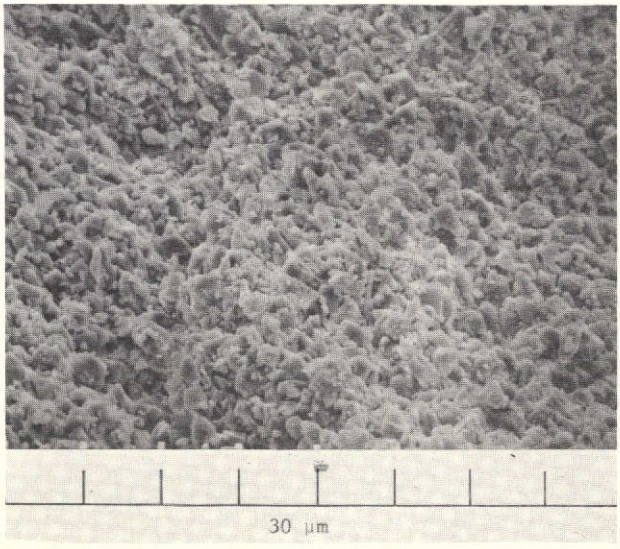

Figure 59.- SEM photograph of 75/25% blend configuration, 75% particle size 6 (5 to 11 µm), 25% particle size 8, fired 4 hr at 1478°K (2200°F)